

Neural Connectivity with Hidden Gaussian Graphical State-Model

Deirel Paz-Linares ^{a,b,1}, Eduardo Gonzalez-Moreira ^{a,c,d,1}, Jorge Bosch-Bayard ^{a,d,e}, Ariosky Areces-Gonzalez ^{a,f},

Maria L. Bringas-Vega ^{a,b} and Pedro A. Valdés-Sosa ^{a,b,2}

^a The Clinical Hospital of Chengdu Brain Science Institute, MOE Key Lab for Neuroinformation, University of Electronic Science and Technology of China, Chengdu, China; ^b Cuban Neuroscience Center, La Habana, Cuba; ^c Centro de Investigaciones de la Informática, Universidad Central “Marta Abreu” de las Villas, Santa Clara, Cuba;

^d Unit of Neurodevelopment, Institute of Neurobiology, UNAM, Campus Juriquilla, Santiago de Querétaro, Querétaro, México; ^e Montreal Neurological Institute, Montreal, Canada; ^f Departamento de Matematica, Universidad de Pinar del Rio, Pinar del Rio, Cuba.

¹ contributed equally to this research ² senior and correspondence author

Abstract

The noninvasive procedures for neural connectivity are under questioning. Theoretical models sustain that the electromagnetic field registered at external sensors is elicited by currents at neural space. Nevertheless, what we observe at the sensor space is a superposition of projected fields, from the whole gray-matter. This is the reason for a major pitfall of noninvasive Electrophysiology methods: distorted reconstruction of neural activity and its connectivity or “leakage”. It has been proven that current methods produce incorrect connectomes. Somewhat related to the incorrect connectivity modelling: they disregard either Systems Theory and Bayesian Information Theory. We introduce a new formalism that attains for it: Hidden Gaussian Graphical State-Model (HIGGS). A neural Gaussian Graphical Model (GGM) hidden by the observation equation of Magneto-encephalographic (M/EEG) signals. HIGGS is equivalent to a frequency domain Linear State Space Model (LSSM) but with sparse connectivity prior. The mathematical contribution here is the theory for high-dimensional and frequency-domain HIGGS solvers. We demonstrate that HIGGS can attenuate the leakage effect in the most critical case: the distortion EEG signal due to head volume conduction heterogeneities. Its application in EEG is illustrated with retrieved connectivity patterns from human Steady State Visual Evoked Potentials (SSVEP). We provide for the first time confirmatory evidence for noninvasive procedures of neural connectivity: concurrent EEG and Electrocorticography (ECoG) recordings on monkey. Open source packages are freely available online, to reproduce the results presented in this paper and to analyze external M/EEG databases.

M/EEG-connectivity | leakage | systems-theory | bayesian-theory | gaussian-graphical-model

1 Introduction

The band specific synchronized activity is the underlying mechanism for Brain large scale integration from which coherent behavior and cognition emerges (Engel et al., 2001; Varela et al. 2001). Synchronized activity is driven by the neural connectivity: this is physically interpreted in terms of synaptic gain (efficiency in synaptic transmission). Somewhat not accessible by noninvasive techniques. Nevertheless, the

Primary Current Density (PCD) caused by spatially and temporally organized synaptic events can be noninvasively observed through scalp M/EEG signals (Lopes da Silva, 2013). The PCD pathway towards the scalp potential is governed uniquely by the laws of electromagnetic field in media: Lead Field (LF) driven (Valdés-Hernández et al. 2009). It does not involve biological mechanisms as with fMRI.

M/EEG connectivity is studied by statistical dependencies of the PCD time series at the space of gray-matter generators. Doing so requires estimating the PCD in the first place. Electrophysiology Source Imaging (ESI) methods can tackle this by inverting the Lead Field forward equation. Lead Field ill-conditioning constitutes a major cause for the uncertainty of source activations. This has motivated the development of source penalization models, indistinctively used by the three large mathematical frameworks: Tikhonov Regularization, Bayesian Analysis and Beamformer Spatial Filtering.

A common issue of ESI methods was the “Activation Leakage” (AL): ghost activations present in the reconstructed source. It has been demonstrated that sparse models can reduce the AL: as with L1 norm based penalization or combined L1/L2 norms (Vega-Hernández et al., 2008;) or Linearly Constrained Minimum Variance (Van Veen et al., 1997).

Solving AL would improve connectivity estimation, but it does not prevent “Connectivity Leakage” (CL). In both MEG and EEG, the estimated time series of neural generators are contaminated with activity of the remaining ones: due to the mixing when they are projected forth (M/EEG signal generation) and back (ESI analysis) between source and sensor space (Van de Steen et al., 2016).

The situation worsens for EEG due to inhomogeneities of head volume conductance, that have a distortive effect on the tangential component of the electric Lead Field. Also, the high conductivity of scalp tissue blurs the electric potential at sensor space. It causes spurious correlations of the adjacent sensor’s time series, which are carried down to source space by ESI. MEG technique has been the choice of leading connectome projects. In the interim, the wearability of EEG systems remains the main argument to center efforts on methods that might ameliorate this effect.

Simulation studies have not attained yet for the isolated effect of these factors on the connectivity: they do not

compare against different head model and their results are perturbed by AL (Anzolin et al., 2019).

Recently, the analysis of source times series with Graphical LASSO has been proposed as the solution to CL (Colclough et al., 2016). This pursues the sparse (de-mixed) estimation of Source Partial Correlations (SPC), from band limited Empirical Source Covariance (ESC) in Real domain.

This idea meets the classical Gaussian Graphical Models (GGM) theory, since the SPC represents the graph edges structure (Friedman et al., 2008). But still incurs in severe theoretical errors: it does not attain to modelling the effect of connectivity estimation (sparse SPC) back to the source time series (ESC). In addition, Real SPC models can only be related to zero-lag interactions within time domain models. Such procedure constitutes a contravention of Systems Theory (Von Bertalanffy, 1950) and Bayesian Information Theory (MacKay, 2003). A deeper discussion on how the current models produce incorrect connectomes was given by (Pascual-Marqui et al., 2017; Biscay et al., 2018).

A physically plausible connectivity model can only be attained by using Systems Theory, as with the Linear State Space Models (LSSM). The Source Partial Coherence of the LSSM frequency domain transformation represents multiple-lag interactions (Faes et al., 2012; Baccalá and Sameshima, 2001).¹ Making reliable inference should consider the probabilistic conditioning between all ontological levels in the Bayesian hierarchy: data (M/EEG observations) <-> parameters (neural dynamics) <-> hyperparameters (neural connectivity). There are two options for the inference of hidden variables from the Bayesian information viewpoint: direct estimation of the connectivity, after the marginalization of neural dynamic variables (which ultimately affects the inference of the latter), or the estimation of both with mutually dependent formulas.

Unfortunately, previous ESI methods based on Bayesian Information Theory do not make use of adequate connectivity models. This is the case of univariate methods (using diagonal connectivity models) like Automatic Relevance Determination (ARD) (Neal, 1998), Structured Sparse Bayesian Learning (SSBL) (Wipf et al., 2009) and multivariate methods that model connectivity through Real Covariance (Friston et al., 2008).

An early frequency domain method based on system theory is the Variable Resolution Tomographic Analysis (VARETA) (Bosch-Bayard, et al., 2001). VARETA uses Bayesian inference: mutual estimation of neural states and connectivity, with the Expectation Maximization (EM) algorithm. Here, we formalize this in the context of system theory. We solve Leakage with sparse prior of VARETA's SPC. The mathematical principle is the Hidden Gaussian Graphical State-Model (HIGGS): a model that meets the Systems Theory and the methodology of GGM connectivity.

¹ From now on we use SPC to denote Source Partial Coherence. For Source Partial Correlations we will use Real SPC.

Significance

Accessing connectivity noninvasively is a key issue. M/EEG signals stand out for its purely electromagnetic link to neural events. Inverting M/EEG towards its source would reveal the connectivity at the mesoscopic scale (millimetric), something not accessible by current analysis methods. This is done here with a new frequency domain Bayesian formalism (H-HGGM). H-HGGM directly models the partial correlations (connectivity) and grounds in mesoscopic neural models (system theory). Here, we propose an approach to solve the severe issues to implement GGM: complex-variable and high-dimensionality.

2 Theory

A ubiquitous system theoretic representation of M/EEG time series is the Linear State Space Model (LSSM). The state (source) is represented by the vector $\iota(t)$, on the q-size discretized gray-matter \mathbb{G} and in time domain ($t \in \mathbb{T}$). Its dynamical regime is governed by a stochastic integral equation (state equation), with a kernel that represents the directed connectivity at multiple time lags $\mathbf{K}_u(\tau)$ ($\tau \in \mathbb{T}$). Activity at source space is transferred to M/EEG signal $\nu(t)$, at the p-size Sensor Space \mathbb{E} , by the Lead Field $\mathbf{L}_{\nu t}(\tau)$ (observation equation). The Lead Field at multiple time lags represents the kernel of the Maxwell equation integral solution. In practice, an instantaneous effect operator $\mathbf{L}_{\nu t}$ is a useful simplification, but we keep this formulation for more generality of the framework.²

The stochastic character of the state and observation equations is driven by additive noise processes at both levels: source $\zeta(t)$ and sensor $\xi(t)$.

$$\nu(t) = \int_0^t \mathbf{L}_{\nu t}(\tau) \iota(t - \tau) d\tau + \xi(t) \quad (1)$$

$$\iota(t) = \int_0^t \mathbf{K}_u(\tau) \iota(t - \tau) d\tau + \zeta(t) \quad (2)$$

Fourier transforming (1) and (2) allows for a more compact representation in frequency domain ($\omega \in \mathbb{F}$), when $\nu(t)$, $\xi(t)$ and $\zeta(t)$ are square-integrable. The stochastic properties of the transformed “realizations” (of observations and states) are driven by a Hermitian Gaussian model ($N^{\mathbb{C}}$), it is direct if one assumes noise Gaussianity ($N^{\mathbb{R}}$): $\xi(t) \sim N_p^{\mathbb{R}}(\xi(t) | \mathbf{0}, \Sigma_{\xi\xi})$ and $\zeta(t) \sim N_q^{\mathbb{R}}(\zeta(t) | \mathbf{0}, \Sigma_{\zeta\zeta})$. This is strongly motivated by central limit theory (Rosenblatt, 1956). See SI section C for further information about this model’s fundament and frequency domain analysis. See also SI sections A and B for notation and nomenclature.

² Observable quantities are denoted by Latin scripts and unobserved by Greek scripts. Check Appendices for mathematical notation and nomenclature.

The Bayesian model is compactly expressed by the Data Likelihood and Parameters Prior: the Hidden Gaussian Graphical State-Model (HIGGS).

$$\mathbf{v}(\nu) | \boldsymbol{\iota}(\nu), \boldsymbol{\Sigma}_{\xi\xi}(\nu) \sim N_p^{\mathbb{C}}(\mathbf{v}(\nu) | \mathbf{L}_{\nu\iota}(\nu) \boldsymbol{\iota}(\nu), \boldsymbol{\Sigma}_{\xi\xi}) \quad (3)$$

$$\boldsymbol{\iota}(\nu) | \boldsymbol{\Sigma}_{\mathbf{u}}(\nu) \sim N_q^{\mathbb{C}}(\boldsymbol{\iota}(\nu) | \mathbf{0}, \boldsymbol{\Sigma}_{\mathbf{u}}(\nu)) \quad (4)$$

The signal spectral properties are stored in the Hermitic Covariance matrices of states/noise ($\boldsymbol{\Sigma}_{\mathbf{u}}(\nu) / \boldsymbol{\Sigma}_{\xi\xi}$). Due to equivalence between time and frequency domain system identification, its knowledge would allow retrieving the states and observations in time domain (Schoukens et al, 2004). The Hermitic matrix $\boldsymbol{\Sigma}_{\mathbf{u}}(\nu)$ encodes the Directed Transfer Function (DTF) $\mathbf{K}_{\mathbf{u}}(\nu)$ or connectivity (Kaminski and Blinowska, 1991). Its inverse: the SPC ($\boldsymbol{\Theta}_{\mathbf{u}}(\nu) = \boldsymbol{\Sigma}_{\mathbf{u}}^{-1}(\nu)$), is regarded as an “undirected connectivity” measure. This is a consequence of the Spectral Factorization Theorem (Faes and Nollo, 2011).

$$\boldsymbol{\Theta}_{\mathbf{u}}(\nu) = (\mathbf{I}_q - \mathbf{K}_{\mathbf{u}}^{\dagger}(\nu)) \boldsymbol{\Sigma}_{\zeta\zeta}^{-1} (\mathbf{I}_q - \mathbf{K}_{\mathbf{u}}(\nu)) \quad (5)$$

Assuming in formula (5) a univariate biological noise model $\boldsymbol{\Sigma}_{\zeta\zeta} = \text{diag}(\sigma_{\zeta}^2)$, the following “necessary condition” can be verified: in relation to node’s directed and undirected connectivity.

“For the existence of undirected connectivity $i \leftrightarrow j$ ($\{\boldsymbol{\Theta}_{\mathbf{u}}(\nu)\}_{ij} \neq 0$) it must hold that either: There exists one of the directed connectivities $i \leftarrow j$ ($\{\mathbf{K}_{\mathbf{u}}(\nu)\}_{ij} \neq 0$) or $j \leftarrow i$ ($\{\mathbf{K}_{\mathbf{u}}(\nu)\}_{ji} \neq 0$). Or there exists directed connectivity from a third node $i \leftarrow k$ ($\{\mathbf{K}_{\mathbf{u}}(\nu)\}_{ik} \neq 0$) or $j \leftarrow k$ ($\{\mathbf{K}_{\mathbf{u}}(\nu)\}_{jk} \neq 0$).”

The Graphical LASSO in Real domain uses this argument, but only its extrapolation to complex variable (Hermitian Graphical LASSO) is totally consistent to Systems Theory. Determining the SPC $\boldsymbol{\Theta}_{\mathbf{u}}(\nu)$ would allow estimating the directionality encoded by the DTF $\mathbf{K}_{\mathbf{u}}(\nu)$, due to the uniqueness of the spectral factors in (5).

Here we will be limited to estimate the undirected connectivity or SPC $\boldsymbol{\Theta}_{\mathbf{u}}(\nu)$. This can be done by the analysis of the GGM (prior) hidden by the Likelihood in formula (4): a consequence of the Observation Equation (1). It can be unhidden after computing the Expected Log-Likelihood (ELL): Local approximation to the Type II Log-Likelihood (T2L) Logarithm, inside the EM loop. This is done by integrating the model (3-4) over the parameters $\boldsymbol{\iota}(\nu)$.

For realizations of the observations $\mathbf{V}(\nu) = \{\mathbf{v}_m(\nu)\}_{m \in \mathbb{M}}$ and states $\mathbf{I}(\nu) = \{\boldsymbol{\iota}_m(\nu)\}_{m \in \mathbb{M}}$, in the Fourier’s coefficient sample space \mathbb{M} (size m), the derived Gibbs form of the ELL unfolds into two marginal Wishart ($W^{\mathbb{C}}$) models. Which arguments are two auxiliary quantities specific of each ontological level. These are computed for fixed values of the hyperparameters at the k -th Expectation step: Effective

Residual Empirical Covariance (EREC) $\boldsymbol{\Psi}_{\xi\xi}^{(k)}(\nu)$ and the Effective Source Empirical Covariance (ESEC) $\boldsymbol{\Psi}_{\mathbf{u}}^{(k)}(\nu)$. This provides for a full interpretation of the EM algorithm in terms of GGM theory (Liu and Rubin, 1994): to unhide HIGGS. See Lemma 1 in Materials and Methods (SI section D and E).

$$\mathbf{V}(\nu) | \boldsymbol{\Sigma}_{\xi\xi}(\nu) \sim W_p^{\mathbb{C}}(\boldsymbol{\Psi}_{\xi\xi}^{(k)}(\nu) | m^{-1} \boldsymbol{\Theta}_{\xi\xi}^{-1}, m) \quad (6)$$

$$\mathbf{V}(\nu) | \boldsymbol{\Sigma}_{\mathbf{u}}(\nu) \sim W_q^{\mathbb{C}}(\boldsymbol{\Psi}_{\mathbf{u}}^{(k)}(\nu) | m^{-1} \boldsymbol{\Theta}_{\mathbf{u}}^{-1}(\nu), m) \quad (7)$$

Solvers for Hermitian Graphical LASSO are not fully developed yet. An important part here is its estimation for the unhidden HIGGS. This will be done by leveraging a Complex Variable Local Quadratic Approximation (CV-LQA) of sparse Gibbs priors, see Lemma 2 and 3 in Materials and Methods (SI section F and G). This is corollary of Andrews and Mallows Lemma (AML) that provides explicit formulas able to tackle estimation in high dimensionality (Andrews and Mallows, 1974), see Lemma 4-5 in Materials and Methods (SI section H and I). The Gibbs prior distribution has exponential form with scale (regularization) parameter α_t and argument $\Pi(\mathbf{A}_{\mathbf{u}} \odot \boldsymbol{\Theta}_{\mathbf{u}}(\nu))$. Here Π represents a given scalar function (penalty) and $\mathbf{A}_{\mathbf{u}}$ a selection matrix of connectivity that may encode neuro-anatomical information (SI section E).

We assume that the Residuals Partial Coherence (RPC) is known but a scalar factor θ_{ξ}^2 to be estimated: $\boldsymbol{\Theta}_{\xi\xi} = \theta_{\xi}^2 \mathbf{A}_{\xi\xi}$. We use an exponential prior with scale parameter α_{ξ} for this factor, which provides an explicit solution. This formulation of the RPC formulation is interpretable in terms of experimental information: spurious EEG sensor connectivity due to scalp leakage currents can be encoded into $\mathbf{A}_{\xi\xi}$ and instrumental noise inferior threshold encoded into α_{ξ} .

$$\theta_{\xi}^2 | \alpha_{\xi} \sim \exp(\theta_{\xi}^2 | m \alpha_{\xi}) \quad (8)$$

$$\boldsymbol{\Theta}_{\mathbf{u}}(\nu) \sim \exp(\Pi(\mathbf{A}_{\mathbf{u}} \odot \boldsymbol{\Theta}_{\mathbf{u}}(\nu)) | m \alpha_t) \quad (9)$$

The fitting of Π and α_t biases the estimation of $\boldsymbol{\Theta}_{\mathbf{u}}^{(k+1)}(\nu)$. We solve this by implementing an unbiased estimator (desparsened) that provides for statistically justified limits to control the connectivity Leakage. This is an extrapolation to complex domain from the Graphical LASSO real domain theory of (Jankova and Van De Geer, 2018), that we validate in simulations. It also holds for the Hermitian Graphical LASSO ($\Pi = \|\cdot\|_1$), with fixed value of the regularization parameter $\alpha_t = \sqrt{m \log(q)}$ with $m \gg q$. See section J of SI.

$$(\widehat{\boldsymbol{\Theta}}_{\mathbf{u}})^{(k+1)}_{unb}(\nu) = 2\widehat{\boldsymbol{\Theta}}_{\mathbf{u}}^{(k+1)}(\nu) - \widehat{\boldsymbol{\Theta}}_{\mathbf{u}}^{(k+1)}(\nu) \widehat{\boldsymbol{\Psi}}_{\mathbf{u}}^{(k)}(\nu) \widehat{\boldsymbol{\Theta}}_{\mathbf{u}}^{(k+1)}(\nu) \quad (10)$$

For complex variable this limit is determined by Rayleigh tendency, in contrast to the Chi-Squared tendency for real variable, i.e. consequence of Jankova and Van De Geer (JVDG) theory. We implemented along other priors for the H-HGGM: based on Naïve (prior free) $\Pi = 0$ and Ridge $\Pi = \|\cdot\|_2$ model. The Naïve case is precisely VARETA model: this is an extension of the LORETA (Pascual-Marqui et al., 1994) with actual statistical fundament. Comparing these models in multiple scenarios of leakage demonstrates the robustness of the HIGGS LASSO.

3 Results and Discussion

We validate HIGGS 4 steps: 1-Statistical properties of the Hermitian Graphical LASSO: Lemmas 2-5, JVDG unbiasing formula (10) and Rayleigh correction. 2-Comparison of HIGGS models (Naïve, Ridge and LASSO penalization) against eLORETA and LCMV postprocessing Hermitian LASSO GGM, for two different Head Models: ideal EEG Lead Field (without the effect of volume conduction) and realistic SPM Human Lead Field. 3- SSVEP analysis with HIGGS (Naïve, Ridge and LASSO). 4-ECOG/EEG confirmatory study of LASSO HIGGS.

Rayleigh statistic of Hermitian Graphical LASSO

We generate 100 PC matrices (size 60x60), with block sparsity structure, and its corresponding empirical covariances for 600 samples of a Hermitian Gaussian generator ($m \gg q$).

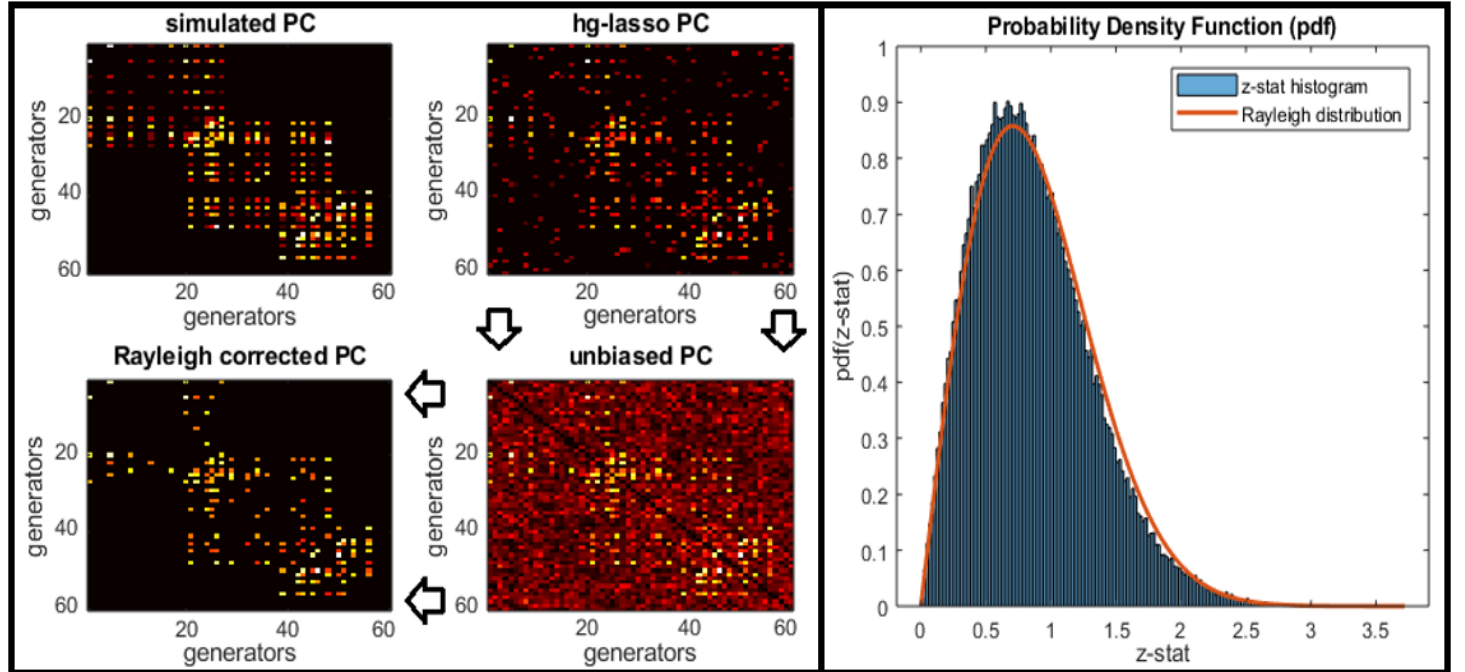


Figure 1: Experiment to evaluate JVDG conditions and statistical goodness of the proposed Hermitian Graphical LASSO (hg-lasso) solution. Top row: in “hot” colormap the typical simulated PC and its estimators, “hg-lasso” solution, “unbiased PC” derived from applying to the former unbiasing operation (10), thresholded unbiased PC (Rayleigh corrected PC). Bottom row: histogram of the z-statistic computed across the 100 trials for null hypothesis cases.

For each trial we compute the Hermitian Graphical LASSO solution (hgmm-lasso PC) and the unbiased statistic proposed by JVDG theory (unbiased PC). From the latter we remove the values under threshold: obtained from the limit value of the Rayleigh distribution (Rayleigh corrected PC).

Figure 1 shows the retrieved sparsity pattern for a typical trial (upper row left), the likelihood evolution with iterations for all trials and for each of the models (upper row right) and histograms with the z-statistic at the null hypothesis subspace (bottom row). Computing the z-statistic was done by scaling the unbiased PC using JVDG theoretical variances.

With Rayleigh threshold, from the originally dense unbiased PC, we obtain an improved sparse result in comparison to the hg-lasso PC, as it is shown in the bidimensional maps of Figure 1. The Hermitian Graphical LASSO shows a robust convergence pattern for any trial, according, see in SI section L the likelihood evolution for all simulations and real data. to the plots of the likelihood in Figure 1. The z-statistic histogram reflects the high coincidence with the theoretical Rayleigh probability density function.

These results demonstrate the Hermitian Graphical LASSO consistency to JVDG theory. The Rayleigh tendency of the unbiased PC absolute values is a natural extension of the real case Chi-Square tendency in the Real case. Furthermore, this analysis validates the solution given in Lemmas 2-5. The complexity of the proposed solution is bounded by the matrix square root of Formula (19): this is an optimal procedure in sight of GGM theory.

HIGGS robustness under volume conductance

We recreate EEG simulations considering two different Lead Field models: pseudo-LF and realistic human-LF, see Figure 2 top row. The pseudo-LF was defined upon two concentric circles: a pseudo-cortex and pseudo-scalp of bidimensional geometry. A basic electrostatic rule was implemented to construct the projected fields, from normally oriented pseudo-cortical dipoles to 30 homogeneously distributed pseudo-scalp sensors. The human-LF was computed for a healthy subject T1 image, with SPM Boundary Element Method (BEM), from normally oriented cortical dipoles to 30 sensors in the 10-20 extended system.

We simulated distributed activity on approximately 20 generators, following similar procedure as with the previous simulation study. The gaussian engine samples were projected to the sensor space via the LF of either pseudo and realistic head models. Additionally, we used a binarized SPC for consistency to ROC performance analysis, i.e. binary

classification measures. We incorporated 7 dB noise at both and sensor and generator space. The operating principle of the simulation was taking the pseudo-cortical sources to a random assortment that spanned homogeneously all long the human cortex (selecting one generator for area and avoiding deeper regions). The differences in performance between the pseudo and human cortical assortment are used to demonstrate the major EEG shortcoming: volume conduction distortion of connectivity.

As Figure 2 (bottom row) shows, the reconstructed SPC deteriorates dramatically when moving from the ideal to realistic case. The HIGGS model with LASSO penalization was the most robust to volume conduction effect, when compared to Ridge and Naïve (VARETA) estimators and the Hermitian Graphical LASSO postprocessing of either eLORETA or LCMV. The simulation conditions isolate this effect from the possible distortion of source localization: we assumed knowledge about the active sources.

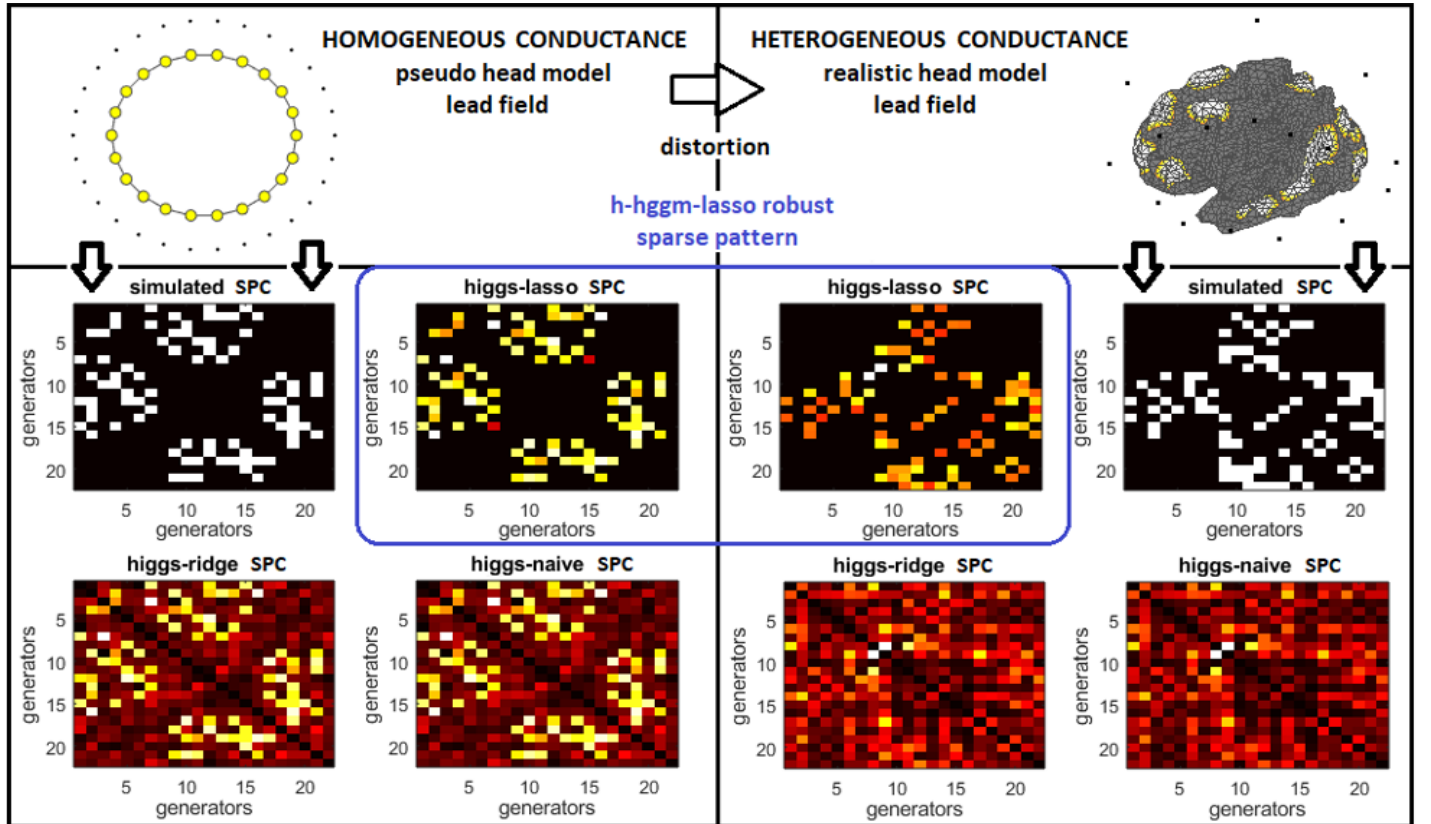


Figure 2: Experiment to evaluate the volume conductance effect. We use first a pseudo lead field with no volume conductance distortion (left) and second a realistic one that has it (right). The former was defined through a purely electrostatic rule: projecting the inner circle (pseudo cortex) dipolar elements onto the outer circle (pseudo cortex) sensor potential (top row left). The latter was computed by SPM software over three layers (cortex, skull and scalp): inhomogeneous conductance model extracted from a healthy human T1 image (top row right). The activity of approximately 20 sources was defined given 600 samples from Hermitian random Gaussian generator, with 100 random binary SPCs of which a single trial is shown. Then, for either model the activity was projected to the sensor space and corrupted with noise (at source and sensor level). See “hot” colormaps of the simulated and estimated SPC in bottom row.

Table 1: Measures of binary classification in connectivity: global AUC and partial measures computed for the optimal ROC threshold (SENS, SPEC, PREC and RECALL). We evaluate the connectivity retrieved with the proposed HIGGS penalty models (LASSO, Ridge and Naive) and with the Hermitian Graphical LASSO postprocessing of eLORETA and LCMV source cross-spectra.

Measures/ Model	AUC		SENS		SPEC		PREC		RECALL	
	pseudo	realistic								
higgs-lasso	100+/-0	84+/-6	100+/-1	69+/-12	100+/-0	99+/-1	100+/-0	91+/-6	100+/-0	78+/-10
higgs-ridge	100+/-0	89+/-3	100+/-0	61+/-24	100+/-0	92+/-4	100+/-0	64+/-10	100+/-0	60+/-16
higgs-naive	100+/-0	86+/-4	100+/-0	43+/-29	100+/-0	94+/-5	100+/-0	62+/-11	100+/-0	50+/-18
eloreta	55+/-6	51+/-1	11+/-11	2+/-2	100+/-0	100+/-0	95+/-15	72+/-24	23+/-17	27+/-22
lcmv	50+/-1	51+/-2	0+/-1	1+/-3	100+/-0	100+/-0	58+/-18	60+/-19	43+/-16	39+/-19

The binary classification performance across 100 simulation trials confirms what we illustrated in Figure 1, see Table 1. For the ideal case perfect classification was achieved, as shown by the ROC derived measures: AUC (total area under curve), SENS (sensitivity), SPEC (specificity), PREC (precision) and RECALL (F1 measure). Strong measures like PREC and RECAL evidence that, the large number of false positives, for Ridge and Naïve estimates situated under optimal ROC threshold in all cases (trials). The Rayleigh threshold of the maps estimated with LASSO model were in total correspondence with (not higher than) the optimal binary classification thresholds, due to the absence of false negative estimated values in the ideal case. That is the reason of its robustness under the volume conduction effect (realistic Lead Field).

Neural connectivity in human SSVEP with HIGGS

We extract the cortical connectivity by the analysis of the sources are involved in processing a light flickering at 4Hz stimulation frequency, i.e. Steady State Visual Evoked Potential (Bayram et al., 2011; Duru et al., 2011). This constitutes an advantageous experimental set up for demonstrating the application of our formalism. Cortical generators involved are expected to have multiple harmonic response of the input frequency (Müller-Putz et al., 2005), see Figure 3 top row-left.

Either harmonic represents the brain response caused by the nonlinear neural response in processing the stimulus. They carry on common signature of source activity and connectivity. Indeed, all harmonics can be regarded as replicas of the slowest harmonic under analysis: the phase shift between them is an “entire number” times 2π (full phase shift). Meanwhile analyzing the main harmonic only would rule out a large amount of information that is encoded by secondary harmonics.

For every experimental condition (flickering frequency) a single section was recorded. The aligned task segments spanned over 133 seconds approximately. The Fourier analysis with an acceptable frequency resolution (0.22Hz) reported 29 time segments. This sample number is insufficient for cross-spectral estimation, in relation to number of sensors (30 in total). To sort this, we consider the band limited cross-spectra: for a narrow band of frequency components adjacent to three central harmonics. The band limited cross-spectra operates under the restriction that all the frequency components have a unique cortical and connectivity signature. This is equivalent to consider analogous time domain LSSM for the dynamical

regime of the band filtered signal. This reported a sample size of several hundred ($m = 435$) in computing the band limited cross-spectra.

To determine the source response to the stimulus (target) we use a special implementation of the Elastic Net Structured Sparse Bayesian Learning (ENET-SSBL) (Paz-Linares et al., 2017). This implementation uses similar assumptions to HIGGS but with diagonal SPC structure. It allows to screen out the active sources by thresholding the posterior distribution statistic: ratio of the posterior mean and posterior variances, see technical details in section K of SI. The ENET-SSBL statistic reveals target areas that extended over the Occipital (OL), Temporal (TL) and Frontal (FL) Lobe at both hemispheres, see Figure 4 (top row right). Previous studies with fMRI BOLD evoked responses evidenced participation of OL (spatially encoding the stimulus) and its functional correlate with the higher level FL processing (Srinivasan et al., 2007).

Electrophysiology supports this fact, but it also detaches the TL mediation in OL \leftrightarrow FL communication. The spatio temporal analysis Visual Evoked Potentials (VEP) have pointed out that FL activations are preceded by earlier and stronger TL activations. Something that was verified with two different SSBL methods: Elastic Net and Elitist LASSO (Paz-Linares et al., 2017). Also, in contradistinction with the results provided by other classical (Tikhonov Regularization) methods (Vega-Hernández et al., 2008). But in high correspondence with neurophysiological information (Boner and Price, 2013). The information flow at sensor space determined with different functional connectivity metrics is also in agreement with this (Miskovic and Keil, 2015). In this sense other studies fail in neglecting the TL participations (Li et al., 2015).

HIGGS connectivity was computed for the most actively ranked generators across the target areas: according to the activity level up to 10 per area were selected. Those were the OL, TL and FL of both hemispheres: Left (L) and Right (R). See in Figure 4 second row the node wise connectivity (SPC) maps, and the qualitatively different results of the three penalization models (LASSO, Ridge and Naive). The lower performance methods eLORETA and LCMV were excluded.

Roughly, the LASSO model exhibited the higher sparsity level and relevancy of the estimates. Ridge and naïve estimation were biased to a single connectivity block. Even when ridge performed much better, most of the connections were smaller and blurred. Nevertheless, all models revealed that the +larger connectivity was OL-L \leftrightarrow OL-R.

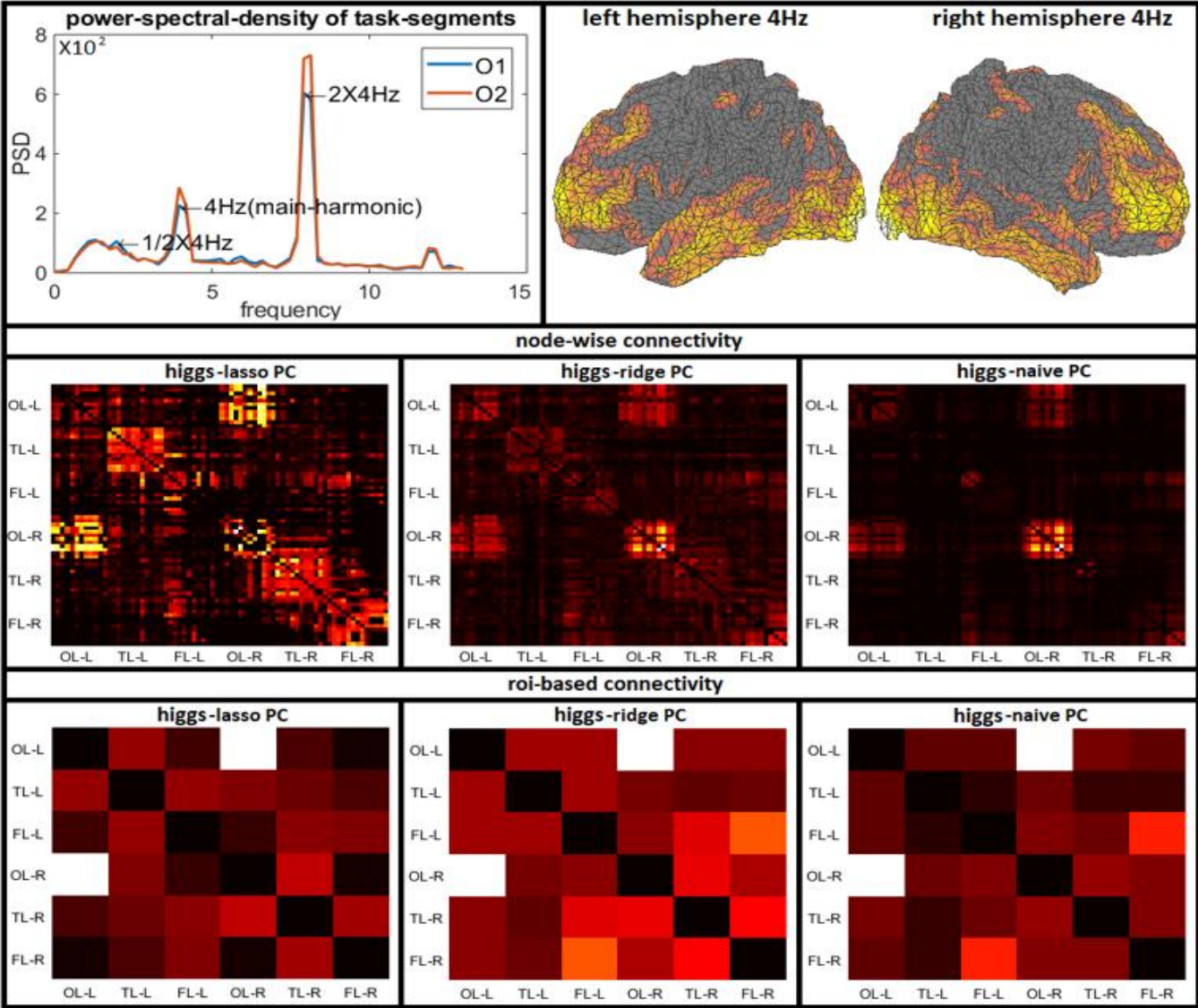


Figure 3: Connectivity analysis in the Steady State Visual Evoked Potential (4Hz stimulation frequency) from a healthy subject. The typical harmonic responses to stimulus of Occipital sensors ($O1$ and $O2$) are shown in top row left. The target areas of the stimulus, reconstructed with ENET-SSBL at the three main harmonics, extend over (top row right) the Occipital, Temporal and Frontal Lobes at both hemispheres. Second row shows the connectivity estimated with the three penalty models in block matrix plots, in hierarchical (functional) order of the target areas (higher levels go down in the plot) and hemispherical organization (left hemisphere in the superior part). The estimation was restricted to the 10 better ranked active generators across the target areas to preserve JVDG condition ($m \gg q$). The roi-based average connectivity analysis (third row) reveals the quantitatively different pathways retrieved with the three models (lasso, ridge and naive).

This was expected since the same information is being processed by the visual cortex at both hemispheres. To interpret the information flow between areas we analyze the average connectivity between regions of interest (ROIs), see Figure 4 third row. LASSO model connectivity was stronger for the $OL \leftrightarrow TL \leftrightarrow FL$ hemispheric pathway. The neurophysiological interpretation of this pattern relies on the mediation by TL in $OL \leftrightarrow FL$ communication. Ridge and naïve models reinforced also the $OL \leftrightarrow FL$ hemispheric pathway due to its sensitivity to Leakage (this has been pinpointed as crosstalk). LASSO model also selected the interhemispheric pathway $OL-R \leftrightarrow TL-L$ and $TL-R \leftrightarrow FL-L$, something more in

correspondence with previous studies on sensor space connectivity of SSVEP (Yan and Gao, 2011; Zhang et al., 2015). Meanwhile Ridge and Naïve model reinforced totally different interhemispheric paths due to Leakage effect. That was also present between frontal areas: it has been demonstrated that not the $FL-L \leftrightarrow FL-R$ but $OL \leftrightarrow FL$ pathway carries on the mayor information flow (Li et al., 2015). In fact, that was the second highest connectivity guessed by Ridge and Naïve models. For LASSO model estimation it was tremendously reduced, at a level that reflects some physiologically plausible statistical dependency.

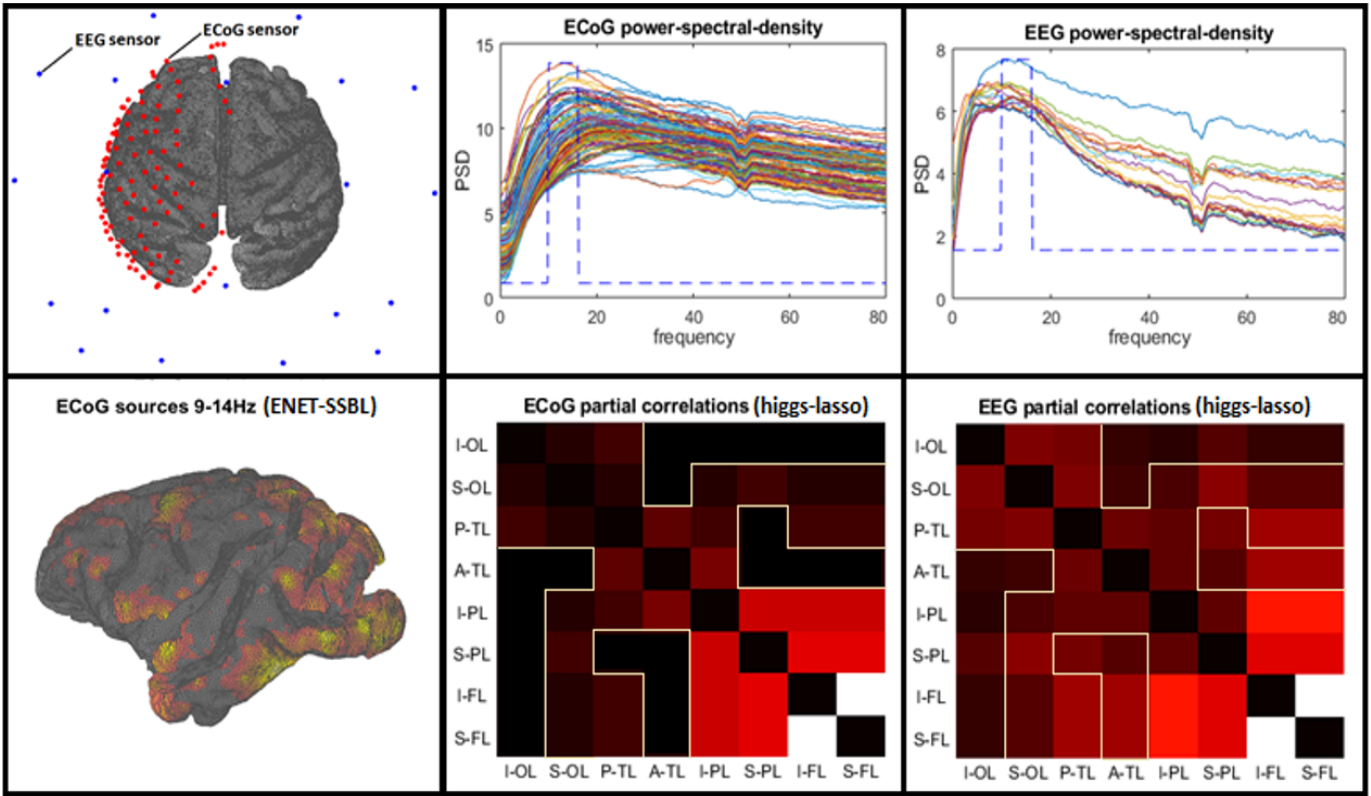


Figure 4: Connectivity analysis in Resting State EEG/ECoG recordings from a healthy monkey. Top row: distribution of sensors relative to the monkey's cortical surface (right) for the ECoG (red) and the EEG (blue), and power spectral density of ECoG (middle) and EEG (right). ENET-SSBL reconstructed sources for the ECoG alpha band (9-14Hz) left hemisphere (bottom row-left). The active areas extend over the Occipital, Temporal, Parietal and Frontal Lobes. Roi-based connectivity retrieved with the higgs-lasso in ECoG (middle) and EEG (right). The minimum value of all connectivity distances was achieved by the HIGGS-LASSO, the largest value corresponded to the Hermitian Graphical LASSO postprocessing of the LCMV, see Table 2.

Concurrent study in EEG/ECoG with HIGGS

For a confirmatory study of HIGGS connectivity in EEG we use the concurrent comparison against a higher resolution technique: electrocorticography (ECoG). The EEG/ECoG signals were recorded simultaneously for the brain's resting state activity of a healthy monkey. During the experimental session the monkey was awake, blindfolded and constrained to sitting position (Nagasaki et al., 2011).

The monkey sensor's layout consisted on 128 ECoG sensors placed surgically on the cortical surface at the left hemisphere and 20 EEG scalp sensors. See in Figure 4 (top row-left) its relative distribution regarding the monkey's cortical surface. The ECoG and EEG Lead Fields were obtained from a head conductivity model, through BEM computations in SimBio, using the monkey's individual T1 MRI segmentation. The head model included 5 conductivity compartments: cortex, ECoG silicon layer, inner skull, outer skull and scalp.

Both EEG and ECoG were synchronized to the trigger signal and down-sampled to 1000 Hz, keeping in total 2 minutes of recordings. The artifact removal procedure included linear detrending with L1TF package, average DC subtraction and 50

Hz notch filtering. The spectral analysis of Figure 4 (top row), of both ECoG (middle) and EEG (right) signals, reveals a larger power spectral density within the band (9-14 Hz). This can be associated to the monkey's alpha rhythm.

Previous studies were limited to the analysis of PL \leftrightarrow FL interactions at ECoG sensor space (Papadopoulou et al., 2011). Here we compute the alpha band cortical signature at left hemisphere (Figure 3 bottom row-left) using ENET-SSBL. This large scale network has strong correspondence with the pattern at the ECoG space (Qing Wang et al., 2019). The larger Occipital Lobe (OL) activations were accompanied with secondary activations extended over the Temporal (TL), Parietal (PL) and Frontal (FL) Lobes at the left (L) hemisphere.

For all neural connectivity models, we compared the distortion of EEG regarding ECoG with several matrix distances, see Table 2. The HIGGS with LASSO model was the less affected by volume conduction according to all distances, see section L of SI. All HIGGS models were less distorted than eLORETA-GGM and LCMV-GGM. The later was the most distorted.

Table 2: Distances between EEG and ECoG connectivity: retrieved with the proposed HIGGS penalty models (LASSO, Ridge and Naive) and with the Hermitian Graphical LASSO postprocessing of eLORETA and LCMV source cross-spectra.

Model/ Measures	higgs-lasso	higgs-ridge	higgs-naive	eloreta	lcmv
Alpha-Diversity	0,0049	0,0080	0,2392	0,9256	1,6366
Kullback-Leibel	0,0404	0,0519	0,2737	0,4263	0,5380
Linkeage-Desequilibrium	0,0202	0,0259	0,1361	0,2131	0,2690
Log-Euclidian	0,0033	0,0054	0,1488	0,3633	0,5788
Optimal-Transport	0,0288	0,0369	0,2073	0,3012	0,3797
Riemann	0,0572	0,0733	0,3857	0,6027	0,7608

The ECoG roi-based connectivity map with HIGGS LASSO model (Figure 4 bottom row-middle) reveals similarities to the one extracted with the minimal EEG layout (Figure 4 bottom row-right). The envelope of the pathways in figure 4 bottom row (non-zero values of the PC) highlights these similarities and leakage also. The effect of leakage on the EEG, due to the three additional tissue layers (inner skull, outer skull and scalp), is represented by the overestimated PC values laying out of the envelope. Maximum PC values were found for the I-FL \leftrightarrow S-FL interaction. This is physically plausible for the resting state, in contrast to the findings of human SSVEP biased by the visual stimulation. Due to the information flow from larger OL, TL and PL that converges in the less extended active area of the FL, reinforcing the FL intrinsic communication. The gradual increment of the PC's amplitude with the hierarchy also responded to this physical fact.

4 Materials and Methods

An approximated expression to the T2L at the k -th EM step is given through ELL $Q(\Omega, \Omega^{(k)})$. The symbol Ω summarizes the hyperparameters for a single frequency component ν , i.e. $\Omega = \{\Theta_{\xi\xi}, \Theta_u(\nu)\}$. Formally, the model spans the entire frequency domain, for the sake of simplicity we hereinafter remove ν from the formulation.

$$p(\mathbf{V}|\Omega) \approx \exp(-Q(\Omega, \Omega^{(k)})) \quad (11)$$

$$Q(\Omega, \Omega^{(k)}) = \int_{\mathbb{Z}^q} p(\mathbf{V}, \mathbf{I}|\Omega) p(\mathbf{I}|\Omega^{(k)}) d\mathbf{I} \quad (12)$$

Lemma 1 (bimodal log-Wishart form of the ELL)

For the model in (3) and (4) the ELL $Q(\Omega, \Omega^{(k)})$ admits a decomposition into two sequentially independent factors of log-Wishart form, of the observation residuals and source:

$$Q(\Omega, \Omega^{(k)}) = m \log |\Theta_{\xi\xi}| - m \text{tr}(\Theta_{\xi\xi} \tilde{\Psi}_{\xi\xi}^{(k)}) - m \log |\Theta_u| - m \text{tr}(\Theta_u \tilde{\Psi}_u^{(k)}) \quad (13)$$

Lemma 2 (CV-LQA of AML corollary)

The measurable space with normalized Gibbs density (pdf) $p(\Theta) \propto \exp(\Pi(\mathbf{A} \odot \Theta)|\alpha)$, with penalization function of the

complex LASSO model ($\Pi = \|\cdot\|_1$), admits a hierarchical (conditional) representation of measurable spaces product: One of the conditional expectation $\Theta|\Gamma$ with (unnormalized) Gaussian density and the random variable Γ with (normalized) Gamma pdf.

$$\Theta|\Gamma \sim \prod_{ij=1}^q N_1(|\Theta_{ij}| | 0, \Gamma_{ij}^2 / m) \quad (14)$$

$$\Gamma \sim \prod_{ij}^q Ga(\Gamma_{ij}^2 | 1, m \alpha^2 A_{ij}^2 / 2) \quad (15)$$

Lemma 3 (concavity of the CV-LQA)

The target function $\mathcal{L}(\Theta, \Gamma)$ (minus-log-density of the measurable product space $\Theta \times \Gamma$) is strictly concave on the intercept of the region of positive definiteness of its arguments $\{\Theta \geq 0, \Gamma \geq 0\}$ and the region comprehended by the set of inequalities:

$$\{3m\Theta_{ij}\Theta_{ij}^\dagger - \Gamma_{ij}^2 + m\alpha^2 A_{ij}^2 \Gamma_{ij}^4 \geq 0\}_{ij=1}^q \quad (16)$$

Then, $\mathcal{L}(\Theta, \Gamma)$ has a minimum within this region given by the intercept of the system of equations:

$$-\Theta^{-1} + \Psi + \Theta \odot \Gamma^2 = \mathbf{0}_q \quad (17)$$

$$\{-m\Theta_{ij}\Theta_{ij}^\dagger + \Gamma_{ij}^2 + m\alpha^2 A_{ij}^2 \Gamma_{ij}^4 = 0\}_{ij=1}^q \quad (18)$$

Lemma 4 (standardization of the Wishart distribution)

Let Ψ and $\tilde{\Psi}$ (referred as "Standard") be $(q \times q)$ Hermitian random matrices with complex Wishart density of m degrees of freedom and positive definite hermitic scale matrix Σ and $\tilde{\Sigma} = (\Sigma^{-1} \odot \Gamma)^{-1}$ (Γ is a $(q \times q)$ positive definite matrix of positive weights), i.e. $\Psi \sim W_q^{\mathbb{C}}(\Psi | \Sigma, m)$ and $\tilde{\Psi} \sim W_q^{\mathbb{C}}(\tilde{\Psi} | \tilde{\Sigma}, m)$. Then for Φ (called "Version") defined by the relationship to the Standard $\tilde{\Psi} = (\Phi^{-1} \odot \Gamma)^{-1}$ (or $\Phi = (\tilde{\Psi}^{-1} \odot \Gamma)^{-1}$) (called "Unstandardization" of $\tilde{\Psi}$), it can be verified:

a) All entries $(\Phi^{-1})_{ij}$ of the Version inverse Φ^{-1} keep the Wishart density independency property: they are stochastically independent among them and from the set $\{\Phi_{i'j'}\}_{(i',j') \neq (i,j)}$.

b) All entries $(\Phi^{-1})_{ij}$ of the Version inverse Φ^{-1} keep the Wishart marginal density: complex Inverse Gamma with parameter of shape $(m - q + 1)$ and scale $(\Sigma^{-1})_{ij}$.

Lemma 5 (local graphical Ridge estimator)

Given the equivalence of Lemma 4 the graphical LASSO admits a graphical Ridge local representation: the pair given by the Likelihood $W_q^C(\tilde{\Psi} | m^{-1}\tilde{\Theta}^{-1}, m)$ and prior $\exp(\tilde{\Theta} | m)$. Furthermore, the graphical Ridge estimator is the solution of the Riccati matrix equation: $\tilde{\Theta}^2 + \tilde{\Psi}\tilde{\Theta} - \mathbf{I}_q = \mathbf{0}_q$. That is the unique solution that shares the eigenspace with $\tilde{\Psi}$, which is also positive definite and hermitic, expressed by the following matrix square root formula:

$$\tilde{\Theta} = -\frac{1}{2}\tilde{\Psi} + \frac{1}{2}\sqrt{\tilde{\Psi}^2 + 4\lambda\mathbf{I}_q} \quad (19)$$

5 Conclusions

Brain Connectivity methods are currently flawed due their lack of interpretability in terms of Systems Theory and Bayesian Formalism. We proposed a new procedure that fills this gap: modelling functional connectivity by the Partial Correlations of a Hidden Gaussian Graphical State-Model (HIGGS). Such quantity (SPC) is a bi-univocal representation of the neural system's Directed Transfer Function. Its inference is leveraged by two combined theoretical elements: 1-the marginal gaussian graphical models of residuals and states, derived from the Type II Likelihood approximation (Lemma 1). 2 - the solution of the hermitian graphical LASSO (Lemma 2-5), alongside its statistical guarantees.

Doing so provided the link of two statistical modelling branches: Linear State Space Models and Gaussian Graphical Models. This strode for the solution to the Leakage problem: a fundamental limitation for M/EEG source space connectivity. It also constitutes a natural extension to the theory of Hidden Markov Models.

The computational cost of our solution to the Hermitian Graphical LASSO, also extendible to real variable, is bound by the matrix square root operation. It is rendered a prospective approach for its entire field of applications. The accuracy of the implementation proposed here was tested in terms of the theoretically expected statistical tendency: the Rayleigh distribution (or complex circular extension of Jankova and Van Der Geer theoretical distribution). This is precisely the way to undertake Leakage control, with enough statistical guarantees, iteratively into the hidden hermitian gaussian graphical model scheme.

The higher performance of HIGGS, in comparison to the connectivity postprocessing of eLORETA and LCMV, demonstrated the necessity to consider Systems Theory and

Bayesian Information Theory to assess connectivity. This is with and without the effect of volume conduction heterogeneities. The HIGGS LASSO model was the most robust in any case, as we illustrated with typical reconstructed connectivity maps and robust binary classification measures (precision and recall). Different regularization models suffered substantial distortion under volume conduction effect. As it was the case with VARETA model: Bayesian generalization of the LORETA. Also, the case of the hidden Hermitian Graphical Ridge: an efficient alternative to LASSO model that we tested here. Either hidden models (LASSO and Ridge) represent a potential assessment to state space inference in multiple scenarios (beyond M/EEG source connectivity).

We were able to extract a meaningful cortical connectivity pattern with the LASSO model in steady state visual evoked potentials, recorded with EEG at fixed light flicker (stimulus) frequency. We regard this experiment as the ideal scenario to validate frequency domain methods: in this case to explore the Leakage effect on the retrieved cortical connectivity at a single response frequency (in relation to the stimulus).

The connectivity study spanned across cortical areas that were first screened with a cross-spectral extension of ENET-SSBL, also a sparse source activity (not connectivity) method with statistical guarantees. Previous studies have proven these areas have a strong involvement in visual processing: a large scale network including the Occipital, Temporal and Frontal Lobes of both hemispheres.

Unfortunately, a large scale analysis as such has not been ever reported in similar experiments and at source space: for fMRI studies only Occipital \leftrightarrow Frontal connection patterns were analyzed and for EEG it was take out only limited to Occipital intrinsic connections. Relevantly, previous studies of connectivity at sensor space have considered a large scale network, which agree with the cortical pathway revealed the sensor space connectivity analysis. These are not interpretable in terms of cortical connections, what they provide at most is a rough idea about the interareal information flow: something we use here as external verification.

These sensor space studies were corrupted by the effect of Leakage: the estimated sensor level network is denser than the original one at neural level. In part due to volume conduction but also because of the mixture of activity projected at the scalp.

The source space methods here used for comparison purpose (Hermitian Graphical Ridge and VARETA), were also sensitive to Leakage and in contradiction with LASSO results. Great differences featured the recovered Occipital \leftrightarrow Frontal pathway Frontal \leftrightarrow Frontal interhemispheric communication. This is a typical example of Leakage, as critical reports point out, which provides an ideal scenario for the verification of the proposed theory of the hidden graphical LASSO.

Our results with the human SSVEP in EEG were supported with the multimodal (EEG/ECoG) comparison in monkey. The connectivity patterns revealed by a minimal EEG array

(influenced by multiple tissue layers) were in correspondence with the ECoG results.

This connectivity model will be further studied: in Human Connectome Project data-bases and on simulations to test both activation and connectivity Leakage. Something that would also involve testing its behavior along with that of the ENET-SSBL source screening. We offer freely an open source software package to reproduce automatically all the results presented in this manuscript: do it so by executing the script "h_hgmm_simpack.m" from the following GitHub link:

https://github.com/CCC-members/MEEG_Source_Connectivity_SoftPack

An independent package is also offered for the general purpose of analyzing M/EEG databases, along with an example to help with the format of the inputting data. Do it so by executing the script "BC-VARETA.m" from the GitHub link:

https://github.com/CCC-members/BC-VARETA_Toolbox

6 Acknowledgements

This study was funded by the Grant No. 61673090 from the National Nature Science Foundation of China.

References

- [1] Andrews, D.F. and Mallows, C.L., 1974. Scale mixtures of normal distributions. *Journal of the Royal Statistical Society. Series B (Methodological)*, pp.99-102.
<https://www.jstor.org/stable/2984774>
- [2] Anzolin, A., Presti, P., Van De Steen, F., Astolfi, L., Haufe, S. and Marinazzo, D., 2019. Quantifying the effect of demixing approaches on directed connectivity estimated between reconstructed EEG sources. *Brain topography*, pp.1-20.
<https://doi.org/10.1007/s10548-019-00705-z>
- [3] Bayram, A., Bayraktaroglu, Z., Karahan, E., Erdogan, B., Bilgic, B., Özker, M., Kasikci, I., Duru, A.D., Ademoglu, A., Öztürk, C. and Arikan, K., 2011. Simultaneous EEG/fMRI analysis of the resonance phenomena in steady-state visual evoked responses. *Clinical EEG and neuroscience*, 42(2), pp.98-106.
<https://doi.org/10.1177/155005941104200210>
- [4] Biscay, R.J., Bosch-Bayard, J.F. and Pascual-Marqui, R.D., 2018. Unmixing EEG Inverse Solutions Based on Brain Segmentation. *Frontiers in neuroscience*, 12, p.325.
<https://doi.org/10.3389/fnins.2018.00325>
- [5] Bosch-Bayard, J., Valdes-Sosa, P., Virués-Alba, T., Aubert-Vazquez, E., John, E.R., Harmony, T., Riera-Díaz, J. and Trujillo-Barreto, N., 2001. 3D statistical parametric mapping of EEG source spectra by means of variable resolution electromagnetic tomography (VARETA). *Clinical Electroencephalography*, 32(2), pp.47-61.
<https://doi.org/10.1177/155005940103200203>
- [6] Bonner, M. F., and Price, A. R., 2013. Where is the anterior temporal lobe and what does it do? *Journal of Neurosciences*, 33, pp.4213-4215.
<https://doi.org/10.1523/JNEUROSCI.0041-13.2013>
- [7] Baccalá, L.A. and Sameshima, K., 2001. Partial directed coherence: a new concept in neural structure determination. *Biological cybernetics*, 84(6), pp.463-474.
<https://doi.org/10.1007/PL000079>
- [8] Brookes, M.J., Woolrich, M., Luckhoo, H., Price, D., Hale, J.R., Stephenson, M.C., Barnes, G.R., Smith, S.M. and Morris, P.G., 2011. Investigating the electrophysiological basis of resting state networks using magnetoencephalography. *Proceedings of the National Academy of Sciences*, 108(40), pp.16783-16788.
<https://doi.org/10.1073/pnas.1112685108>
- [9] Dempster, A.P., Laird, N.M. and Rubin, D.B., 1977. Maximum likelihood from incomplete data via the EM algorithm. *Journal of the royal statistical society. Series B (methodological)*, pp.1-38.
<https://www.jstor.org/stable/2984875>
- [10] Duru, A.D., Erdogan, S.B., Kasikci, I., Bayram, A., Ademoglu, A. and Demiralp, T., 2011, August. Investigation of the neuronal efficacy and EEG source power under steady-state visual stimulation. In 2011 Annual International Conference of the IEEE Engineering in Medicine and Biology Society (pp. 6576-6579). IEEE.
<https://doi.org/10.1109/IEMBS.2011.6091622>
- [11] Engel, A.K., Fries, P. and Singer, W., 2001. Dynamic predictions: oscillations and synchrony in top-down processing. *Nature Reviews Neuroscience*, 2(10), p.704.
<https://doi.org/10.1038/35094565>
- [12] Friston, K., Harrison, L., Daunizeau, J., Kiebel, S., Phillips, C., Trujillo-Barreto, N., Henson, R., Flandin, G. and Mattout, J., 2008. Multiple sparse priors for the M/EEG inverse problem. *NeuroImage*, 39(3), pp.1104-1120.
<https://doi.org/10.1016/j.neuroimage.2007.09.048>
- [13] Friedman, J., Hastie, T. and Tibshirani, R., 2008. Sparse inverse covariance estimation with the graphical lasso. *Biostatistics*, 9(3), pp.432-441.
<https://doi.org/10.1093/biostatistics/kxm045>
- [14] Faes, L. and Nollo, G., 2011. Multivariate frequency domain analysis of causal interactions in physiological time series. In *Biomedical Engineering, Trends in Electronics, Communications and Software*. InTech.
<https://doi.org/10.5772/13065>
- [15] Faes, L., Erla, S. and Nollo, G., 2012. Measuring connectivity in linear multivariate processes: definitions, interpretation, and practical analysis. *Computational and mathematical methods in medicine*, 2012.

[16] <http://dx.doi.org/10.1155/2012/140513>
 [16] Jankova, J. and van de Geer, S., 2018. Inference in high-dimensional graphical models. arXiv preprint arXiv:1801.08512.
<https://arxiv.org/abs/1801.08512>

[17] Li, F., Tian, Y., Zhang, Y., Qiu, K., Tian, C., Jing, W., Liu, T., Xia, Y., Guo, D., Yao, D. and Xu, P., 2015. The enhanced information flow from visual cortex to frontal area facilitates SSVEP response: evidence from model-driven and data-driven causality analysis. *Scientific reports*, 5, p.14765.
<https://doi.org/10.1038/srep14765>

[18] Liu, C. and Rubin, D.B., 1994. The ECME algorithm: a simple extension of EM and ECM with faster monotone convergence. *Biometrika*, 81(4), pp.633-648.
<https://doi.org/10.1093/biomet/81.4.633>

[19] Lopes da Silva, F. 2013. EEG and MEG: Relevance to Neuroscience, *Neuron*, 80(5), pp.1112-1128,
<https://doi.org/10.1016/j.neuron>

[20] MacKay D J C. *Information Theory, Inference, and Learning Algorithms*. Cambridge University Press 2003.
<https://doi.org/10.2277/0521642981>

[21] Miskovic, V. and Keil, A., 2015. Reliability of event-related EEG functional connectivity during visual entrainment: Magnitude squared coherence and phase synchrony estimates. *Psychophysiology*, 52(1), pp.81-89.
<https://doi.org/10.1111/psyp.12287>

[22] Müller-Putz, G.R., Scherer, R., Brauneis, C. and Pfurtscheller, G., 2005. Steady-state visual evoked potential (SSVEP)-based communication: impact of harmonic frequency components. *Journal of neural engineering*, 2(4), p.123.
<https://doi.org/10.1088/1741-2560/2/4/008>

[23] Nagasaka, Y., Shimoda, K. and Fujii, N., 2011. Multidimensional recording (MDR) and data sharing: an ecological open research and educational platform for neuroscience. *PloS one*, 6(7), p.e22561.
<https://doi.org/10.1371/journal.pone.0022561>

[24] Papadopoulou, M., Friston, K. and Marinazzo, D., 2015. Estimating directed connectivity from cortical recordings and reconstructed sources. *Brain topography*, pp.1-12.
<https://doi.org/10.1007/s10548-015-0450-6>

[25] Pascual-Marqui, R.D., Michel, C.M. and Lehmann, D., 1994. Low resolution electromagnetic tomography: a new method for localizing electrical activity in the brain. *International Journal of psychophysiology*, 18(1), pp.49-65.
[https://doi.org/10.1016/0167-8760\(84\)90014-X](https://doi.org/10.1016/0167-8760(84)90014-X)

[26] Pascual-Marqui, R.D., Biscay, R.J., Bosch-Bayard, J., Faber, P., Kinoshita, T., Kochi, K., Milz, P., Nishida, K. and Yoshimura, M., 2017. Innovations orthogonalization: a solution to the major pitfalls of EEG/MEG" leakage correction". arXiv preprint arXiv:1708.05931.
<https://arxiv.org/abs/1708.05931>

[27] Pascual-Marqui, R.D., Pascual-Montano, A.D., Lehmann, D., Kochi, K., Esslen, M., Jancke, L., Anderer, P., Saletu, B., Tanaka, H., Hirata, K. and John, E.R., 2006. Exact low resolution brain electromagnetic tomography (eLORETA). *NeuroImage*, 31(Suppl 1).

[28] Paz-Linares, D., Vega-Hernandez, M., Rojas-Lopez, P.A., Valdes-Hernandez, P.A., Martinez-Montes, E. and Valdes-Sosa, P.A., 2017. Spatio temporal EEG source imaging with the hierarchical bayesian elastic net and elitist lasso models. *Frontiers in neuroscience*, 11, p.635.
<https://doi.org/10.3389/fnins.2017.00635>

[29] Rosenblatt, M., 1956. A central limit theorem and a strong mixing condition. *Proceedings of the National Academy of Sciences*, 42(1), pp.43-47.
<https://doi.org/10.1073/pnas.42.1.43>

[30] Schoukens, J., Pintelon, R. and Rolain, Y., 2004, June. Time domain identification, frequency domain identification. Equivalencies! Differences?. In *American Control Conference*, 2004. *Proceedings of the 2004* (Vol. 1, pp. 661-666). IEEE.
<https://doi.org/10.23919/ACC.2004.1383679>

[31] Srinivasan, R., Fornari, E., Knyazeva, M.G., Meuli, R. and Maeder, P., 2007. fMRI responses in medial frontal cortex that depend on the temporal frequency of visual input. *Experimental brain research*, 180(4), pp.677-691.
<https://doi.org/10.1007/s00221-007-0886-3>

[32] Srivastava, M.S., 1965. On the complex Wishart distribution. *The Annals of mathematical statistics*, 36(1), pp.313-315.
<https://www.jstor.org/stable/2238098>

[33] Valdés-Hernández, P.A., von Ellenrieder, N., Ojeda-Gonzalez, A., Kochen, S., Alemán-Gómez, Y., Muravchik, C. and Valdés-Sosa, P.A., 2009. Approximate average head models for EEG source imaging. *Journal of neuroscience methods*, 185(1), pp.125-132.
<https://doi.org/10.1016/j.jneumeth.2009.09.005>

[34] Van de Steen, F., Faes, L., Karahan, E., Songsiri, J., Valdes-Sosa, P.A. and Marinazzo, D., 2016. Critical comments on EEG sensor space dynamical connectivity analysis. *Brain topography*, pp.1-12.
<http://dx.doi.org/10.1007/s10548-016-0538-7>

[35] Van Veen, B. D., Van Drongelen, W., Yuchtman, M., & Suzuki, A. (1997). Localization of brain electrical activity via linearly constrained minimum variance spatial filtering. *IEEE Transactions on biomedical engineering*, 44(9), 867-880.
<https://doi.org/10.1109/10.623056>

[36] Varela, F., Lachaux, J.P., Rodriguez, E. and Martinerie, J., 2001. The brainweb: phase synchronization and large-scale integration. *Nature reviews neuroscience*, 2(4), p.229.
<https://doi.org/10.1038/35067550>

[37] Vega-Hernández, M., Martínez-Montes, E., Sánchez-Bornot, J.M., Lage-Castellanos, A. and Valdés-Sosa, P.A., 2008. Penalized least squares methods for solving the EEG inverse problem. *Statistica Sinica*, pp.1535-1551.
<https://www.jstor.org/stable/24308568>

[38] Von Bertalanffy, L., 1950. An outline of general system theory. *British Journal for the Philosophy of science*.
<https://doi.org/10.1093/bjps/1.2.134>

[39] Wipf, D. and Nagarajan, S., 2009. A unified Bayesian framework for MEG/EEG source imaging. *NeuroImage*, 44(3), pp.947-966.

[40] Yan, Z. and Gao, X., 2011. Functional connectivity analysis of steady-state visual evoked potentials. *Neuroscience letters*, 499(3), pp.199-203.
<https://doi.org/10.1016/j.neulet.2011.05.061>

[41] Yuan, G., Tan, H. and Zheng, W.S., 2017. A Coordinate-wise Optimization Algorithm for Sparse Inverse Covariance Selection. *arXiv preprint arXiv:1711.07038*.
<https://arxiv.org/abs/1711.07038>

[42] Zhang, Y., Guo, D., Cheng, K., Yao, D. and Xu, P., 2015. The graph theoretical analysis of the SSVEP harmonic response networks. *Cognitive neurodynamics*, 9(3), pp.305-315.
<https://doi.org/10.1007/s11571-015-9327-3>

SUPPLEMENTARY INFORMATION

Neural Connectivity with Hidden Gaussian Graphical State-Model

Deirel Paz-Linares ^{a,b,1}, Eduardo Gonzalez-Moreira ^{a,c,d,1}, Jorge Bosch-Bayard ^{a,d,e}, Ariosky Areces-Gonzalez ^{a,f},
 Maria L. Bringas-Vega ^{a,b} and Pedro A. Valdés-Sosa ^{a,b,2}

^a The Clinical Hospital of Chengdu Brain Science Institute, MOE Key Lab for Neuroinformatics, University of Electronic Science and Technology of China, Chengdu, China; ^b Cuban Neuroscience Center, La Habana, Cuba; ^c Centro de Investigaciones de la Informática, Universidad Central “Marta Abreu” de las Villas, Santa Clara, Cuba;

^d Unit of Neurodevelopment, Institute of Neurobiology, UNAM, Campus Juriquilla, Santiago de Querétaro, Querétaro, México; ^e Montreal Neurological Institute, Montreal, Canada; ^f Departamento de Matemática, Universidad de Pinar del Río, Pinar del Río, Cuba.

¹ contributed equally to this research ² senior and correspondence author

Pedro A. Valdés-Sosa

pedro.valdes@neuroinformatics-collaboratory.org

This PDF file includes:

Mathematical Notation (section A)

Nomenclature (section B)

Frequency Domain Transformation of the Linear State Space Model (section C)

Proof of Lemma 1: bimodal log-wishart form of the expected log-likelihood (section D)

Hyperparameter Posterior Analysis: maximization of the expected log-likelihood (section E)

Proof of Lemma 2: Complex Variable Local Quadratic Approximation of Andrews and Mallows Lemma (section F)

Proof of Lemma 3: Concavity of the Complex Variable Local Quadratic Approximation (section G)

Proof of Lemma 4: standardization of the Wishart distribution (section H)

Proof of Lemma 5: local graphical Ridge estimator (section I)

Connectivity estimator of the Local Quadratic Approximation (section J)

Cross-spectral formulation of the Elastic Net Structured Sparse Bayesian Learning (section K)

Model's statistical goodness (section L)

References for the Supplementary Information

A-Mathematical Notation

[A.1]	$\mathbf{x}, \mathbf{X}, \mathbb{X}$	The following symbols denote respectively a vector (bold italic lowercase) a matrix (bold capital) a set (double struck capital).
[A.2]	\mathbf{x}_m	Subscript indicating with lowercase script the m -th vector sample.
[A.3]	$\mathbf{X}_{ij}, (\mathbf{X})_{ij}, x_i, (x)_i$	Subscript indicating with lowercase the ij (i) element of a matrix \mathbf{X} (vector \mathbf{x}). Light captions denote matrix (vectors) elements.
[A.4]	$N_p(\mathbf{x} \mathbf{y}, \mathbf{Z})$	Normal distribution of a (p) size vector \mathbf{x} with mean \mathbf{y} and Covariance Matrix \mathbf{Z} .
[A.5]	$N_p^C(\mathbf{x} \mathbf{y}, \mathbf{Z})$	Circularly Symmetric Complex Normal distribution of a (p) size complex vector \mathbf{x} with complex mean \mathbf{y} and Complex Covariance Matrix \mathbf{Z} .
[A.6]	$exp(x y)$	Exponential distribution of the scalar x with parameter of shape y .
[A.7]	$Ga(x y, z)$	Gamma distribution of the scalar x with parameters of shape y and rate z .
[A.8]	$ \mathbf{X} $	Determinant of a matrix \mathbf{X} .
[A.9]	$tr(\mathbf{X})$	Trace of a matrix \mathbf{X} .
[A.10]	\mathbf{X}^{-1}	Inverse of a matrix \mathbf{X} .
[A.11]	\mathbf{X}^T	Transpose of a matrix \mathbf{X} .
[A.12]	\mathbf{X}^\dagger	Conjugate transpose of a matrix \mathbf{X} .
[A.13]	$\hat{\mathbf{X}}, \hat{\mathbf{x}}$	Estimator Parameters or Hyperparameters random matrix (\mathbf{X}) or vector (\mathbf{x}).
[A.14]	$\tilde{\mathbf{X}}$	Estimator of auxiliary magnitudes random matrix (\mathbf{X}), dependent on Parameters or Hyperparameters estimators.
[A.15]	$\hat{\mathbf{X}}^{(k)}, \tilde{\mathbf{X}}^{(k)}$	Updates at the k -th iteration of estimators.
[A.16]	$\sum_{m=1}^m$	Sum operator along index m .
[A.17]	$\prod_{m=1}^m$	Product operator along index m .
[A.18]	$p(\mathbf{X})$	Probability density function of a random variable \mathbf{X} .

[A.19]	$p(\mathbf{X} \mathbf{Y})$	Conditional probability density function of a random variable \mathbf{X} regarding the state of the variable \mathbf{Y} .
[A.20]	$p(\mathbf{X}, \mathbf{Y} \mathbf{Z})$	Conditional joint probability density function of random variables \mathbf{X} and \mathbf{Y} regarding the state of the variable \mathbf{Z} .
[A.21]	$\mathbf{X} \mathbf{Y} \sim p(\mathbf{X} \mathbf{Y})$	Indicates that the variable \mathbf{X} probability density function is conditioned to \mathbf{Y} .
[A.22]	$\ \mathbf{X}\ _{i,\mathbf{A}}, i = 1,2$	L1 or L2 norm of the matrix \mathbf{X} with weights or elementwise precisions defined by the mask matrix \mathbf{A} .
[A.23]	$\mathbf{I}_p, \mathbf{1}_p, \mathbf{0}_p$	Denotes respectively Identity, Ones and Ceros matrices of size p .
[A.24]	\odot, \oslash	Elementwise matrix product a division operators (Hadamard).
[A.28]	$\text{argmin}_{\mathbf{X}}\{f(\mathbf{X})\}$ or $\text{argmax}_{\mathbf{X}}\{f(\mathbf{X})\}$	Extreme values of the scalar function f , correspondingly minimum or maximum, in the argument \mathbf{X} .
[A.29]	$\text{zeros}_{\mathbf{X}}\{f(\mathbf{X})\}$	Zeros of the scalar function f in the argument \mathbf{X} .

B-Nomenclature

[B.1]	\mathbb{E}	Scalp Sensors (Electrodes) Space.
[B.2]	\mathbb{M}	Random Samples space.
[B.3]	\mathbb{G}	Discretized Gray Matter (Generators) Space.
[B.4]	p	Number of MEEG sensors at the scalp.
[B.5]	m	Number of data samples obtained from MEEG single frequency bin Fourier coefficients from a number (m) of segments.
[B.6]	q	Number of MEEG generators at the Cortex surface.
[B.7]	\mathbf{v}_m	Complex size MEEG data Fourier coefficients sample vector for a single frequency component (observed variables or Data).
[B.8]	\mathbf{t}_m	Complex size MEEG source's Fourier coefficients sample vector for a single frequency component (unobserved variables or parameters).
[B.9]	\mathbf{L}	Lead Field matrix of $n \times q$ size.
[B.10]	ξ_m	Complex Fourier coefficients vector for a single frequency component from MEEG forward model residuals (sensors' noise).
[B.11]	Σ_u	Complex size Hermitian and positive semidefinite matrix of EEG/MEG sources' Fourier coefficients (unobserved variables or Parameters) Covariance matrix.
[B.12]	Θ_u	Complex size Hermitian and positive semidefinite matrix of EEG/MEG source's Fourier coefficients (unobserved variables or Parameters) Inverse Covariance matrix.
[B.13]	$\Sigma_{\xi\xi}$	Complex Hermitian and positive semidefinite matrix of EEG/MEG forward model residuals' Fourier coefficients (sensors' noise) Covariance matrix.
[B.14]	\mathbf{A}	Known Complex Hermitian and positive semidefinite matrix.
[B.15]	θ_{ξ}^2	Positive nuisance level hyperparameter σ_e^2 .
[B.16]	Ξ	General variable defining the set of hyperparameters.
[B.17]	$Q(\Xi, \widehat{\Xi})$	Data expected log likelihood, obtained after the expectation operation of the data and parameters log joint conditional probability density function over the parameters accounting for the parameters posterior density function with estimated values of the hyperparameters.
[B.18]	$\Pi(\Theta_u, \mathbf{A})$	Scalar general penalty function or exponent of the prior distribution Precision matrix Θ_u parametrized in the regularization parameters or mask matrix \mathbf{A} .
[B.19]	λ	Regularization parameters or tuning hyperparameters vector of the general penalty function.
[B.20]	$\mathbf{T}^{(k)}$	MEEG Data to Source Transfer Function.
[B.21]	$\widecheck{\Sigma}_u^{(k)}$	Complex Hermitian and positive semidefinite matrix of MEEG source Fourier coefficients (unobserved variables or parameters) posterior Covariance matrix.
[B.22]	$\check{\mathbf{S}}_u^{(k)}$	Complex Hermitian and positive semidefinite matrix of MEEG sources' Fourier coefficients (unobserved variables or parameters) empirical Covariance matrix.
[B.23]	$\Psi_u^{(k)}$	Effective Sources Empirical Covariance (ESEC). It carries the information about sources correlations that will effectively influence the sources Covariance matrix estimator in the maximization step (sources Graphical Model solution), thus, it becomes the sources Covariance matrix estimator in the especial case of prior free model.

[B.24]	S_{vv}	Complex Hermitian matrix MEEG data Fourier coefficients Covariance matrix.
--------	----------	--

C-Frequency Domain Transformation of the Linear State Space Model

The LSSM representation is settled in a more general context of State Space Model (SSM) like formulations, representing neural model that underlies MEEG signal generation. This is supported by previous experimental studies, evidencing the existence of deterministic dynamic regimes of neural populations (neural masses or equivalently Gray Matter generators) (Freeman, 1974). See an excellent review about these models and its biophysical basis in (Deco et al, 2008). Two SSM formulations can be accounted among the most stablished within the state of the art: Nonlinear Continuous Time models in either differential or integrodifferential form (Lopes da Silva et al., 1980; Valdes-Sosa 2004; David et al., 2003; Jirsa et al., 1997). Linear Discrete Autoregressive models (Faes et al., 2012; Galka et al., 2004; Pascual-Marqui et al., 2014; Baccalá and Sameshima, 2001; Babiloni et al., 2005).

Given its simplicity and generality, a ubiquitous formulation is that given by a dynamical integral representation of the source activity $\iota(t)$, in the continuous time domain ($t \in \mathbb{T}$), i.e. State Equation. Thus, the associated LSSM builds upon the coupling of that with the Forward Model of the MEEG signal $v(t)$ also in integral form, i.e. Observation Equation. See the expression (MEEG-LSSM) below, observable quantities are denoted by Latin scripts while the unobserved by Greek scripts. Check the mathematical notation and definition of variables across this document in sections A and B.

$$v(t) = \int_0^t L_{vt}(\tau) \iota(t - \tau) d\tau + \xi(t) \quad \text{"Time Domain Observation Equation"} \quad (C-1)$$

$$\iota(t) = \int_0^t K_u(\tau) \iota(t - \tau) d\tau + \zeta(t) \quad \text{"Time Domain Neural State Equation"} \quad (C-2)$$

Above $L_{vt}(\tau)$ represents the Source to Data Transfer Function (SDTO) of size $p \times q$, i.e. Lead Field. Where p and q are respectively the number of sensors (at the p -size Sensor Space \mathbb{E}) and the number of generators (at the q -size discretized Gray Matter Space \mathbb{G}). The Lead Field is a result of the Maxwell Equations integration, expressed as temporal convolution ($\tau \in \mathbb{T}$), for a specific model of head conductivity and numerical integration method for partial differential equations. The lowercases $\xi(t)$ and $\zeta(t)$ represent respectively additive noise vectors of the MEEG signal and sources activity. The uppercase Kappa $K_u(\tau)$ denotes the sources directed connectivity matrix at multiple lags ($\tau \in \mathbb{T}$), of a mesoscopic neural mass model. At the mesoscopic scale, the connectivity between neural populations (masses) is expressed by unidirectional coupling strength coefficients. This represents the efficiency in neural communication, given by the spatio-temporal density of synaptic events. (Valdes-Sosa et al., 1999; Valdes-Sosa et al., 2005; Valdes-Sosa et al., 2006; Friston, 2009; Valdes-Sosa et al., 2009; Friston, 2011; Valdes-Sosa et al., 2011).

Strongly motivated by the central limit theory (Rosenblatt, 1956) and/or analytical tractability (Roweis and Ghahramani, 1999), the noise (residuals) are modeled as stationary gaussian processes. See the stochastic model below, built on Multivariate Real Gaussian distributions $N^{\mathbb{R}}$, with time invariant parametrization in the covariance matrices of sensor $\Sigma_{\xi\xi}$ and source $\Sigma_{\zeta\zeta}$ noise.

$$\xi(t) \sim N^{\mathbb{R}}(\xi(t) | \mathbf{0}, \Sigma_{\xi\xi}) \quad \text{"MEEG Residuals Process"} \quad (C-3)$$

$$\zeta(t) \sim N^{\mathbb{R}}(\zeta(t) | \mathbf{0}, \Sigma_{\zeta\zeta}) \quad \text{"Source Residuals Process"} \quad (C-4)$$

The identification of the MEEG signal underlying model, when the periodicity of time series holds, is better suited by its representation in transformed spaces. The most interpretable and commonly used is the Fourier Transform, relevant discussion points about the use of time domain vs frequency domain system identification techniques are surveyed in (Ljung and Glover, 1981; Schoukens et al, 2004). In the frequency domain ($\nu \in \mathbb{F}$), the MEEG signal and source activity are respectively denoted by Fourier coefficients $v_m(\nu)$ and $\iota_m(\nu)$, that correspond to different time windows $m \in \mathbb{M}$. Because of the Fourier Transform properties (linearity, convolution factorization), the model in (C-1) and (C-2) is expressed in the frequency domain as a linear system of equations. The spectral properties of the States are fully characterized by the Directed Transfer Function (DFT) $K_u(\nu)$, i.e. Fourier transform of $K_u(\tau)$. The DFT approach was introduced in the context of MEEG sensor connectivity analysis by (Kaminski and Blinowska, 1991).

$$v_m(\nu) = L_{vt}(\nu) \iota_m(\nu) + \xi_m(\nu) \quad \text{"Frequency Domain Observation Equation"} \quad (C-5)$$

$$\iota_m(\nu) = K_u(\nu) \iota_m(\nu) + \zeta_m(\nu) \quad \text{"Frequency Domain Neural State Equation"} \quad (C-6)$$

In formulas (C-5) and (C-6), the assumptions on the LSSM noise vectors stochastic properties predefine a frequency domain Bayesian model: For the MEEG signal (Data) $\mathbf{v}_m(\nu)$ and the source activity (Parameters) $\boldsymbol{\iota}_m(\nu)$ Fourier coefficients, categorized as independent random variables, consequently with the Bayesian formalism (MacKay, 2003). This can be demonstrated in virtue of the stochastic invariance under the Fourier Transform of the gaussian process (B-3) and (B-4) and few algebraic transformations of equation (C-6). Thereby shaping the Data Likelihood and Parameters Prior, i.e. hierarchically conditioned CSG distribution $N^{\mathbb{C}}$.

$$\mathbf{v}_m(\nu) | \boldsymbol{\iota}_m(\nu), \boldsymbol{\Sigma}_{\xi\xi}(\nu) \sim N^{\mathbb{C}}(\mathbf{v}_m(\nu) | \mathbf{L}_{\nu\iota} \boldsymbol{\iota}_m(\nu), \boldsymbol{\Sigma}_{\xi\xi}(\nu)) \quad \text{"Data Likelihood"} \quad (\text{C-7})$$

$$\boldsymbol{\iota}_m(\nu) | \boldsymbol{\Sigma}_u(\nu) \sim N^{\mathbb{C}}(\boldsymbol{\iota}_m(\nu) | \mathbf{0}, \boldsymbol{\Sigma}_u(\nu)) \quad \text{"Parameters Prior"} \quad (\text{C-8})$$

Above, the former distribution is explicitly conditioned to the Parameters $\boldsymbol{\iota}_m(\nu)$ and the MEEG noise covariance $\boldsymbol{\Sigma}_{\xi\xi}(\nu)$ (Hyperparameters). The latter is implicitly conditioned to the DTF $\mathbf{K}_u(\nu)$ and source noise covariance $\boldsymbol{\Sigma}_{\zeta\zeta}(\nu)$, through the frequency dependent covariance matrix $\boldsymbol{\Sigma}_u(\nu)$ (Hyperparameters). The frequency independency condition of the noise covariances is usually relaxed, i.e. $\boldsymbol{\Sigma}_{\xi\xi} \leftarrow \boldsymbol{\Sigma}_{\xi\xi}(\nu)$ and $\boldsymbol{\Sigma}_{\zeta\zeta} \leftarrow \boldsymbol{\Sigma}_{\zeta\zeta}(\nu)$. This relaxation still encompasses the LSSM frequency domain representation but enriches the model with generality of the noise dynamic model, e.g. non stationarity. Importantly, the DFT can be extracted by the decomposition into stable spectral factors of the covariance matrix inverse, i.e. precision matrix $\boldsymbol{\Theta}_u(\nu) = \boldsymbol{\Sigma}_u^{-1}(\nu)$. This is known as Spectral Factorization Theorem (Sayad and Kailath, 2001; Janashia et al, 2011; Jafarian and McWhirter et al, 2012; Faes and Nollo, 2011; Ephremidze et al, 2007).

$$\boldsymbol{\Theta}_u(\nu) = (\mathbf{I}_q - \mathbf{K}_u^\dagger(\nu)) \boldsymbol{\Sigma}_{\zeta\zeta}^{-1}(\nu) (\mathbf{I}_q - \mathbf{K}_u(\nu)) \quad \text{"Spectral Factorization"} \quad (\text{C-9})$$

As a direct consequence of this parametric representation an additional category of random variables to be estimated (Hyperparameters) is introduced, i.e. Residuals (noise) Covariance (RC) and Source Covariance (SC). These are denoted by the Greek letter "Xi" $\boldsymbol{\Omega}$. The symbol $\boldsymbol{\Omega}$ summarizes the hyperparameters for a single frequency component ν , i.e. $\boldsymbol{\Omega} = \{\boldsymbol{\Theta}_{\xi\xi}, \boldsymbol{\Theta}_u(\nu)\}$. Formally, the model spans the entire frequency domain, for the sake of simplicity we hereinafter remove ν from the formulation.

D-Proof of Lemma 1 (bimodal log-wishart form of the expected log-likelihood)

The general strategy for the estimation of the H-HGGM model, is based on the EM algorithm for the Bayesian formalism of maximum posterior analysis at the first (Parameters) and second (Hyperparameters) levels of inference (Dempster et al., 1977; Liu and Rubin, 1994; McLachlan and Krishnan, 2007; Wills et al., 2009). The First Level of Inference consists on maximizing the Gaussian distribution derived from Parameter Posterior Analysis. Under the H-GGM of formulas (C-7) and (C-9) (Likelihood and Parameters Prior), the Parameters $\boldsymbol{\iota}_m$ are independent and have a posterior distribution proportional to the factor of the Data likelihood and the Parameters prior. This can be expressed upon fixed values of the Hyperparameters $\widehat{\boldsymbol{\Omega}}^{(k)} = \{\widehat{\boldsymbol{\Theta}}_{\xi\xi}^{(k)}, \boldsymbol{\Theta}_u^{(k)}\}$ (or equivalently $\widehat{\boldsymbol{\Omega}}^{(k)} = \{\widehat{\boldsymbol{\Sigma}}_{\xi\xi}^{(k)}, \widehat{\boldsymbol{\Sigma}}_u^{(k)}\}$), within an outer cycle indexed (k) of the Parameters and Hyperparameters iterated computation.

$$p(\boldsymbol{\iota}_m | \mathbf{v}_m, \widehat{\boldsymbol{\Omega}}^{(k)}) \propto N_p^{\mathbb{C}}(\mathbf{v}_m | \mathbf{L}_{\nu\iota} \boldsymbol{\iota}_m, \widehat{\boldsymbol{\Sigma}}_{\xi\xi}^{(k)}) N_q^{\mathbb{C}}(\boldsymbol{\iota}_m | \mathbf{0}, \widehat{\boldsymbol{\Sigma}}_u^{(k)}) \quad (\text{D-1})$$

Analyzing the exponent in (D-1) is enough to find the structure of the posterior distribution:

$$-(\mathbf{v}_m - \mathbf{L}_{\nu\iota} \boldsymbol{\iota}_m)^\dagger \widehat{\boldsymbol{\Sigma}}_{\xi\xi}^{(k)} (\mathbf{v}_m - \mathbf{L}_{\nu\iota} \boldsymbol{\iota}_m) - \boldsymbol{\iota}_m^\dagger \widehat{\boldsymbol{\Sigma}}_u^{(k)} \boldsymbol{\iota}_m \quad (\text{D-2})$$

Reorganizing terms in [C.4]:

$$-\boldsymbol{\iota}_m^\dagger (\mathbf{L}_{\nu\iota}^\dagger \widehat{\boldsymbol{\Sigma}}_{\xi\xi}^{(k)} \mathbf{L}_{\nu\iota} + \widehat{\boldsymbol{\Sigma}}_u^{(k)} \mathbf{I}_q) \boldsymbol{\iota}_m + \mathbf{v}_m^\dagger \widehat{\boldsymbol{\Sigma}}_{\xi\xi}^{(k)} \mathbf{L}_{\nu\iota} \boldsymbol{\iota}_m + \boldsymbol{\iota}_m^\dagger \mathbf{L}_{\nu\iota}^\dagger \widehat{\boldsymbol{\Sigma}}_{\xi\xi}^{(k)} \mathbf{v}_m \quad (\text{D-3})$$

Defining the auxiliary quantity Posterior Source Covariance (PSC) $\widehat{\boldsymbol{\Sigma}}_u^{(k)} \leftarrow (\mathbf{L}_{\nu\iota}^\dagger \widehat{\boldsymbol{\Sigma}}_{\xi\xi}^{(k)} \mathbf{L}_{\nu\iota} + \widehat{\boldsymbol{\Sigma}}_u^{(k)} \mathbf{I}_q)^{-1}$ and completing terms in (D-3):

$$-\boldsymbol{\iota}_m^\dagger \tilde{\boldsymbol{\Sigma}}_u^{(k)} \boldsymbol{\iota}_m + \boldsymbol{v}_m^\dagger \tilde{\boldsymbol{\Sigma}}_{\xi\xi}^{(k)} \boldsymbol{\iota}_m + \boldsymbol{v}_m^\dagger \tilde{\boldsymbol{\Sigma}}_u^{(k)} \boldsymbol{\iota}_m^\dagger \tilde{\boldsymbol{\Sigma}}_u^{(k)} \boldsymbol{v}_m \quad (D-4)$$

The second and third terms in (D-4) can be reorganized into the auxiliary quantity Data to Sources Transfer Function (DSTF) $\tilde{\mathbf{T}}_{\nu}^{(k)} \leftarrow \tilde{\boldsymbol{\Sigma}}_u^{(k)} \mathbf{L}_{\nu}^T \tilde{\boldsymbol{\Sigma}}_{\xi\xi}^{(k)} \boldsymbol{\iota}_m^\dagger$. Its left product with the Data samples \boldsymbol{v}_m defines the source activity estimator $\hat{\boldsymbol{\iota}}_m^{(k)}$.

$$\hat{\boldsymbol{\iota}}_m^{(k)} \leftarrow \tilde{\mathbf{T}}_{\nu}^{(k)} \boldsymbol{v}_m \quad (D-5)$$

Substituting (D-5) in (D-4) and completing with the term $\hat{\boldsymbol{\iota}}_m^{(k)T} \tilde{\boldsymbol{\Sigma}}_u^{(k)} \hat{\boldsymbol{\iota}}_m^{(k)}$ we obtain the following expression for the exponent of the parameters posterior distribution.

$$-(\boldsymbol{\iota}_m - \hat{\boldsymbol{\iota}}_m^{(k)})^\dagger \tilde{\boldsymbol{\Sigma}}_u^{(k)} \boldsymbol{\iota}_m + \hat{\boldsymbol{\iota}}_m^{(k)T} \tilde{\boldsymbol{\Sigma}}_u^{(k)} \hat{\boldsymbol{\iota}}_m^{(k)} \quad (D-6)$$

In virtue of (D-6) is clear that parameters posterior distribution constitutes a Circularly Symmetric Complex Gaussian, with posterior mean $\hat{\boldsymbol{\iota}}_m^{(k)}$ and posterior covariance matrix $\tilde{\boldsymbol{\Sigma}}_u^{(k)}$.

$$\boldsymbol{\iota}_m | \boldsymbol{v}_m, \hat{\boldsymbol{\Omega}}^{(k)} \sim N_q^{\mathbb{C}}(\boldsymbol{\iota}_m | \hat{\boldsymbol{\iota}}_m^{(k)}, \tilde{\boldsymbol{\Sigma}}_u^{(k)}) \quad (D-7)$$

The Second Level of inference or Hyperparameter Posterior Analysis, formulated through the EM algorithm, constitutes an explicit and interpretable way to tackle the Hyperparameters estimation. This is done by iteratively maximizing its approximated representation of the intractable Type II likelihood (T2L) $p(\{\boldsymbol{v}_m\}_{m=1}^m | \boldsymbol{\Omega})$, by the so-called Expected Log-Likelihood (ELL) $Q(\boldsymbol{\Omega}, \hat{\boldsymbol{\Omega}}^{(k)})$. The latter is construed by the Expectation of the Data and Parameters Joint distribution given by the parameters Posterior distribution.

$$Q(\boldsymbol{\Omega}, \hat{\boldsymbol{\Omega}}^{(k)}) = \sum_{m=1}^m \int \log(p(\boldsymbol{v}_m, \boldsymbol{\iota}_m | \boldsymbol{\Omega})) p(\boldsymbol{\iota}_m | \boldsymbol{v}_m, \hat{\boldsymbol{\Omega}}^{(k)}) d\boldsymbol{\iota}_m \quad (D-8)$$

The Bayesian formalism, based on the HEGGM, can be reformulated regarding the Parameters as missing Data within the Complete Data defined as the pair $\{\boldsymbol{v}_m, \boldsymbol{\iota}_m\}$. The complete Data Likelihood $p(\boldsymbol{v}_m, \boldsymbol{\iota}_m | \boldsymbol{\Omega})$ can be factorized into the following expression:

$$p(\boldsymbol{v}_m, \boldsymbol{\iota}_m | \boldsymbol{\Omega}) = p(\boldsymbol{v}_m | \boldsymbol{\iota}_m, \boldsymbol{\Sigma}_{\xi\xi}) p(\boldsymbol{\iota}_m | \boldsymbol{\Sigma}_u) = N_p^{\mathbb{C}}(\boldsymbol{v}_m | \mathbf{L}\boldsymbol{\iota}_m, \boldsymbol{\Sigma}_{\xi\xi}) N_q^{\mathbb{C}}(\boldsymbol{\iota}_m | 0, \boldsymbol{\Sigma}_u) \quad (D-9)$$

A single sample element of the Data Expected Log-Likelihood $Q_m(\boldsymbol{\Omega}, \hat{\boldsymbol{\Omega}}^{(k)}) = E_{\hat{\boldsymbol{\Omega}}^{(k)}} \{\log p(\boldsymbol{v}_m, \boldsymbol{\iota}_m | \boldsymbol{\Omega}) | \boldsymbol{v}_m\}$, in virtue of (D-9), can be expressed as follows.

$$Q(\boldsymbol{\Omega}, \hat{\boldsymbol{\Omega}}^{(k)}) = \int N_q^{\mathbb{C}}(\boldsymbol{\iota}_m | \hat{\boldsymbol{\iota}}_m^{(k)}, \tilde{\boldsymbol{\Sigma}}_u^{(k)}) \log(N_p^{\mathbb{C}}(\boldsymbol{v}_m | \mathbf{L}\boldsymbol{\iota}_m, \boldsymbol{\Sigma}_{\xi\xi}) N_q^{\mathbb{C}}(\boldsymbol{\iota}_m | 0, \boldsymbol{\Sigma}_u)) d\boldsymbol{\iota}_m \quad (D-10)$$

Since the logarithm $\log(N_p^{\mathbb{C}}(\boldsymbol{v}_m | \mathbf{L}\boldsymbol{\iota}_m, \boldsymbol{\Sigma}_{\xi\xi}) N_q^{\mathbb{C}}(\boldsymbol{\iota}_m | 0, \boldsymbol{\Sigma}_u))$ can be expressed as:

$$\log|\boldsymbol{\Sigma}_{\xi\xi}^{-1}| - (\boldsymbol{v}_m - \mathbf{L}\boldsymbol{\iota}_m)^\dagger \boldsymbol{\Sigma}_{\xi\xi}^{-1} (\boldsymbol{v}_m - \mathbf{L}\boldsymbol{\iota}_m) + \log|\boldsymbol{\Sigma}_u^{-1}| - \boldsymbol{\iota}_m^\dagger \boldsymbol{\Sigma}_u^{-1} \boldsymbol{\iota}_m \quad (D-11)$$

Using the trace properties on the second and fourth term in (D-11), and after some algebraic transformations we obtain:

$$\log|\boldsymbol{\Sigma}_{\xi\xi}^{-1}| - \text{tr}(\boldsymbol{\Sigma}_{\xi\xi}^{-1} (\boldsymbol{v}_m \boldsymbol{v}_m^\dagger - \boldsymbol{v}_m \boldsymbol{\iota}_m^\dagger \mathbf{L}_{\nu}^T - \mathbf{L}_{\nu} \boldsymbol{\iota}_m \boldsymbol{v}_m^\dagger + \mathbf{L}_{\nu} \boldsymbol{\iota}_m \boldsymbol{\iota}_m^\dagger \mathbf{L}_{\nu}^T)) + \log|\boldsymbol{\Sigma}_u^{-1}| - \boldsymbol{\iota}_m^\dagger \boldsymbol{\Sigma}_u^{-1} \boldsymbol{\iota}_m \quad (D-12)$$

From (D-12) we can deduce that the integral (D-8) can be rearranged as:

$$Q_m(\boldsymbol{\Omega}, \hat{\boldsymbol{\Omega}}^{(k)}) = \log|\boldsymbol{\Sigma}_{\xi\xi}^{-1}| - \text{tr}(\boldsymbol{\Sigma}_{\xi\xi}^{-1} \boldsymbol{v}_m \boldsymbol{v}_m^\dagger) + \text{tr}(\boldsymbol{\Sigma}_{\xi\xi}^{-1} \boldsymbol{v}_m E_{\hat{\boldsymbol{\Omega}}^{(k)}} \{\boldsymbol{\iota}_m | \boldsymbol{v}_m\}^\dagger \mathbf{L}_{\nu}^T) + \text{tr}(\boldsymbol{\Sigma}_{\xi\xi}^{-1} \mathbf{L}_{\nu} E_{\hat{\boldsymbol{\Omega}}^{(k)}} \{\boldsymbol{\iota}_m | \boldsymbol{v}_m\} \boldsymbol{v}_m^\dagger) - \text{tr}(\boldsymbol{\Sigma}_{\xi\xi}^{-1} \mathbf{L}_{\nu} E_{\hat{\boldsymbol{\Omega}}^{(k)}} \{\boldsymbol{\iota}_m \boldsymbol{\iota}_m^\dagger | \boldsymbol{v}_m\} \mathbf{L}_{\nu}^T) + \log|\boldsymbol{\Sigma}_u^{-1}| - \text{tr}(\boldsymbol{\Sigma}_u^{-1} E_{\hat{\boldsymbol{\Omega}}^{(k)}} \{\boldsymbol{\iota}_m \boldsymbol{\iota}_m^\dagger | \boldsymbol{v}_m\}) \quad (D-13)$$

It can be easily checked that for the expectation terms inside [D.5] the following expressions hold:

$$E_{\widehat{\Omega}^{(k)}}\{\boldsymbol{\iota}_m|\boldsymbol{v}_m\} = \widehat{\boldsymbol{\iota}}_m^{(k)} \quad (D-14)$$

$$E_{\widehat{\Omega}^{(k)}}\{\boldsymbol{\iota}_m \boldsymbol{\iota}_m^\dagger|\boldsymbol{v}_m\} = \widehat{\boldsymbol{\Sigma}}_u^{(k)} + \widehat{\boldsymbol{\iota}}_m^{(k)} \widehat{\boldsymbol{\iota}}_m^{(k)\dagger} \quad (D-15)$$

Then, plugging (D-14) and (D-15) in equation (D-13):

$$\begin{aligned} Q_m(\boldsymbol{\Omega}, \boldsymbol{\Omega}^{(k)}) &= \log |\boldsymbol{\Sigma}_{\xi\xi}^{-1}| - \text{tr}(\boldsymbol{\Sigma}_{\xi\xi}^{-1} \boldsymbol{v}_m \boldsymbol{v}_m^\dagger) + \text{tr}(\boldsymbol{\Sigma}_{\xi\xi}^{-1} \boldsymbol{v}_m \widehat{\boldsymbol{\iota}}_m^{(k)\dagger} \mathbf{L}_{\nu\nu}^T) + \text{tr}(\boldsymbol{\Sigma}_{\xi\xi}^{-1} \mathbf{L}_{\nu\nu} \widehat{\boldsymbol{\iota}}_m^{(k)} \boldsymbol{v}_m^\dagger) - \text{tr}(\boldsymbol{\Sigma}_{\xi\xi}^{-1} \mathbf{L}_{\nu\nu} \widehat{\boldsymbol{\iota}}_m^{(k)} \widehat{\boldsymbol{\iota}}_m^{(k)\dagger} \mathbf{L}_{\nu\nu}^T) - \\ &\text{tr}(\boldsymbol{\Sigma}_{\xi\xi}^{-1} \mathbf{L}_{\nu\nu} \widehat{\boldsymbol{\Sigma}}_u^{(k)} \mathbf{L}_{\nu\nu}^T) + \log |\boldsymbol{\Sigma}_u^{-1}| - \text{tr}\left(\boldsymbol{\Sigma}_u^{-1} \left(\widehat{\boldsymbol{\Sigma}}_u^{(k)} + \widehat{\boldsymbol{\iota}}_m^{(k)} \widehat{\boldsymbol{\iota}}_m^{(k)\dagger}\right)\right) \end{aligned} \quad (D-16)$$

The previous analysis can be replicated for m samples of the Complete Data, defined as the set of independent pairs Samples $\{\boldsymbol{v}_m, \boldsymbol{\iota}_m\}$, $m = 1 \dots m$, to obtain the Data Expected Log-Likelihood. It is computed formulating the Complete Data Likelihood $\prod_{m=1}^m p(\boldsymbol{v}_m, \boldsymbol{\iota}_m | \boldsymbol{\Omega})$ and the parameters posterior distribution $\prod_{m=1}^m p(\boldsymbol{\iota}_m | \widehat{\boldsymbol{\iota}}_m^{(k)}, \widehat{\boldsymbol{\Omega}}^{(k)})$, and in virtue of the linearity of the Integral in equation (D-8):

$$Q(\boldsymbol{\Omega}, \widehat{\boldsymbol{\Omega}}^{(k)}) = \sum_{m=1}^m Q_m(\boldsymbol{\Omega}, \widehat{\boldsymbol{\Omega}}^{(k)}) \quad (D-17)$$

The Expectation leads to a compact form, representing the two levels of the HEGGM hierarchical structure, i.e. MEEG noise (residuals) and source covariances. The ELL is through auxiliary quantities that can be interpreted as empirical covariances: Effective Empirical Residuals Covariance (EERC) matrix $\widehat{\boldsymbol{\Psi}}_{\xi\xi}^{(k)}$ and Effective Empirical Source Covariance (EESC) matrix $\widehat{\boldsymbol{\Psi}}_u^{(k)}(\omega)$.

The EESC is given by the additive combination of the auxiliary quantities PSC $\widehat{\boldsymbol{\Sigma}}_u^{(k)}$ and Empirical Source Covariance (ESC) $\widehat{\boldsymbol{S}}_u^{(k)}$. The ESC is the estimated Parameters empirical covariance $\widehat{\boldsymbol{S}}_u^{(k)} = \frac{1}{m} \sum_{m=1}^m \widehat{\boldsymbol{\iota}}_m^{(k)} \widehat{\boldsymbol{\iota}}_m^{(k)\dagger}$. It can be expressed compactly by explicitly expressing $\widehat{\boldsymbol{\iota}}_m^{(k)}$ through the DSTF of and effectuating empirical covariance of the Data, i.e. Empirical Data Covariance (EDC) $\boldsymbol{S}_{vv} = \frac{1}{m} \sum_{m=1}^m \boldsymbol{v}_m \boldsymbol{v}_m^\dagger$. See in formulas below the expression of the EESC and ESC.

$$\widehat{\boldsymbol{\Psi}}_u^{(k)} = \widehat{\boldsymbol{\Sigma}}_u^{(k)} + \widehat{\boldsymbol{S}}_u^{(k)} \quad (D-18)$$

$$\widehat{\boldsymbol{S}}_u^{(k)} = \mathbf{T}_{\xi\nu}^{(k)} \boldsymbol{S}_{vv} \mathbf{T}_{\xi\nu}^{(k)\dagger} \quad (D-19)$$

The EERC $\widehat{\boldsymbol{\Psi}}_{\xi\xi}^{(k)}$ depends on the EDC \boldsymbol{S}_{vv} and the auxiliary quantities PSC $\widehat{\boldsymbol{\Sigma}}_u^{(k)}$ and DRTF $\mathbf{T}_{\xi\nu}^{(k)} \leftarrow \mathbf{I}_p - \mathbf{L}_{\nu\nu} \mathbf{T}_{\xi\nu}^{(k)}$ through the following expression.

$$\widehat{\boldsymbol{\Psi}}_{\xi\xi}^{(k)} = \mathbf{T}_{\xi\nu}^{(k)} \boldsymbol{S}_{vv} \mathbf{T}_{\xi\nu}^{(k)\dagger} + \mathbf{L}_{\nu\nu} \widehat{\boldsymbol{\Sigma}}_u^{(k)} \mathbf{L}_{\nu\nu}^T \quad (D-20)$$

Effectuating the sum (D-17) and rearranging the terms into (D-16) to conform the EERC and EESC we obtain the final expression of the Expected Log-Likelihood.

$$\begin{aligned} Q(\boldsymbol{\Omega}(\omega), \widehat{\boldsymbol{\Omega}}^{(k)}(\omega)) &= m \log |\boldsymbol{\Sigma}_{\xi\xi}^{-1}(\omega)| - m \text{tr}(\boldsymbol{\Sigma}_{\xi\xi}^{-1}(\omega) \widehat{\boldsymbol{\Psi}}_{\xi\xi}^{(k)}(\omega)) \dots \\ &+ m \log |\boldsymbol{\Sigma}_u^{-1}(\omega)| - m \text{tr}(\boldsymbol{\Sigma}_u^{-1}(\omega) \widehat{\boldsymbol{\Psi}}_u^{(k)}(\omega)) \quad \text{“Data Expected Log-Likelihood”} \end{aligned} \quad (D-21)$$

Or equivalently formulated in terms of the Source Partial Correlations (SPC).

$$\begin{aligned} Q(\boldsymbol{\Omega}(\omega), \widehat{\boldsymbol{\Omega}}^{(k)}(\omega)) &= m \log |\boldsymbol{\Theta}_{\xi\xi}(\omega)| - m \text{tr}(\boldsymbol{\Theta}_{\xi\xi}(\omega) \widehat{\boldsymbol{\Psi}}_{\xi\xi}^{(k)}(\omega)) \dots \\ &+ m \log |\boldsymbol{\Theta}_u(\omega)| - m \text{tr}(\boldsymbol{\Theta}_u(\omega) \widehat{\boldsymbol{\Psi}}_u^{(k)}(\omega)) \quad \text{“Data Expected Log-Likelihood”} \end{aligned} \quad (D-22)$$

E-Hyperparameter Posterior Analysis (maximization of the expected log-likelihood)

The Hyperparameters probabilistic posterior map is thus expressed analytically by the combination of the Type II Likelihood approximated (iterated) representation and the Hyperparameter priors. The former builds on the exponentiation of the DELL of formula (D-22).

$$\Omega | \{v_m\}_{m=1}^m, \widehat{\Omega}^{(k)} \sim e^{Q(\Omega, \widehat{\Omega}^{(k)})} p(\Omega) \quad \text{"Hyperparameters Posterior Distribution"} \quad (\text{E-1})$$

$$\Theta_u \sim \exp(\Pi(\mathbf{A}_u \odot \Theta_u) | m\alpha_t) \quad \text{"Source Partial Correlations Prior"} \quad (\text{E-2})$$

$$\theta_{\xi}^2 \sim \exp(\theta_{\xi}^2 | m\alpha_{\xi}) \quad \text{"Residual Partial Correlations Prior"} \quad (\text{E-3})$$

The SPC estimator can be computed by maximizing the Hyperparameters Posterior distribution of formula (E-1) over Θ_u . See Figure E-1 for the schematic representation of expectation computations and hyperparameters posterior maps:

$$\widehat{\Theta}_u^{(k+1)} \leftarrow \operatorname{argmax}_{\Theta_u} \left\{ e^{Q(\Omega, \widehat{\Omega}^{(k)})} p(\Theta_u) \right\} \quad (\text{E-4})$$

Equivalently, it can be done by direct differentiation after taking minus Logarithm in (E-4), by substituting formula (D-22) and the SPC Prior in formula (E-2):

$$\widehat{\Theta}_u^{(k+1)} \leftarrow \operatorname{argmin}_{\Theta_u} \left\{ -\log |\Theta_u| + \operatorname{tr}(\Theta_u \Psi_u^{(k)}) + \alpha_t \Pi(\mathbf{A}_u \odot \Theta_u) \right\} \quad (\text{E-5})$$

The Nuisance Hyperparameter can be computed by maximizing the Posterior distribution in formula [E.1] over θ_{ξ}^2 :

$$\widehat{\theta}_{\xi}^{2(k+1)} \leftarrow \operatorname{argmax}_{\theta_{\xi}^2} \left\{ e^{Q(\Omega, \widehat{\Omega}^{(k)})} p(\theta_{\xi}^2) \right\} \quad (\text{E-6})$$

Equivalently, it can be done by direct differentiation after taking the Logarithm in (E-6) and substituting the Prior of formula (E-3):

$$\widehat{\theta}_{\xi}^{2(k+1)} \leftarrow \operatorname{zero}_{\theta_{\xi}^2} \left\{ \frac{\partial}{\partial \theta_{\xi}^2} Q(\Omega, \widehat{\Omega}^{(k)}) + \frac{\partial}{\partial \theta_{\xi}^2} \log p(\theta_{\xi}^2) \right\} \quad (\text{E-7})$$

Effectuating the derivative $\frac{\partial}{\partial \theta_{\xi}^2}$ of the first term inside (E-7) and in virtue of formula (D-22):

$$\frac{\partial}{\partial \theta_{\xi}^2} Q(\Omega, \widehat{\Omega}^{(k)}) = -mp\theta_{\xi}^2 + \operatorname{mtr}(\mathbf{A}_{\xi\xi} \mathbf{T}_{\xi\nu}^{(k)} \mathbf{S}_{\nu\nu} \mathbf{T}_{\xi\nu}^{(k)\dagger}) \theta_{\xi}^2 + \operatorname{mtr}(\mathbf{A}_{\xi\xi} \mathbf{L}_{\nu\ell} \mathbf{\Sigma}_u^{(k)} \mathbf{L}_{\nu\ell}^T) \theta_{\xi}^4 \quad (\text{E-8})$$

Assuming $\alpha_{\xi} = \epsilon p$ and computing the derivative of the Nuisance Hyperparameter Log-Prior in the second term of [E.7]:

$$\frac{\partial}{\partial \theta_{\xi}^2} \log p(\theta_{\xi}^2) = \epsilon mp \quad (\text{E-9})$$

Substituting (E-8) and (E-9) in formula (E-7) we obtain:

$$\widehat{\theta}_{\xi}^{2(k+1)} \leftarrow \frac{\operatorname{tr}(\mathbf{A}_{\xi\xi} \Psi_{\xi\xi}^{(k)}(\omega))}{p} + \epsilon \quad (\text{E-10})$$

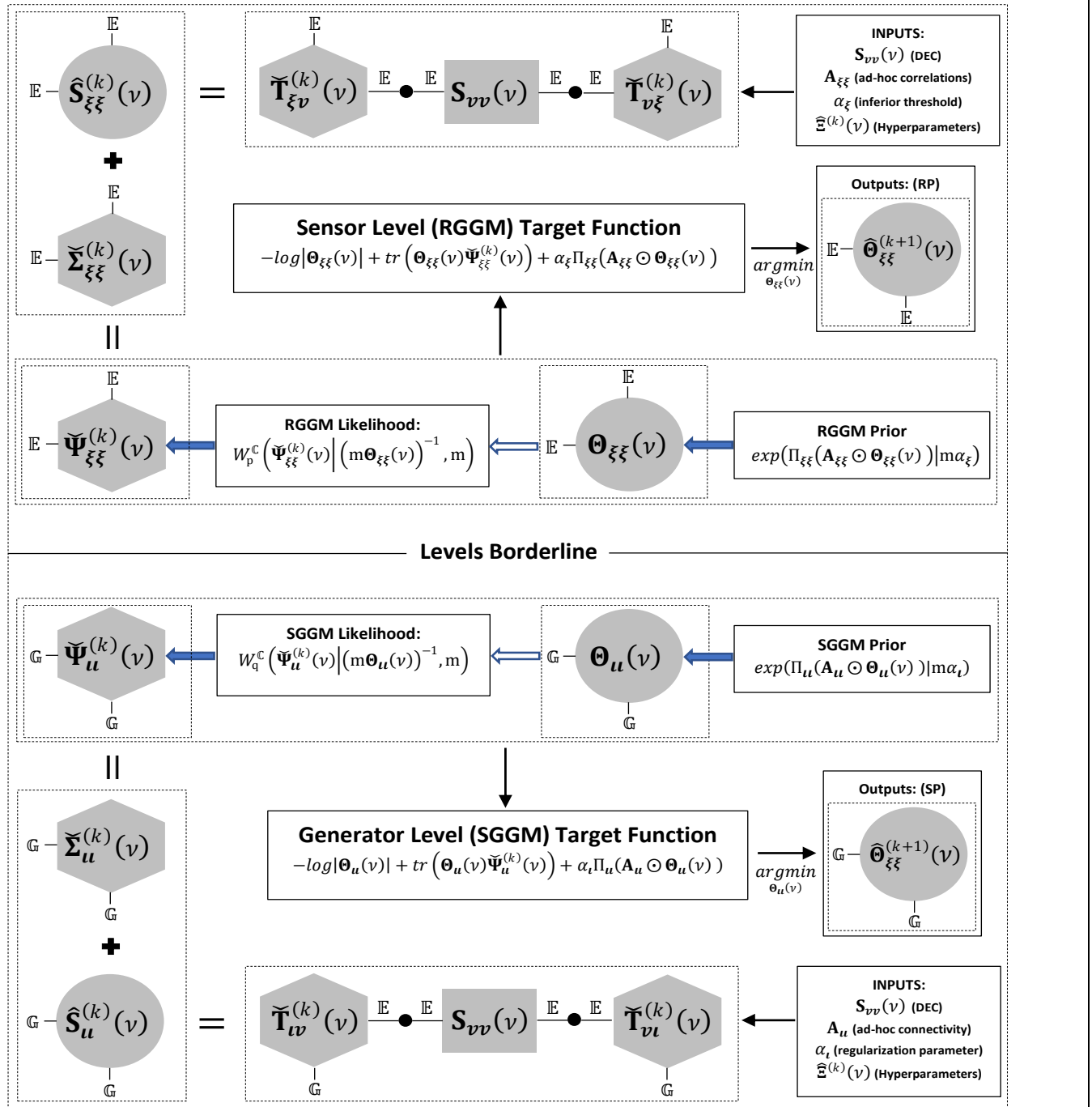


Figure E-1: More-Penrose diagram of the H-HGGM Posterior Analysis represented at a k -th iteration into the EM scheme and for single component in the Frequency Space $v \in \mathbb{F}$. The gray shapes represent different quantities categories: Observed (squares), Indirectly Observed (hexagons) and Variables/Estimators (circles). Accordingly, they lie on the Cartesian Product built of either Sensor Space \mathbb{E} or Generator Space \mathbb{G} . The filled arrows represent variables generation by a specific distribution and the unfilled arrows the corresponding distribution parametrization. Into the iterative scheme this Posterior distribution is totally conditioned on the EESC matrix $\Psi_{xx}^{(k)}$, $x = \{\xi, \iota\}$. At every iteration, if we consider $\Psi_{xx}^{(k)}$ as an indirectly observed Empirical Covariance, a complete analogy to a GGM can be found by assuming that $\Psi_{xx}^{(k)}$ has Wishart Likelihood with m degrees of freedom and scale matrix $m^{-1}\Theta_{xx}^{-1}$: $W_n^{\mathbb{C}}(\Psi_{xx}^{(k)} | m^{-1}\Theta_{xx}^{-1}, m) = |\Psi_{xx}^{(k)}|^{(m-n)} |\Theta|^{-m} e^{-m \text{tr}(\Theta \Psi_{xx}^{(k)})}$, $n = \{p, q\}$.

F-Proof of Lemma 2 (Complex Variable Local Quadratic Approximation of Andrews and Mallows Lemma)

The hierarchical representation of the Gibbs Prior with LASSO exponent $\Pi(\mathbf{A}_u \odot \Theta_u) = \|\Theta\|_{1,A}$, can be built on corollaries of the Andrews and Mallows Lemma (Andrews and Mallows, 1974) for the extension of Real Laplace pdf to the Real/Complex matrix case, by considering unnormalized density functions or simply more general measurable spaces.

By Andrews and Mallows Lemma in the Real LASSO Gibbs pdf (Laplace), also for the Real/Complex case the integral representation holds $e^{-a|z|} \propto \int N_1(|z| | 0, \tau) \text{Gamma}(\tau | 1, a^2/2) d\tau$. The measurable space in which the variable $z | \tau$ is defined has a unnormalized density function given by the Gaussian pdf $p(z | \tau) = N_1(|z| | 0, \tau)$, where its variance τ has Gamma pdf $p(\tau) = \text{Ga}(\tau | 1, a^2/2)$. So, the measure in the product space of z and τ is has density represented as an unnormalized product of Gaussian and Gamma densities $p(z, \tau) \propto N_1(|z| | 0, \tau) \text{Ga}(\tau | 1, a^2/2)$. We call this the generalization of Andrews and Mallows Lemma for Real/Complex LASSO Gibbs pdf.

The GLASSO Gibbs pdf is expressed as $p(\Theta) \propto \exp(\|\Theta\|_{1,A} | m\alpha)$, where there's a priori independence between the Precision matrix elements, thus its pdf is factorizable as follows $p(\Theta) \propto \prod_{ij=1}^q \exp(A_{ij} | \Theta_{ij} | | m\alpha)$. If we apply the generalization Andrews and Mallows Lemma in Real/Complex variable to the Precision matrix elements, by substituting $a = m^{1/2} \alpha A_{ij}$, $z = m^{1/2} \Theta_{ij}$ and $\tau = \Gamma_{ij}^2$ after some minor algebraic considerations we obtain $p(\Theta_{ij}, \Gamma_{ij}) \propto N_1(|\Theta_{ij}| | 0, \Gamma_{ij}^2/m) \text{Ga}(\Gamma_{ij}^2 | 1, m\alpha^2 A_{ij}^2/2)$. For the measure in the product space of the Precision matrix Θ and variances matrix Γ we can write the joint density.

$$p(\Theta, \Gamma) = \prod_{ij=1}^q N_1(|\Theta_{ij}| | 0, \Gamma_{ij}^2/m) \text{Ga}(\Gamma_{ij}^2 | 1, m\alpha^2 A_{ij}^2/2) \blacksquare$$

Remark: In Lemma 2 we establish a statistical equivalence between the Gibbs Prior pdf with argument in the Complex LASSO and a hierarchical representation through a Second Level unnormalized density function $p(\Theta | \Gamma)$, which is parametrized in a Third Level pdf. Remarkably, at this Second Level we are not using a pdf in the strict mathematical sense but a density function of a measurable space in which the variable $\Theta | \Gamma$ is defined. The equivalence relies in that the probability measure in the space of Θ defined by the Gibbs pdf can be expressed by a measure in the product space of $\Theta | \Gamma$ and Γ , where the Second Level cannot be considered a probabilistic space but a general measurable space. Setting up Sparse Models as General Penalty Function has been established in similar scenarios of Variable Selection, i.e. Graphical Models estimation (Jordan, 1998; Attias, 2000; Friedman et al, 2008; Mazumder et al. 2012; Wang, 2012; Wang, 2014; Schmidt, 2010; Hsieh, 2014; Witten et al., 2014; Zhang and Zou, 2014; Yuan and Zheng, 2017; Drton and Maathuis, 2017). Some of the most common Penalty Functions are referred into the family of Graphical LASSO Models, see Table 1 below.

Table 1: Graphical LASSO family Penalty Functions Models

	Penalty function $\Pi(\Theta_u, A)$
Graphical LASSO (GLASSO)	$\ \Theta_u\ _{1,A}$
Graphical Elastic Net (GENET)	$\ \Theta_u\ _{1,A_1} + \ \Theta_u\ _{2,A_2}^2$
Graphical Group Lasso (GGLASSO)	$\sum_{j=1}^q \left\ \Theta_{u(\mathbb{K}_j)} \right\ _{2,A_{(\mathbb{K}_j)}}$; $\mathbb{K}_j \subset \mathbb{G} \times \mathbb{G}; j = 1 \dots n$

G-Proof of Lemma 3 (Concavity of the Complex Variable Local Quadratic Approximation)

With the hierarchical representation of the Real/Complex LASSO, Lemma 2, we attain a modified Target Function of the Precisions matrix built on a Local Quadratic Approximation of the SGGM, i.e. combination of the EC Wishart Likelihood and the Precisions matrix univariate Gaussian Prior. Other terms are related to the normalization constant of the Precisions matrix Gaussian prior and the Precisions matrix variances (Weights) Gamma Prior.

To build the Target Function mofied by AML, it is enough to formulate the posterior pdf of the PC and the PC variances as $p(\Theta, \Gamma | \Psi) \propto p(\Psi | \Theta) p(\Theta | \Gamma) p(\Gamma)$, i.e. according to the distributions defined in formulas Lemma 1 and Lemma 2.

$$p(\Theta, \Gamma | \Psi) \propto W_q^{\mathbb{C}}(\Psi | m^{-1} \Theta^{-1}, m) \prod_{ij=1}^q N_1(|\Theta_{ij}| | 0, \Gamma_{ij}^2/m) p(\Gamma) \quad (G-1)$$

We define the Target Function as the terms dependent on the Precisions matrix \mathbf{X} and Precisions matrix variances Γ as $\mathcal{L}(\Theta, \Gamma) \propto -\log p(\Theta, \Gamma | \Psi)$, it is thus expressed as follows:

$$\mathcal{L}(\Theta, \Gamma) = -m \log|\Theta| + m \text{tr}(\Theta \Psi) - \sum_{ij=1}^q \log N_1(|\Theta_{ij}| | 0, \Gamma_{ij}^2 / m) - \log p(\Gamma) \quad (G-2)$$

Given the definition of the univariate Gaussian pdf $\log N_1(|\Theta_{ij}| | 0, \Gamma_{ij}^2 / m) \propto -\log \Gamma_{ij} - m\Theta_{ij}\Theta_{ij}^\dagger / 2\Gamma_{ij}^2$, the independence of the Γ s and defining $\|\Theta\|_{2,1_q \otimes \Gamma}^2 = \sum_{ij=1}^q \Theta_{ij}\Theta_{ij}^\dagger / \Gamma_{ij}^2$, we can write the target function as:

$$\mathcal{L}(\Theta, \Gamma) = -m \log|\Theta| + m \text{tr}(\Theta \Psi) + \frac{m}{2} \|\Theta\|_{2,1_q \otimes \Gamma}^2 + \sum_{ij=1}^q \log \Gamma_{ij} - \sum_{ij=1}^q \log p(\Gamma_{ij}) \quad (G-3)$$

The target function $\mathcal{L}(\Theta, \Gamma)$ of arguments Θ and Γ can be rearranged as a function of a vector argument $\mathcal{L}\left(\begin{bmatrix} \Theta \\ \Gamma \end{bmatrix}\right)$, where $\Theta = \text{vect}(\Theta)$ and $\Gamma = \text{vect}(\Gamma)$. The Hessian can be computed by a block array of the second derivatives over Θ and Γ :

$$\begin{bmatrix} \frac{\partial^2 \mathcal{L}\left(\begin{bmatrix} \Theta \\ \Gamma \end{bmatrix}\right)}{\partial \Theta \partial \Theta} & \frac{\partial^2 \mathcal{L}\left(\begin{bmatrix} \Theta \\ \Gamma \end{bmatrix}\right)}{\partial \Theta \partial \Gamma} \\ \frac{\partial^2 \mathcal{L}\left(\begin{bmatrix} \Theta \\ \Gamma \end{bmatrix}\right)}{\partial \Gamma \partial \Theta} & \frac{\partial^2 \mathcal{L}\left(\begin{bmatrix} \Theta \\ \Gamma \end{bmatrix}\right)}{\partial \Gamma \partial \Gamma} \end{bmatrix} \quad (G-4)$$

The block Hessian matrix is Positive Definite if and only if its diagonal blocks are Positive Definite. Given the expression of $\mathcal{L}(\Theta, \Gamma)$ in formula (G-3) we can deduce the structure of the diagonal blocks in (G-4) in the following expressions:

$$\frac{\partial^2 \mathcal{L}\left(\begin{bmatrix} \Theta \\ \Gamma \end{bmatrix}\right)}{\partial \Theta \partial \Theta} = \frac{\partial^2}{\partial \Theta \partial \Theta} \left(-m \log|\Theta| + m \text{tr}(\Theta \Psi) + \frac{m}{2} \sum_{ij=1}^q \frac{\Theta_{ij}\Theta_{ij}^\dagger}{\Gamma_{ij}^2} \right) \quad (G-5)$$

$$\frac{\partial^2 \mathcal{L}\left(\begin{bmatrix} \Theta \\ \Gamma \end{bmatrix}\right)}{\partial \Gamma \partial \Gamma} = \frac{\partial^2}{\partial \Gamma \partial \Gamma} \left(\frac{m}{2} \sum_{ij=1}^q \frac{\Theta_{ij}\Theta_{ij}^\dagger}{\Gamma_{ij}^2} + \sum_{ij=1}^q \log \Gamma_{ij} - \sum_{ij=1}^q \log p(\Gamma_{ij}) \right) \quad (G-6)$$

By considering the matrix differential properties the first block in expression (G-5) can be expressed as:

$$\frac{\partial^2 \mathcal{L}\left(\begin{bmatrix} \Theta \\ \Gamma \end{bmatrix}\right)}{\partial \Theta \partial \Theta} = m\Theta^{-1} \otimes \Theta^{-1} + \frac{m}{2} \text{diag}(\text{vect}(\mathbf{1}_q \otimes \Gamma^2)) \quad (G-7)$$

In the region of Positive Definiteness of Θ the Kronecker product $\Theta^{-1} \otimes \Theta^{-1}$ is Positive Definite. Since the second term in [G1.13] is Positive Definite³ also the whole expression is Positive Definite, thus, the first block of the Hessian $\frac{\partial^2 \mathcal{L}\left(\begin{bmatrix} \Theta \\ \Gamma \end{bmatrix}\right)}{\partial \Theta \partial \Theta}$ is Positive Definite. To analyze the Positive Definiteness of $\frac{\partial^2 \mathcal{L}\left(\begin{bmatrix} \Theta \\ \Gamma \end{bmatrix}\right)}{\partial \Gamma \partial \Gamma}$ it is enough to analyze the positivity of the expression $\frac{\partial^2}{\partial \Gamma_{ij} \partial \Gamma_{ij}} \left(\frac{m}{2} \frac{\Theta_{ij}\Theta_{ij}^\dagger}{\Gamma_{ij}^2} + \log \Gamma_{ij} - \log p(\Gamma_{ij}) \right)$ for all ij . Substituting the term of the Gamma prior for the LASSO case, $\log p(\Gamma_{ij}) \propto -\frac{m\alpha^2 A_{ij}^2}{2} \Gamma_{ij}^2$, in the expression above we obtain:

$$\frac{\partial^2 \mathcal{L}\left(\begin{bmatrix} \Theta \\ \Gamma \end{bmatrix}\right)}{\partial \Gamma_{ij} \partial \Gamma_{ij}} = \frac{\partial^2}{\partial \Gamma_{ij} \partial \Gamma_{ij}} \left(\frac{m}{2} \frac{\Theta_{ij}\Theta_{ij}^\dagger}{\Gamma_{ij}^2} + \log \Gamma_{ij} + \frac{m\alpha^2 A_{ij}^2}{2} \Gamma_{ij}^2 \right) = 3m \frac{\Theta_{ij}\Theta_{ij}^\dagger}{\Gamma_{ij}^4} - \frac{1}{\Gamma_{ij}^2} + m\alpha^2 A_{ij}^2 \quad (G-8)$$

In virtue of (G-8), the Hessian is Positive Definite in the region of the product space $\Theta \times \Gamma$ defined by the intercept of the region of Positive Definiteness of Θ the region where the following set of inequalities $\left\{ 3m \frac{\Theta_{ij}\Theta_{ij}^\dagger}{\Gamma_{ij}^4} - \frac{1}{\Gamma_{ij}^2} + m\alpha^2 A_{ij}^2 > 0 \right\}_{ij=1}^q$ hold. From this result the target function $\mathcal{L}(\Theta, \Gamma)$ is strictly convex within this region. Then, applying derivatives of $\mathcal{L}(\Theta, \Gamma)$ over Θ and Γ we obtain:

³ See **Proposition 3 of Lemma 4** in Section H to corroborate this.

$$\frac{\partial}{\partial \Theta} \left\{ -m \log |\Theta| + m \operatorname{tr}(\Theta \Psi) + \frac{m}{2} \sum_{ij=1}^q \frac{\Theta_{ij} \Theta_{ij}^\dagger}{\Gamma_{ij}^2} \right\} = -m(\Theta^{-1})^T + m\Psi^T + m\Theta^T \oslash \Gamma^2 \quad (G-9)$$

$$\frac{\partial}{\partial \Gamma_{ij}} \left\{ \frac{m}{2} \frac{\Theta_{ij} \Theta_{ij}^\dagger}{\Gamma_{ij}^2} + \log \Gamma_{ij} + \frac{m\alpha^2}{2} A_{ij}^2 \Gamma_{ij}^2 \right\} = -m \frac{\Theta_{ij} \Theta_{ij}^\dagger}{\Gamma_{ij}^3} + \frac{1}{\Gamma_{ij}} + m\alpha^2 A_{ij}^2 \Gamma_{ij} \quad (G-10)$$

Equating (G-9) and (G-10) to zero and with some algebraic transformations we obtain the system of equations:

$$-\Theta^{-1} + \Psi + \Theta \oslash \Gamma^2 = \mathbf{0}_q \quad (G-11)$$

$$\left\{ -m \frac{\Theta_{ij} \Theta_{ij}^\dagger}{\Gamma_{ij}^4} + \frac{1}{\Gamma_{ij}^2} + m\alpha^2 A_{ij}^2 = 0 \right\}_{ij=1}^q \quad (G-12)$$

It can be checked that the point of the product space that satisfies the equation (G-12) also belongs to the region defined by the set of inequalities $\left\{ 3m \frac{\Theta_{ij} \Theta_{ij}^\dagger}{\Gamma_{ij}^4} - \frac{1}{\Gamma_{ij}^2} + m\alpha^2 A_{ij}^2 > 0 \right\}_{ij=1}^q$. This can be checked by substituting into the inequality the term $m \frac{\Theta_{ij} \Theta_{ij}^\dagger}{\Gamma_{ij}^4}$ given by (G-12), which leads to $3 \left(\frac{1}{\Gamma_{ij}^2} + m\alpha^2 A_{ij}^2 \right) - \frac{1}{\Gamma_{ij}^2} + m\alpha^2 A_{ij}^2 = \frac{2}{\Gamma_{ij}^2} + 4m\alpha^2 A_{ij}^2 \geq 0$.

For every element Γ_{ij}^2 of the system of quadratic equations (G-12) it can be shown that it has a unique Real and Positive solution amongst the Discriminant formula Roots of Second Order Polynomials. This solution can be compactly expressed through the elementwise matrix operations \odot (Hadamard product), \oslash (Hadamard division), $\operatorname{abs}(\cdot)$ (elementwise matrix absolute value), $(\cdot)^2$ (elementwise matrix Square exponentiation), $(\cdot)^{\frac{1}{2}}$ (elementwise matrix Square Root) and $\mathbf{1}_q$ ($q \times q$ matrix of ones):

$$\Gamma^2 = \left(-\mathbf{1}_q + (\mathbf{1}_q + 4\alpha^2 \mathbf{A}^2 \odot \operatorname{abs}(\Theta)^2)^{\frac{1}{2}} \right) \oslash (2\alpha \mathbf{A}^2) \quad (G-13)$$

Given the Positive Definiteness of \mathbf{A} and Θ , it can also be deduced that Γ is Positive Definite by following the steps in Proposition 3 of Lemma 4. ■

According to the hierarchical representation of the Real/Complex LASSO, through the Prior $p(\Theta|\Gamma)$ of equation (G-1), we can define a new random matrix through the Hadamard division scaling transformation $\tilde{\Theta} = \Theta \oslash \Gamma$ (Standard Precision matrix), so that its Prior is a Gibbs pdf of the Squared L2 norm:

$$\Theta \sim e^{-\frac{m}{2} \|\Theta\|_{2,1q}^2} \quad (G-14)$$

$$\tilde{\Theta} \propto e^{-\frac{m}{2} \|\tilde{\Theta}\|_2^2} \quad (G-15)$$

Now we define a Standardization transformation on the ESEC $\tilde{\Psi} = (\Psi^{-1} \oslash \Gamma)^{-1}$ that keeps the stochastic properties of the Wishart distribution (Likelihood) when conditioned to the Standard Precision matrix $\tilde{\Theta}$. See next seccion.

H-Proof of Lemma 4 (standardization of the Wishart distribution)

Proposition 1

If Ψ is a $(q \times q)$ Real/Complex Random matrix with Complex Wishart pdf of m degrees of freedom and positive definite scale matrix Σ . Then the Random matrix obtained from the consecutive rows and columns permutation operations, denoted $\mathbf{P}_{i \leftrightarrow i'}^{\text{row}}$ and $\mathbf{P}_{j \leftrightarrow j'}^{\text{col}}$ respectively, has Wishart pdf of m degrees of freedom and positive definite scale matrix.

$$\left(\mathbf{P}_{j \leftrightarrow j'}^{\text{col}} \mathbf{P}_{i \leftrightarrow i'}^{\text{row}} \Sigma^{-1} \right)^{-1}$$

Proof of Proposition 1:

The Wishart pdf of the posterior probability maps in Figure E-1 can be expressed as $W_q^C(\Psi|\Sigma, m) \propto |\Psi|^{(m-q)} |\Sigma^{-1}|^m e^{-tr(\Sigma^{-1}\Psi)}$. These determinants and trace terms of the Wishart are invariant to consecutive rows and columns permutation operations $\mathbf{P}_{j \leftrightarrow j'}^{col}, \mathbf{P}_{i \leftrightarrow i'}^{row}$. So that:

$$|\Sigma^{-1}| = \left| \mathbf{P}_{j \leftrightarrow j'}^{col} \mathbf{P}_{i \leftrightarrow i'}^{row} \Sigma^{-1} \right|, |\Psi| = \left| \mathbf{P}_{j \leftrightarrow j'}^{col} \mathbf{P}_{i \leftrightarrow i'}^{row} \Psi \right| \text{ and } tr(\Sigma^{-1}\Psi) = tr \left(\mathbf{P}_{j \leftrightarrow j'}^{col} \mathbf{P}_{i \leftrightarrow i'}^{row} \Sigma^{-1} \mathbf{P}_{j \leftrightarrow j'}^{col} \mathbf{P}_{i \leftrightarrow i'}^{row} \Psi \right).$$

Thus the Wishart distribution can be expressed as a function of the Random matrix $\mathbf{P}_{j \leftrightarrow j'}^{col} \mathbf{P}_{i \leftrightarrow i'}^{row} \Psi$, $W_q^C(\Psi|\Sigma, m) = W_q^C \left(\mathbf{P}_{j \leftrightarrow j'}^{col} \mathbf{P}_{i \leftrightarrow i'}^{row} \Psi \left| \left(\mathbf{P}_{j \leftrightarrow j'}^{col} \mathbf{P}_{i \leftrightarrow i'}^{row} \Sigma^{-1} \right)^{-1}, m \right. \right)$. Then, since the pdf is invariant to the organization of variables within the set $\{\Psi_{ij}: i, j = 1 \dots q\}$, $p(\{\Psi_{ij}: i, j = 1 \dots q\}) = p(\Psi) = p \left(\mathbf{P}_{j \leftrightarrow j'}^{col} \mathbf{P}_{i \leftrightarrow i'}^{row} \Psi \right)$, it is clear that:

$$\mathbf{P}_{j \leftrightarrow j'}^{col} \mathbf{P}_{i \leftrightarrow i'}^{row} \Psi \sim W_q^C \left(\mathbf{P}_{j \leftrightarrow j'}^{col} \mathbf{P}_{i \leftrightarrow i'}^{row} \Psi \left| \left(\mathbf{P}_{j \leftrightarrow j'}^{col} \mathbf{P}_{i \leftrightarrow i'}^{row} \Sigma^{-1} \right)^{-1}, m \right. \right). \blacksquare$$

For the conditional pdf of an element Ψ_{ij} in the Wishart distributed complex random matrix \mathbf{S} regarding the remaining elements $\{\Psi_{\bar{i}\bar{j}}\} = \{\Psi_{i'j'}: (i'j') \neq (ij)\}$ the following holds:

$$p(\Psi_{ij} | \{\Psi_{\bar{i}\bar{j}}\}) \propto |\Psi|^{(m-q)} e^{-tr(\Sigma^{-1}\Psi)} \quad (H-1)$$

To find this conditional pdf it is enough to apply the consecutive permutation operation $\mathbf{P}_{j \leftrightarrow 1}^{col} \mathbf{P}_{i \leftrightarrow 1}^{row} \Psi$ and then consider the conditional pdf of the element $(\mathbf{P}_{j \leftrightarrow 1}^{col} \mathbf{P}_{i \leftrightarrow 1}^{row} \Psi)_{11}$. In virtue of Proposition 1 the pdf of $\mathbf{P}_{j \leftrightarrow 1}^{col} \mathbf{P}_{i \leftrightarrow 1}^{row} \Psi$ is also Wishart. Thus, for $(\mathbf{P}_{j \leftrightarrow 1}^{col} \mathbf{P}_{i \leftrightarrow 1}^{row} \Psi)_{11}$ a conditional pdf equivalent to the one in equation (F-1) can also be written. Without losing generality we can consider first the element Ψ_{11} and then any result will also apply for all Ψ_{ij} :

$$p(\Psi_{11} | \{\Psi_{\bar{1}\bar{1}}\}) \propto |\Psi|^{(m-q)} e^{-tr(\Sigma^{-1}\Psi)} \quad (H-2)$$

Partitioning the random matrix Ψ into the following block structure we can find a simplified expression of the determinant in the conditional pdf of equation (H-2):

$$\Psi = \begin{pmatrix} \Psi_{11} & \Psi_{12} \\ \Psi_{21} & \Psi_{22} \end{pmatrix} \quad (H-3)$$

$$|\Psi| = |\Psi_{22}|(\Psi_{11} - \Psi_{12} \Psi_{22}^{-1} \Psi_{21}) \quad (H-4)$$

If we consider applying the same block structure as in expression (H-3) to Σ^{-1} in the trace term if equation (H-2), completing the exponent with the term $\Psi_{12} \Psi_{22}^{-1} \Psi_{21}$ and by the determinant formula (H-4) we obtain:

$$p(\Psi_{11} | \{\Psi_{\bar{1}\bar{1}}\}) \propto (\Psi_{11} - \Psi_{12} \Psi_{22}^{-1} \Psi_{21})^{(m-q)} e^{-(\Sigma^{-1})_{11}(\Psi_{11} - \Psi_{12} \Psi_{22}^{-1} \Psi_{21})} \quad (H-5)$$

The argument $(\Psi_{11} - \Psi_{12} \Psi_{22}^{-1} \Psi_{21})$ in equation (H-5) above can be directly related to the element $(\Psi^{-1})_{11}$ of the inverse Ψ^{-1} though the block inverse identity:

$$\Psi^{-1} = \begin{pmatrix} \frac{1}{(\Psi_{11} - \Psi_{12} \Psi_{22}^{-1} \Psi_{21})} & -\frac{\Psi_{22}^{-1} \Psi_{21}}{(\Psi_{11} - \Psi_{12} \Psi_{22}^{-1} \Psi_{21})} \\ -\frac{\Psi_{22}^{-1} \Psi_{21}}{(\Psi_{11} - \Psi_{12} \Psi_{22}^{-1} \Psi_{21})} & \Psi_{22}^{-1} + \frac{\Psi_{22}^{-1} \Psi_{21} \Psi_{12} \Psi_{22}^{-1}}{(\Psi_{11} - \Psi_{12} \Psi_{22}^{-1} \Psi_{21})} \end{pmatrix} \quad (H-6)$$

$$(\Psi^{-1})_{11} = \frac{1}{(\Psi_{11} - \Psi_{12} \Psi_{22}^{-1} \Psi_{21})} \quad (H-7)$$

From this it is deduced that the random variable $(\Psi^{-1})_{11}$ is independent from $\{\Psi_{11}\}$ and it has Complex Inverse Gamma pdf with shape parameter $(m - q)$ and scale parameter $(\Sigma^{-1})_{11}$:

$$p((\Psi^{-1})_{11}) \propto ((\Psi^{-1})_{11})^{-(m-q)} e^{-\frac{(\Sigma^{-1})_{11}}{(\Psi^{-1})_{11}}} \quad (H-8)$$

Now let's build the following auxiliary random matrix $\tilde{\Psi}$ and scale matrix $\tilde{\Sigma}$, based on scaling the elements $(\Phi^{-1})_{11}$ and $(\Sigma^{-1})_{11}$ respectively by a positive number Γ_{11} :

$$\tilde{\Psi} = \begin{pmatrix} \frac{(\Phi^{-1})_{11}}{\Gamma_{11}} & (\Phi^{-1})_{12} \\ (\Phi^{-1})_{21} & (\Phi^{-1})_{22} \end{pmatrix}^{-1} \quad (H-9)$$

$$\tilde{\Sigma} = \begin{pmatrix} \frac{(\Sigma^{-1})_{11}}{\Gamma_{11}} & (\Sigma^{-1})_{12} \\ (\Sigma^{-1})_{21} & (\Sigma^{-1})_{22} \end{pmatrix}^{-1} \quad (H-10)$$

Proposition 2

The element $(\Phi^{-1})_{11}$ of the matrix Φ has identical marginal pdf that the element $(\Psi^{-1})_{11}$ of the matrix Ψ , when Ψ has Wishart pdf with m degrees of freedom and complex positive definite scale matrix $\tilde{\Sigma}$.

Proof of Proposition 2

Using analogous representation of the conditional probability density of $\tilde{\Psi}_{11}$ given $\{\tilde{\Psi}_{11}\}$, as in formula (H-5), we can write $p(\tilde{\Psi}_{11} | \{\tilde{\Psi}_{11}\}) \propto |\tilde{\Psi}|^{(m-q)} e^{-tr(\tilde{\Sigma}^{-1} \tilde{\Psi})}$. Given the property of the Wishart pdf deduced before in equation (H-8) it is clear that the random variable $(\tilde{\Psi}^{-1})_{11}$ is independent from $\{\tilde{\Psi}_{11}\}$ and it has Real/Complex Inverse Gamma pdf with shape parameter $(m - q)$ and scale parameter $(\tilde{\Sigma}^{-1})_{11}$. By construction of $\tilde{\Psi}$ it holds that $(\Phi^{-1})_{11} = \Gamma_{11}(\tilde{\Phi}^{-1})_{11}$, thus, $(\Phi^{-1})_{11}$ is also independent and it has Real/Complex Inverse Gamma pdf with shape parameter $(m - q)$ and scale parameter $\Gamma_{11}(\tilde{\Sigma}^{-1})_{11} = (\Sigma^{-1})_{11}$. ■

In virtue of **Proposition 1** we can iteratively apply the scaling operation described in equations (H-9) and (H-10) and get an standardized Wishart pdf of m degrees of freedom and positive definite scale matrix $\tilde{\Sigma} = (\Sigma^{-1} \oslash \Gamma)^{-1}$, which argument is the complex random matrix $\tilde{\Psi} = (\Phi^{-1} \oslash \Gamma)^{-1}$, i.e. $p(\tilde{\Psi}) = W_q^C(\tilde{\Psi} | \tilde{\Sigma}, m)$. Which has identical marginal stochastic properties of the inverse Ψ^{-1} .

To complete the proof, it is enough to show that the scale matrix $\tilde{\Sigma} = (\Sigma^{-1} \oslash \Gamma)^{-1}$ of the Wishart pdf keeps being positive definite. This is a direct consequence of the fact that the scaling operation keeps positive definiteness property, as we can check from the following proposition which is a Corollary of Schur product theorem.

Proposition 3

If Σ and Γ are positive definite matrices then the matrix $\tilde{\Sigma} = (\Sigma^{-1} \oslash \Gamma)^{-1}$ from the scaling operation is also positive definite.

Proof of Proposition 3

If Σ is positive definite so it is also the inverse Σ^{-1} . Then, let's analyze the positive definiteness of the Hadamard scaling $\mathbf{1}_q \oslash \Gamma$. This Hadamard scaling can be expressed as an elementwise exponentiation $\mathbf{1}_q \oslash \Gamma = e^{-\log(\Gamma)}$, $\log(\Gamma)$ acts as an elementwise function. The logarithm can be expressed as an infinite Taylor series $\log(\Gamma) = \sum_{\ell=1}^{\infty} \frac{(-1)^{\ell+1}}{\ell} (\Gamma - \mathbf{1}_q)^{\ell}$. Without losing generality we can consider that the elements in Γ belong to the open interval $\Gamma_{ij} \in (0, 1), \forall ij$. Given the assumption before, the odd terms in the Taylor series of $-\log(\Gamma)$ become positive, the series can be rearranged into $-\log(\Gamma) = \sum_{\ell=1}^{\infty} \frac{(\mathbf{1}_q - \Gamma)^{\ell}}{\ell}$. Finally, by substituting in the

elementwise exponential function we can express the Hadamard Scaling as the element wise product of exponentials $\mathbf{1}_q \oslash \boldsymbol{\Gamma} = \prod_{\ell=1}^{\infty} e^{\frac{(\mathbf{1}_q - \boldsymbol{\Gamma})^\ell}{\ell}}$. Here, given the positive definiteness of $\boldsymbol{\Gamma}$ and since $\Gamma_{ij} \in (0,1), \forall ij$ it holds that $(\mathbf{1}_q - \boldsymbol{\Gamma})$ is positive definite. Also, the elementwise exponentiation $(\mathbf{1}_q - \boldsymbol{\Gamma})^\ell$ and $e^{\frac{(\mathbf{1}_q - \boldsymbol{\Gamma})^\ell}{\ell}}$ and element wise product operation $\prod_{\ell=1}^{\infty}$ keep the positive definiteness. Thus, it is clear that $\boldsymbol{\Sigma}^{-1} \oslash \boldsymbol{\Gamma}$ is positive definite so also it is $\tilde{\boldsymbol{\Sigma}}$. ■

Remark: By Lemma 4 we build a statistically equivalent model of the random matrix $\boldsymbol{\Psi}$, the variable denominated ‘Version’ $\boldsymbol{\Phi}$ defined through the Unstandardization of $\tilde{\boldsymbol{\Psi}}$, in the sense that it keeps the same multivariate structure through the Wishart **pdf**, and its inverse $\boldsymbol{\Phi}^{-1}$ keeps the same stochastic properties than $\boldsymbol{\Psi}^{-1}$, i.e. all their elements are independent with identical marginal pdf (Drton et al., 2008). This result prescribes a Statistical equivalence between a Model of the Empirical Covariance $\boldsymbol{\Psi}$ defined by a Wishart **pdf**, of m degrees of freedom and positive definite scale matrix $(m\boldsymbol{\Theta})^{-1}$, with Prior of the Precision matrix $\boldsymbol{\Theta}$ given by [G3.1], and Model of the Standard Empirical Covariance $\tilde{\boldsymbol{\Psi}}$ defined by a Wishart **pdf**, of m degrees of freedom and positive definite scale matrix $(m\tilde{\boldsymbol{\Theta}})^{-1}$, with Prior of the Standard Precision matrix $\tilde{\boldsymbol{\Theta}}$ given by (G-15):

$$\boldsymbol{\Psi} | \tilde{\boldsymbol{\Theta}} \sim W_q^{\mathbb{C}} (\tilde{\boldsymbol{\Psi}} | (m\tilde{\boldsymbol{\Theta}})^{-1}, m) \quad (\text{H-11})$$

$$W_q^{\mathbb{C}} (\tilde{\boldsymbol{\Psi}} | (m\tilde{\boldsymbol{\Theta}})^{-1}, m) \propto |\tilde{\boldsymbol{\Psi}}|^{m-q} |\tilde{\boldsymbol{\Theta}}|^m e^{-m\text{tr}(\tilde{\boldsymbol{\Theta}}\tilde{\boldsymbol{\Psi}})} \quad (\text{H-12})$$

This Statistical Standardization is also consistent when the sample number m tends to infinite, given the Inverse EESC tendency in probability to \mathbf{X} , i.e. $P(\boldsymbol{\Psi}^{-1} \in \mathcal{B}(\boldsymbol{\Theta})) \rightarrow 1$ as $m \rightarrow \infty$ for any open set $\mathcal{B}(\boldsymbol{\Theta})$ containing $\boldsymbol{\Theta}$ in the q^2 -dimensional complex Euclidean space. A natural estimator of the Standard Precision matrix $\tilde{\boldsymbol{\Theta}}$ can be computed by maximum Likelihood through direct differentiation of equation (H-12) $\hat{\tilde{\boldsymbol{\Theta}}} = \tilde{\boldsymbol{\Psi}}^{-1}$, then, in agreement with the conditions and equivalence shown in Lemma 4:

$$\hat{\tilde{\boldsymbol{\Theta}}} = \boldsymbol{\Psi} \oslash \boldsymbol{\Gamma} \quad (\text{H-13})$$

So, given the tendency in probability of $\boldsymbol{\Psi}^{-1}$ it can also be directly deduced the tendency in probability of the Standard Precision matrix estimator, i.e. $P(\hat{\tilde{\boldsymbol{\Theta}}} \in \mathcal{B}(\boldsymbol{\Theta} \oslash \boldsymbol{\Gamma})) \rightarrow 1$ as $m \rightarrow \infty$ for any open set $\mathcal{B}(\boldsymbol{\Theta} \oslash \boldsymbol{\Gamma})$ containing $\boldsymbol{\Theta} \oslash \boldsymbol{\Gamma}$ in the q^2 -dimensional complex Euclidean space. ■

I-Proof of Lemma 5 (local graphical Ridge estimator)

We attain a Standard formulation of the Precision matrix Posterior distribution, combining the equations of the Standard Wishart Likelihood and the Standard Prior:

$$\tilde{\boldsymbol{\Theta}} | \tilde{\boldsymbol{\Psi}} \sim |\tilde{\boldsymbol{\Theta}}|^m e^{-m\text{tr}(\tilde{\boldsymbol{\Theta}}\tilde{\boldsymbol{\Psi}})} e^{-\frac{m}{2}\|\tilde{\boldsymbol{\Theta}}\|_2^2} \quad (\text{I-1})$$

Applying minus Logarithm to the posterior distribution of formula (I-1) we obtain the Local Quadratic Approximation or Standard Target Function:

$$\hat{\tilde{\boldsymbol{\Theta}}} = \text{argmin}_{\tilde{\boldsymbol{\Theta}}} \left\{ -\log|\tilde{\boldsymbol{\Theta}}| + \text{tr}(\tilde{\boldsymbol{\Theta}}\tilde{\boldsymbol{\Psi}}) + \frac{1}{2}\|\tilde{\boldsymbol{\Theta}}\|_2^2 \right\} \quad (\text{I-2})$$

Since (I-2) is a convex differentiable function the necessary and sufficient condition for a minimum is that its first matrix derivative over the argument $\tilde{\boldsymbol{\Theta}}$ equals a matrix made of zeroes $\mathbf{0}_q$, so it is direct that the minimization of (I-2) is reduced to solve the following matrix equation:

$$-\tilde{\boldsymbol{\Theta}}^{-1} + \tilde{\boldsymbol{\Psi}} + \tilde{\boldsymbol{\Theta}} = \mathbf{0}_q \quad (\text{I-3})$$

Remark: The expression (I-3) constitute a special case of the Riccati matrix equation. Positive definiteness and hermiticity of its solution $\widehat{\Theta}$, as a natural property of the Standard Precision matrix estimator, is required. Also, it can be checked that the solution $\widehat{\Theta}$ must share the same eigenspace with $\widehat{\Psi}$, since from (I-3) two auxiliary Second Order matrix equations hold, i.e. $\widehat{\Theta}^2 + \widehat{\Theta}\widehat{\Psi} - \mathbf{I}_q = \mathbf{0}$ and $\widehat{\Theta}^2 + \widehat{\Psi}\widehat{\Theta} - \mathbf{I}_q = \mathbf{0}_q$, given the left and right multiplication by the Standard Precision matrix. This imply that any solution $\widehat{\Theta}$ commute with $\widehat{\Psi}$, thus they share the eigenspace. ■

Let's show first that the proposed solution is positive definite. Given the positive definiteness and hermiticity of the complex matrix $\widehat{\Psi}$ it admits a singular value decomposition $\widehat{\Psi} = \widetilde{\mathbf{U}}\widetilde{\mathbf{D}}\widetilde{\mathbf{U}}^\dagger$ with real and positive singular values $\widetilde{\mathbf{D}}$. Thus, the argument in the matrix square root of formula [G4.4] admits a singular value decomposition of the kind $\widehat{\Psi}^2 + 4\mathbf{I}_q = \widetilde{\mathbf{U}}(\widetilde{\mathbf{D}}^2 + 4\mathbf{I}_q)\widetilde{\mathbf{U}}^\dagger$, where its singular values, given by $\widetilde{\mathbf{D}}^2 + 4\mathbf{I}_q$, are also real and positive. In consequence the square root term has also real and positive singular values given by the following singular value decomposition:

$$\sqrt{\widehat{\Psi}^2 + 4\mathbf{I}_q} = \widetilde{\mathbf{U}}\sqrt{\widetilde{\mathbf{D}}^2 + 4\mathbf{I}_q}\widetilde{\mathbf{U}}^\dagger \quad (\text{I-4})$$

Finally, the singular value decomposition of the Standard Precision matrix estimator can be expressed as:

$$\widehat{\Theta} = \widetilde{\mathbf{U}}\left(\frac{1}{2}\sqrt{\widetilde{\mathbf{D}}^2 + 4\mathbf{I}_q} - \frac{1}{2}\mathbf{I}_q\right)\widetilde{\mathbf{U}}^\dagger \quad (\text{I-5})$$

It is clear, by formula (I-5), that the singular values of the Standard Precision matrix estimator are real and positive numbers. The Standard Precision matrix estimator commutes with the Standard ESEC $\widehat{\Psi}$ since they share the eigenspace, i.e. $\widehat{\Psi}\widehat{\Theta} = \widehat{\Theta}\widehat{\Psi}$. Given the singular value decomposition in equation (I-5) we can get that the singular value decomposition of $\widehat{\Psi}\widehat{\Theta}$ can be expressed as:

$$\widehat{\Psi}\widehat{\Theta} = \widetilde{\mathbf{U}}\left(\widetilde{\mathbf{D}}\left(\frac{1}{2}\sqrt{\widetilde{\mathbf{D}}^2 + 4\mathbf{I}_q} - \frac{1}{2}\mathbf{I}_q\right)\right)\widetilde{\mathbf{U}}^\dagger \quad (\text{I-6})$$

The product of diagonal matrices always commutes, so we can directly check that (I-6) is also the singular value decomposition of $\widehat{\Theta}\widehat{\Psi}$.

To check that the proposed estimator satisfies the equation (I-3) it is enough to check that it also satisfies the pair of equations $\widehat{\Theta}\widehat{\Psi} = \mathbf{I}_q - \widehat{\Theta}^2$ and $\widehat{\Psi}\widehat{\Theta} = \mathbf{I}_q - \widehat{\Theta}^2$. The left side in both equations are equal, i.e. $\widehat{\Theta}\widehat{\Psi} = \widehat{\Psi}\widehat{\Theta}$, and given by formula (I-6), so, lets evaluate the right side:

$$\mathbf{I}_q - \widehat{\Theta}^2 = \mathbf{I}_q - \left(-\frac{1}{2}\widehat{\Psi} + \frac{1}{2}\sqrt{\widehat{\Psi}^2 + 4\lambda\mathbf{I}_q}\right)^2 \quad (\text{I-7})$$

Effectuating the matrix square operation in (I-7) we obtain:

$$\mathbf{I}_q - \widehat{\Theta}^2 = \mathbf{I}_q - \left(\frac{1}{2}\right)^2 \left(\widehat{\Psi}^2 - \widehat{\Psi}\sqrt{\widehat{\Psi}^2 + 4\mathbf{I}_q} - \sqrt{\widehat{\Psi}^2 + 4\mathbf{I}_q}\widehat{\Psi} + \widehat{\Psi}^2 + 4\mathbf{I}_q \right) \quad (\text{I-8})$$

From the singular value decomposition analysis above the matrices $\widehat{\Psi}$ and $\sqrt{\widehat{\Psi}^2 + 4\mathbf{I}_q}$ share the same eigenspace and thus commute, so, rearranging (I-8) it can be obtained that:

$$\mathbf{I}_q - \lambda\widehat{\Theta}^2 = \mathbf{I}_q - 2\left(\frac{1}{2}\right)^2 \widehat{\Psi}^2 + 2\left(\frac{1}{2}\right)^2 \widehat{\Psi}\sqrt{\widehat{\Psi}^2 + 4\mathbf{I}_q} - 4\left(\frac{1}{2}\right)^2 \mathbf{I}_q \quad (\text{I-9})$$

From (I-9) and considering (I-8) it is direct that following identity holds:

$$\mathbf{I}_q - \widehat{\boldsymbol{\Theta}}^2 = -\frac{1}{2}\widehat{\boldsymbol{\Psi}}^2 + \frac{1}{2}\widehat{\boldsymbol{\Psi}}\sqrt{\widehat{\boldsymbol{\Psi}}^2 + 4\mathbf{I}_q} = \widehat{\boldsymbol{\Psi}}\widehat{\boldsymbol{\Theta}} \quad (\text{I-10})$$

Now we need to proof that the proposed estimator is the unique solution of equation (I-3) that commute with $\widehat{\boldsymbol{\Psi}}$. Let $\widehat{\boldsymbol{\Phi}}$ be another solution that also commutes with $\widehat{\boldsymbol{\Psi}}$. Since the matrix $\widehat{\boldsymbol{\Phi}}$ commutes with $\widehat{\boldsymbol{\Psi}}$ it has the same eigenspace, i.e. it admits a singular value decomposition of the kind $\widehat{\boldsymbol{\Phi}} = \widetilde{\mathbf{U}}\widetilde{\mathbf{E}}\widetilde{\mathbf{U}}^\dagger$. Also, since $\widehat{\boldsymbol{\Phi}}$ satisfies equation (I-3) it can be checked that $-\widetilde{\mathbf{E}}^{-1} + \widetilde{\mathbf{D}} + \widetilde{\mathbf{E}} = \mathbf{0}_q$. The solution of this equation is straightforward given diagonal matrices $\widetilde{\mathbf{E}}$ and $\widetilde{\mathbf{D}}$, i.e. $\widetilde{\mathbf{E}} = \frac{1}{2}\sqrt{\widetilde{\mathbf{D}}^2 + 4\mathbf{I}_q} - \frac{1}{2}\mathbf{I}_q$. It shows that $\widehat{\boldsymbol{\Phi}} = \widehat{\boldsymbol{\Theta}}$ since they have identical eigenspace and eigenvalues. ■

The graphical Ridge estimatior is thus expressed by the following matrix square root formula:

$$\widehat{\boldsymbol{\Theta}} = -\frac{1}{2}\widehat{\boldsymbol{\Psi}} + \frac{1}{2}\sqrt{\widehat{\boldsymbol{\Psi}}^2 + 4\mathbf{I}_q} \quad (\text{I-11})$$

J-Connectivity estimator of the Local Quadratic Approximation

As for choosing the Penalty Function and Regularization Parameter there is not ubiquitous rule. It is usually assumed that, for a given Penalty Function, fitting the Regularization Parameter by some Statistical Criteria by would suffice to rule out the ambiguity on the Variable Selection sparsity level (Resolution). This approach does not provide a Statistical guarantee, as discussed in [\(Jankova and Van De Geer, 2015, 2017\)](#), due the biasing introduced in the estimation by the Sparse Penalty in any case. For the typical Graphical LASSO, a solution was recently presented in [\(Jankova and Van De Geer, 2018\)](#) through an unbiased Precision Matrix estimator $(\widehat{\boldsymbol{\Theta}}_u)^{(k+1)}_{unbiased}$.

$$(\widehat{\boldsymbol{\Theta}}_u)^{(k+1)}_{unbiased} = 2\widehat{\boldsymbol{\Theta}}_u^{(k+1)} - \widehat{\boldsymbol{\Theta}}_u^{(k+1)}\boldsymbol{\Psi}_u^{(k)}\widehat{\boldsymbol{\Theta}}_u^{(k+1)} \quad (\text{J-1})$$

For the conditions $\Pi(\mathbf{A}_u \odot \boldsymbol{\Theta}_u) = \|\boldsymbol{\Theta}_u\|_{1,\mathbf{A}_u}$ and $\alpha = \sqrt{\log(q)/m}$, it is demonstrated, for the elements into the unbiased estimator $((\widehat{\boldsymbol{\Theta}}_u)^{(k+1)}_{unbiased})_{ij}$, a tendency to the Model Precision Matrix elements $(\boldsymbol{\Theta}_u)_{ij}$ with Complex Normal pdf of consistent variances $\sigma_{ij}((\widehat{\boldsymbol{\Theta}}_u)^{(k+1)}_{unbiased}) = (\widehat{\boldsymbol{\Theta}}_u^{(k+1)})_{ii}(\widehat{\boldsymbol{\Theta}}_u^{(k+1)})_{jj} + (\widehat{\boldsymbol{\Theta}}_u^{(k+1)})_{ij}$ rated by \sqrt{m} :

$$((\widehat{\boldsymbol{\Theta}}_u)^{(k+1)}_{unbiased})_{ij} \sim N_1^{\mathbb{C}} \left(((\widehat{\boldsymbol{\Theta}}_u)^{(k+1)}_{unbiased})_{ij} \left| (\boldsymbol{\Theta}_u)_{ij}, \frac{\sigma_{ij}((\widehat{\boldsymbol{\Theta}}_u)^{(k+1)}_{unbiased})}{\sqrt{m}} \right. \right) \quad (\text{J-2})$$

At every iteration of the outer cycle indexed k -th, of the Parameters $\widehat{\boldsymbol{\iota}}_m^{(k)}$ and Hyperparameter $\widehat{\boldsymbol{\Omega}}^{(k)}$ estimators described in Section E, the unbiased Precision matrix estimator $(\widehat{\boldsymbol{\Theta}}_u)^{(k+1)}_{unbiased}$ should be computed by effectuating an inner cycle indexed l -th, of the Local Quadratic Approximation formulas (G-11) and (G-12). If we denote $\widehat{\boldsymbol{\Theta}}_u^{(k,l)}$ as the Local Quadratic Approximation Precision matrix estimator, the unbiased Precision matrix estimator is given by taking it to the limit:

$$(\widehat{\boldsymbol{\Theta}}_u)^{(k+1)}_{unbiased} \leftarrow \lim_{l \rightarrow \infty} (2\widehat{\boldsymbol{\Theta}}_u^{(k,l)} - \widehat{\boldsymbol{\Theta}}_u^{(k,l)}\boldsymbol{\Psi}_u^{(k)}\widehat{\boldsymbol{\Theta}}_u^{(k,l)}) \quad (\text{J-3})$$

Considering the unstandardization formula of the Precision matrix by its Standard estimator update $\widehat{\boldsymbol{\Theta}}_u^{(k,l+1)}$ at the $(l+1)$ -th iteration of the inner cycle, the Local Quadratic Approximation Precision matrix estimator update $\widehat{\boldsymbol{\Theta}}_u^{(k,l+1)}$ is computed as:

$$\widehat{\boldsymbol{\Theta}}_u^{(k,l+1)} = \widehat{\boldsymbol{\Gamma}}^{(k,l)} \odot \widehat{\boldsymbol{\Theta}}_u^{(k,l+1)} \quad (\text{J-4})$$

By substituting in formula [H.4] the Standard estimator $\widehat{\boldsymbol{\Theta}}_u^{(k,l+1)}$ given in formula (I-11) with Standard ESEC $(\boldsymbol{\Psi}_u^{(k)}{}^{-1} \oslash \widehat{\boldsymbol{\Gamma}}^{(k,l)})^{-1}$ we obtain:

$$\widehat{\Theta}_u^{(k,l+1)} = \frac{1}{2\lambda} \widehat{\Gamma}^{(k,l)} \odot \left(\sqrt{\left(\Psi_u^{(k)} \right)^{-1} \oslash \widehat{\Gamma}^{(k,l)}}^{-2} + 4\lambda \mathbf{I}_q} - \left(\Psi_u^{(k)} \right)^{-1} \oslash \widehat{\Gamma}^{(k,l)} \right)^{-1} \right) \quad (I-5)$$

The solution to the Weights estimator updates at the $(l+1)$ -th iteration of the inner cycle can be computed by (G-13), after substituting the Precision matrix estimator update $\widehat{\Theta}_u^{(k,l+1)}$.

$$\widehat{\Gamma}^{(k,l)} \leftarrow \left(-\mathbf{1}_q + \left(\mathbf{1}_q + 4(\lambda m)^2 \mathbf{A}^2 \odot \text{abs}(\widehat{\Theta}_u^{(k,l)})^2 \right)^{\frac{1}{2}} \right)^{\frac{1}{2}} \oslash \left(2^{\frac{1}{2}} (\lambda m)^{\frac{1}{2}} \mathbf{A} \right) \quad (I-6)$$

K-Cross-spectral formulation of the Elastic Net Structured Sparse Bayesian Learning

The results for complex LASSO of Section F can also be extended to the complex ENET, by the modification of Andrews and Mallows Lemma for Real ENET Gibbs pdf (Gaussian-Laplace). For the Real/Complex case the integral representation holds $e^{-a_1|z|-a_2|z|^2} \propto \int N_1(|z||0, f(\tau)) TGamma \left(\tau \left| \frac{1}{2}, 1, \left(\frac{a_1^2}{4a_2}, \infty \right) \right. \right) d\tau$, where the variance is defined as $f(\tau) = \frac{1}{2a_2} \left(1 - \frac{a_1^2}{4a_2\gamma} \right)$. The measurable space in which the variable $z|\tau$ is defined has a unnormalized density function given by the Gaussian pdf $p(z|\tau) = N_1(|z||0, f(\tau))$ and its variance $\gamma(\tau)$ is dependent on the random variable x which has Truncated Gamma pdf $p(\tau) = TGamma \left(\tau \left| \frac{1}{2}, 1, \left(\frac{a_1^2}{4a_2}, \infty \right) \right. \right)$. So, the measure in the space product of z and τ is has density represented as an unnormalized product of Gaussian and Gamma densities $p(z, \tau) \propto N_1(|z||0, f(\tau)) TGamma \left(\tau \left| \frac{1}{2}, 1, \left(\frac{a_1^2}{4a_2}, \infty \right) \right. \right)$.

If for all parameter component we define the group penalization across samples $z = \sqrt{\sum_{m=1}^m |(\boldsymbol{\iota}_m)_i|^2}$ and $f(\tau) = (\sigma_t^2)_i$. Then the transformed prior of the parameters is described analytically by the following prior distributions: $(\boldsymbol{\iota}_m)_i \sim N(|(\boldsymbol{\iota}_m)_i||0, (\sigma_t^2)_i)$, $\gamma_i \sim TGA \left(\gamma_i \left| \frac{1}{2}, 1, \left(\frac{a_1^2}{4a_2}, \infty \right) \right. \right)$. The full vector Bayesian model is as follows:

$$\mathbf{v}_m \sim N^C(\mathbf{v}_m | \mathbf{L}\boldsymbol{\iota}_m, \sigma_\xi^2 \mathbf{I}) \quad \text{"Likelihood"} \quad (K-1)$$

$$\boldsymbol{\iota}_m \sim N(|\boldsymbol{\iota}_m||0, diag(\boldsymbol{\sigma}_t^2)) \quad \text{"Parameters prior"} \quad (K-2)$$

$$\gamma \sim \prod_i TGA \left(\gamma_i \left| \frac{1}{2}, 1, \left(\frac{a_1^2}{4a_2}, \infty \right) \right. \right) \quad \text{"Hyperparameters prior"} \quad (K-3)$$

Proposition K-1

Let us define $\widehat{\boldsymbol{\mu}}_m = \widecheck{\Sigma}_u \mathbf{L}_{\mathbf{v}\boldsymbol{\iota}}^T (\sigma_\xi^2 \mathbf{I})^{-1} \mathbf{v}_m$ where $\widecheck{\Sigma}_u = \left(\mathbf{L}_{\mathbf{v}\boldsymbol{\iota}}^T (\sigma_\xi^2 \mathbf{I})^{-1} \mathbf{L}_{\mathbf{v}\boldsymbol{\iota}} + \frac{1}{2} (diag(\boldsymbol{\sigma}_t^2))^{-1} \right)^{-1}$ then for the joint distribution of data and parameters, $p(\mathbf{v}_m, \boldsymbol{\iota}_m) = N^C(\mathbf{v}_m | \mathbf{L}_{\mathbf{v}\boldsymbol{\iota}} \boldsymbol{\iota}_m, \sigma_\xi^2 \mathbf{I}) N(|\boldsymbol{\iota}_m||0, diag(\boldsymbol{\sigma}_t^2))$, the following factorization holds:

$$N^C(\mathbf{v}_m | \mathbf{L}_{\mathbf{v}\boldsymbol{\iota}} \boldsymbol{\iota}_m, \sigma_\xi^2 \mathbf{I}) N(|\boldsymbol{\iota}_m||0, diag(\boldsymbol{\sigma}_t^2)) = |\pi \widecheck{\Sigma}_u| N^C(\boldsymbol{\iota}_m | \widehat{\boldsymbol{\mu}}_m, \widecheck{\Sigma}_u) N^C(\mathbf{v}_m | \mathbf{L}_{\mathbf{v}\boldsymbol{\iota}} \widehat{\boldsymbol{\mu}}_m, \sigma_\xi^2 \mathbf{I}) N(|\widehat{\boldsymbol{\mu}}_m||0, diag(\boldsymbol{\sigma}_t^2)) \quad (K-4)$$

Proof of Proposition K-1

Writing explicitly the distributions given in formula (K-4):

$$N^C(\mathbf{v}_m | \mathbf{L}_{\mathbf{v}\boldsymbol{\iota}} \boldsymbol{\iota}, \sigma_\xi^2 \mathbf{I}) N(|\boldsymbol{\iota}_m||0, diag(\boldsymbol{\sigma}_t^2)) = \frac{1}{|\pi \sigma_\xi^2 \mathbf{I}|} e^{-(\mathbf{v}_m - \mathbf{L}_{\mathbf{v}\boldsymbol{\iota}} \boldsymbol{\iota}_m)^T (\sigma_\xi^2 \mathbf{I})^{-1} (\mathbf{v}_m - \mathbf{L}_{\mathbf{v}\boldsymbol{\iota}} \boldsymbol{\iota}_m)} \frac{1}{|2\pi diag(\boldsymbol{\sigma}_t^2)|^{\frac{1}{2}}} e^{-\frac{1}{2} \boldsymbol{\iota}_m^T (diag(\boldsymbol{\sigma}_t^2))^{-1} \boldsymbol{\iota}_m} \quad (K-5)$$

The form of the resultant distribution can be found by analyzing the terms that depend on the parameters (exponential argument) in formula (K-5):

$$-\mathbf{v}_m^\dagger (\sigma_\xi^2 \mathbf{I})^{-1} \mathbf{v}_m - \boldsymbol{\iota}_m^\dagger \mathbf{L}_{\nu\iota}^T (\sigma_\xi^2 \mathbf{I})^{-1} \mathbf{L}_{\nu\iota} \boldsymbol{\iota}_m + \mathbf{v}_m^\dagger (\sigma_\xi^2 \mathbf{I})^{-1} \mathbf{L}_{\nu\iota} \boldsymbol{\iota}_m + \boldsymbol{\iota}_m^\dagger \mathbf{L}_{\nu\iota}^T (\sigma_\xi^2 \mathbf{I})^{-1} \mathbf{v}_m - \frac{1}{2} \boldsymbol{\iota}_m^\dagger (\text{diag}(\boldsymbol{\sigma}_\iota^2))^{-1} \boldsymbol{\iota}_m \quad (\text{K-6})$$

Reorganizing the exponent (K-6) in terms of $\hat{\boldsymbol{\mu}}_m$ and $\check{\boldsymbol{\Sigma}}_u$ we obtain.

$$-(\boldsymbol{\iota}_m - \hat{\boldsymbol{\mu}}_m)^\dagger \check{\boldsymbol{\Sigma}}_u^{-1} (\boldsymbol{\iota}_m - \hat{\boldsymbol{\mu}}_m) - \mathbf{v}_m^\dagger (\sigma_\xi^2 \mathbf{I})^{-1} \mathbf{v}_m + \hat{\boldsymbol{\mu}}_m^\dagger \check{\boldsymbol{\Sigma}}_u^{-1} \hat{\boldsymbol{\mu}}_m \quad (\text{K-7})$$

Completing terms (K-7) with the terms: $-\mathbf{v}_m^\dagger (\sigma_\xi^2 \mathbf{I})^{-1} \mathbf{L}_{\nu\iota} \hat{\boldsymbol{\mu}}_m$, $-\hat{\boldsymbol{\mu}}_m^\dagger \mathbf{L}_{\nu\iota}^T (\sigma_\xi^2 \mathbf{I})^{-1} \mathbf{v}_m$ and $+\hat{\boldsymbol{\mu}}_m^\dagger \mathbf{L}_{\nu\iota}^T (\sigma_\xi^2 \mathbf{I})^{-1} \mathbf{L}_{\nu\iota} \hat{\boldsymbol{\mu}}_m$ we obtain.

$$-(\boldsymbol{\iota}_m - \hat{\boldsymbol{\mu}}_m)^\dagger \check{\boldsymbol{\Sigma}}_u^{-1} (\boldsymbol{\iota}_m - \hat{\boldsymbol{\mu}}_m) - (\mathbf{v}_m - \mathbf{L}_{\nu\iota} \hat{\boldsymbol{\mu}}_m)^\dagger (\sigma_\xi^2 \mathbf{I})^{-1} (\mathbf{v}_m - \mathbf{L}_{\nu\iota} \hat{\boldsymbol{\mu}}_m) - \mathbf{v}_m^\dagger (\sigma_\xi^2 \mathbf{I})^{-1} \mathbf{L}_{\nu\iota} \hat{\boldsymbol{\mu}}_m - \hat{\boldsymbol{\mu}}_m^\dagger \mathbf{L}_{\nu\iota}^T (\sigma_\xi^2 \mathbf{I})^{-1} \mathbf{v}_m + \hat{\boldsymbol{\mu}}_m^\dagger \mathbf{L}_{\nu\iota}^T (\sigma_\xi^2 \mathbf{I})^{-1} \mathbf{L}_{\nu\iota} \hat{\boldsymbol{\mu}}_m + \hat{\boldsymbol{\mu}}_m^\dagger \check{\boldsymbol{\Sigma}}_u^{-1} \hat{\boldsymbol{\mu}}_m \quad (\text{K-8})$$

In formula (K-8) the third and fourth term can be added with the sixth: due to $\mathbf{L}_{\nu\iota}^T (\sigma_\xi^2 \mathbf{I})^{-1} \mathbf{v}_m = \check{\boldsymbol{\Sigma}}_u^{-1} \hat{\boldsymbol{\mu}}_m$.

$$-(\boldsymbol{\iota}_m - \hat{\boldsymbol{\mu}}_m)^\dagger \check{\boldsymbol{\Sigma}}_u^{-1} (\boldsymbol{\iota}_m - \hat{\boldsymbol{\mu}}_m) - (\mathbf{v}_m - \mathbf{L}_{\nu\iota} \hat{\boldsymbol{\mu}}_m)^\dagger (\sigma_\xi^2 \mathbf{I})^{-1} (\mathbf{v}_m - \mathbf{L}_{\nu\iota} \hat{\boldsymbol{\mu}}_m) - \hat{\boldsymbol{\mu}}_m^\dagger \check{\boldsymbol{\Sigma}}_u^{-1} \hat{\boldsymbol{\mu}}_m + \hat{\boldsymbol{\mu}}_m^\dagger \mathbf{L}_{\nu\iota}^T (\sigma_\xi^2 \mathbf{I})^{-1} \mathbf{L}_{\nu\iota} \hat{\boldsymbol{\mu}}_m \quad (\text{K-9})$$

Finally, rearranging terms in (K-9) we obtain.

$$-(\boldsymbol{\iota}_m - \hat{\boldsymbol{\mu}}_m)^\dagger \check{\boldsymbol{\Sigma}}_u^{-1} (\boldsymbol{\iota}_m - \hat{\boldsymbol{\mu}}_m) - (\mathbf{v}_m - \mathbf{L}_{\nu\iota} \hat{\boldsymbol{\mu}}_m)^\dagger (\sigma_\xi^2 \mathbf{I})^{-1} (\mathbf{v}_m - \mathbf{L}_{\nu\iota} \hat{\boldsymbol{\mu}}_m) - \frac{1}{2} \hat{\boldsymbol{\mu}}_m^\dagger (\text{diag}(\boldsymbol{\sigma}_\iota^2))^{-1} \hat{\boldsymbol{\mu}}_m \quad (\text{K-10})$$

From (K-10) it holds that:

$$\mathbf{N}^{\mathbb{C}}(\mathbf{v}_m | \mathbf{L}_{\nu\iota} \boldsymbol{\iota}_m, \sigma_\xi^2 \mathbf{I}) \mathbf{N}(|\boldsymbol{\iota}_m| | 0, \text{diag}(\boldsymbol{\sigma}_\iota^2)) = |\pi \check{\boldsymbol{\Sigma}}_u| \mathbf{N}^{\mathbb{C}}(\boldsymbol{\iota}_m | \hat{\boldsymbol{\mu}}_m, \check{\boldsymbol{\Sigma}}_u) \mathbf{N}^{\mathbb{C}}(\mathbf{v}_m | \mathbf{L}_{\nu\iota} \hat{\boldsymbol{\mu}}_m, \sigma_\xi^2 \mathbf{I}) \mathbf{N}(|\hat{\boldsymbol{\mu}}_m| | 0, \text{diag}(\boldsymbol{\sigma}_\iota^2)) \blacksquare \quad (\text{K-11})$$

The estimation formulas can be derived by applying maximum posterior analysis to the hyperparameters, as in (Paz-Linares et al., 2017). Note the changes in notation used here with respect to the latter manuscript: $\Lambda := \boldsymbol{\sigma}_\iota^2$, $\hat{\Lambda} := \check{\boldsymbol{\sigma}}_\iota^2$, $\beta := \sigma_\xi^2$, $a_1 := a_2$, $a_2 := a_1$, $r := \frac{a_1^2}{4a_2}$, $\bar{\Sigma} := \check{\boldsymbol{\Sigma}}_u$, $S := q$. With starting hyperparameters $\alpha_2^{(0)}$, $r^{(0)}$, $(\sigma_\xi^2)^{(0)}$ and $(\boldsymbol{\sigma}_\iota^2)^{(0)}$ the estimators are as follows:

$$\mathbf{S}_{vv} = \frac{1}{m} \sum_{m=1}^m \mathbf{v}_m \mathbf{v}_m^\dagger \quad (\text{K-12})$$

$$\check{\boldsymbol{\Sigma}}_u^{(k+1)} \leftarrow \left((\sigma_\xi^{-2})^{(k)} \mathbf{L}_{\nu\iota}^T \mathbf{L}_{\nu\iota} + \frac{1}{2} (\text{diag}((\boldsymbol{\sigma}_\iota^2)^{(k)}))^{-1} \right)^{-1} \quad (\text{K-13})$$

$$\mathbf{S}_{\mu\mu}^{(k+1)} \leftarrow \frac{1}{m} \sum_{m=1}^m \hat{\boldsymbol{\mu}}_m^{(k)} (\hat{\boldsymbol{\mu}}_m^{(k)})^\dagger \leftarrow (\sigma_\xi^{-4})^{(k)} \check{\boldsymbol{\Sigma}}_u^{(k+1)} \mathbf{L}_{\nu\iota}^T \mathbf{S}_{vv} \mathbf{L}_{\nu\iota} \check{\boldsymbol{\Sigma}}_u^{(k+1)} \quad (\text{K-14})$$

$$(\boldsymbol{\sigma}_\iota^2)_i^{(k+1)} = \frac{1}{2\alpha_2^{(k)}} (\check{\boldsymbol{\sigma}}_\iota^2)_i^{(k+1)} \quad (\text{K-15})$$

Where $(\check{\boldsymbol{\sigma}}_\iota^2)_i^{(k+1)} = \eta_i^{(k+1)} / (r^{(k)} + \eta_i^{(k+1)})$, for $i = 1:q$, and $\eta_i^{(k+1)}$ expressed as:

$$\eta_i^{(k+1)} = -\frac{1}{4} + \sqrt{\frac{1}{16} + \left((\mathbf{S}_{\mu\mu}^{(k+1)})_{ii} + (\bar{\Sigma}_u^{(k+1)})_{ii} \right) \alpha_2^{(k)} r^{(k)}}, \text{ for } i = 1:q \quad (K-16)$$

$$\alpha_2^{(k+1)} = \binom{q}{2} / \sum_{i=1}^q \left(\frac{(\mathbf{S}_{\mu\mu}^{(k+1)})_{ii} + (\bar{\Sigma}_u^{(k+1)})_{ii}}{(\sigma_i^2)^{(k+1)}} \right) \quad (K-17)$$

$$r^{(k)} = \text{argmin} |F(r)| \quad (K-18)$$

$$F(r) = \sum_{i=1}^q \left(\frac{1}{1 - (\sigma_i^2)^{(k+1)}} \right) + v - \left(\tau - \frac{q}{2} \right) \frac{1}{r} - q(\pi r)^{-\frac{1}{2}} e^{-r} / \int_r^\infty Ga\left(x \middle| \frac{1}{2}, 1\right) dx \quad (K-19)$$

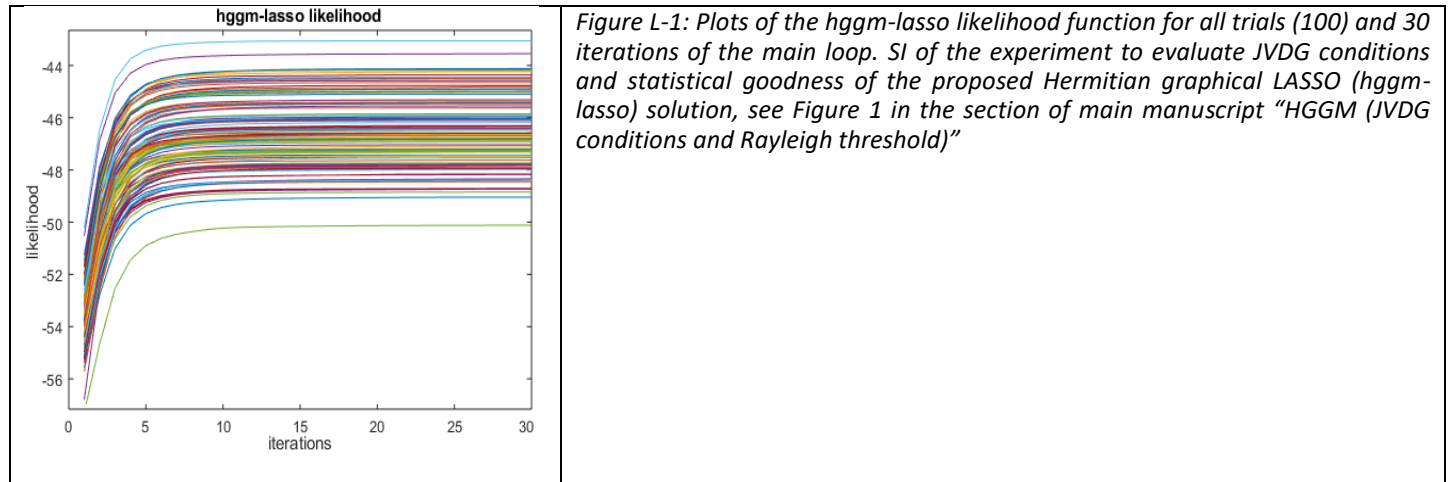
After convergence of the ENET-SSBL we can threshold the estimated source activity by constraining a biased statistic: this is due to the posterior distribution of source activity $N^{\mathbb{C}}(\boldsymbol{\iota}_m | \hat{\boldsymbol{\mu}}_m, \bar{\Sigma}_u)$. In this distribution $\hat{\boldsymbol{\mu}}_m$ is the posterior mean and $\bar{\Sigma}_u$ the posterior covariance. The z-statistic for the analysis of variance has the following form:

$$z_stat = \text{sqrt}(\text{diag}(\mathbf{S}_{\mu\mu}^{(\infty)}). / (\sigma_i^2)^{(\infty)}) \quad (K-20)$$

A plausible way to screen out the active sources is to extract the set of nodes \mathcal{J} that return a value of the z-statistic greater than 1:

$$\mathcal{J} = \{i: z_stat_i \geq 1\} \quad (K-21)$$

L-Model's statistical goodness



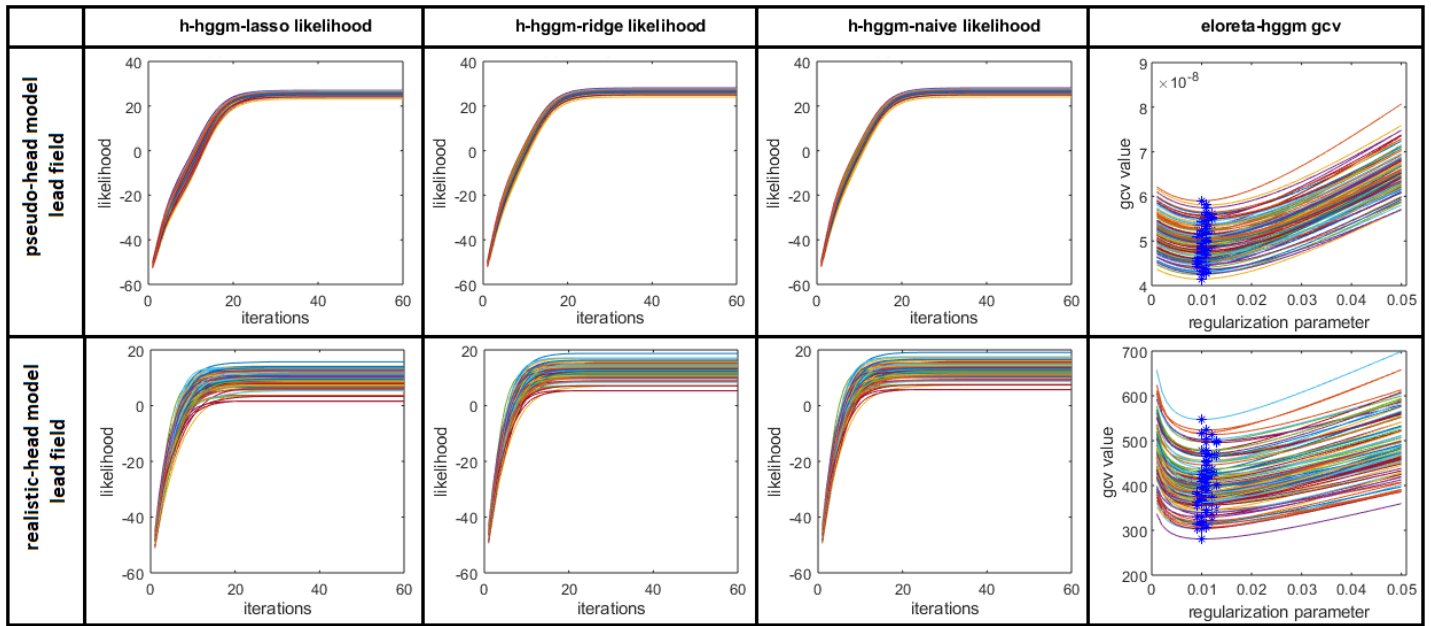


Figure L-2: Likelihood evolution along 60 iterations of the h-hggm main loop and the eloreta-hggm generalized cross-validation for all simulated trials (100). It was computed for both lead fields: pseudo (top row) and realistic (bottom row), see Figure 2 and Table 1 in the section of main manuscript “H-HGGM (connectivity distortion by the Lead Field)”.

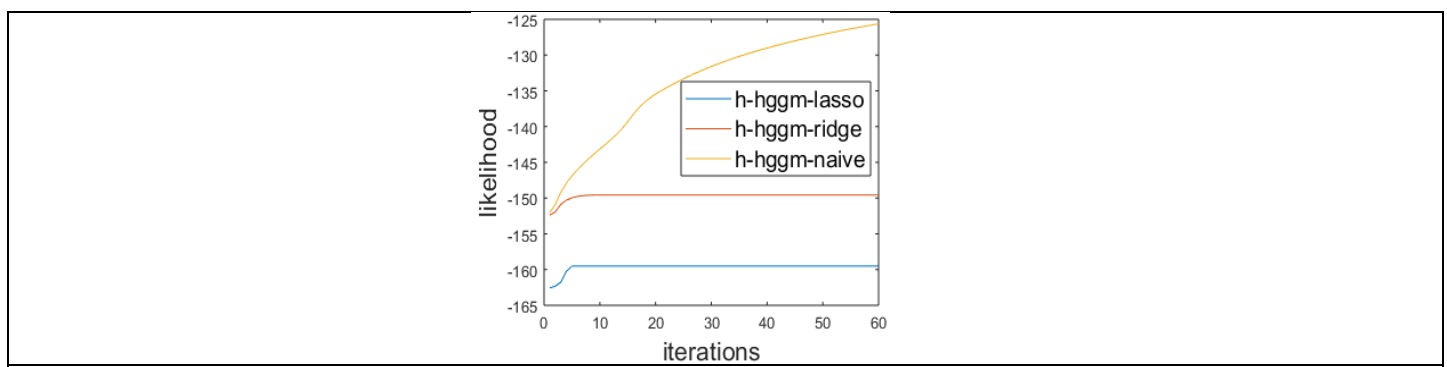


Figure L-3: Likelihood evolution along 60 iterations of the h-hggm main loop in the human SSVEP.

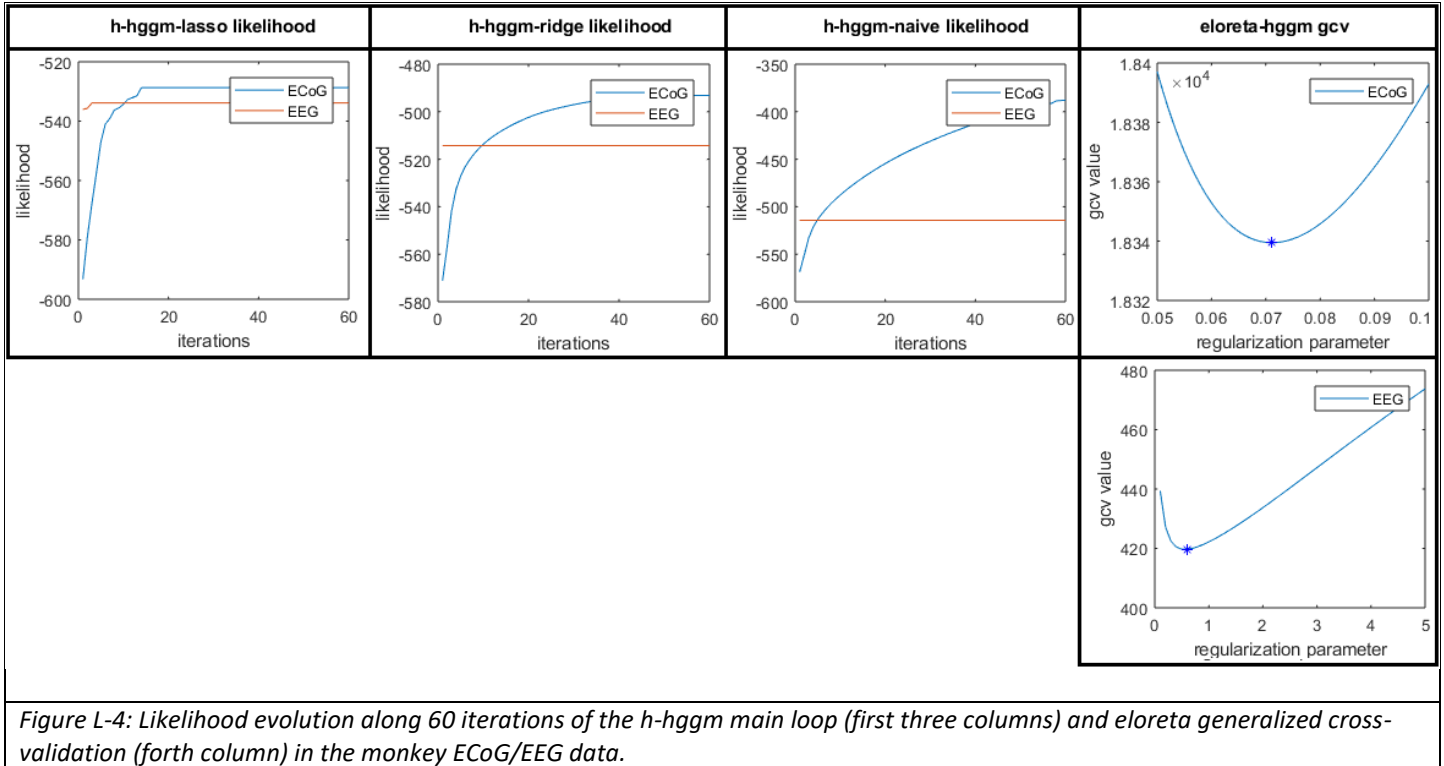


Figure L-4: Likelihood evolution along 60 iterations of the h-hggm main loop (first three columns) and eloreta generalized cross-validation (forth column) in the monkey ECoG/EEG data.

Table L-5: Distances in matrix space between the connectivity estimated from EEG and ECoG for all methods. Alpha-div: . Kullback: Kullback Leibler divergence. LD: . Log-Euclid: Logarithm of the Euclidean distance. Opt-Transp: . Riemann: Riemann distance.						
	Alpha-Div	Kullback	LD	Log-Euclid	Opt-Transp	Riemann
'h-hggm-lasso'	0.0049	0.0404	0.0202	0.0033	0.0288	0.0572
'h-hggm-ridge'	0.008	0.0519	0.0259	0.0054	0.0369	0.0733
'h-hggm-naive'	0.2392	0.2737	0.1361	0.1488	0.2073	0.3857
'eloreta-hggm'	0.9256	0.4263	0.2131	0.3633	0.3012	0.6027
'lcmv-hggm'	1.6366	0.538	0.269	0.5788	0.3797	0.7608

References for the Supplementary Information

[43] Andrews, D.F. and Mallows, C.L., 1974. Scale mixtures of normal distributions. *Journal of the Royal Statistical Society. Series B (Methodological)*, pp.99-102.
<https://www.jstor.org/stable/2984774>

[44] Attias, H., 2000. A variational bayesian framework for graphical models. In *Advances in neural information processing systems* (pp. 209-215).

[45] Bosch-Bayard, J. and Viscay, R.J., 2018. Several drawbacks in brain connectivity assessment based on source estimates - elucidations, practical guidelines, and incentives for further research. Submitted to *Brain Topography*.

[46] Baccalá, L.A. and Sameshima, K., 2001. Partial directed coherence: a new concept in neural structure determination. *Biological cybernetics*, 84(6), pp.463-474.
<https://doi.org/10.1007/PL000079>

[47] Balkan, O., Kreutz-Delgado, K. and Makeig, S., 2014. Localization of more sources than sensors via jointly-sparse Bayesian learning. *IEEE Signal Processing Letters*, 21(2), pp.131-134.
<https://doi.org/10.1109/LSP.2013.2294862>

[48] Belardinelli, P., Ortiz, E., Barnes, G., Noppeney, U. and Preissl, H., 2012. Source reconstruction accuracy of MEG and EEG Bayesian inversion approaches. *PloS one*, 7(12), p.e51985.
<https://doi.org/10.1371/journal.pone.0051985>

[49] Babiloni, F., Cincotti, F., Babiloni, C., Carducci, F., Mattia, D., Astolfi, L., Basilisco, A., Rossini, P.M., Ding, L., Ni, Y. and Cheng, J., 2005. Estimation of the cortical functional connectivity with the multimodal integration of high-resolution EEG and fMRI data by directed transfer function. *Neuroimage*, 24(1), pp.118-131.
<https://doi.org/10.1016/j.neuroimage.2004.09.036>

[50] Danaher, P., Wang, P. and Witten, D.M., 2014. The joint graphical lasso for inverse covariance estimation across multiple classes. *Journal of the Royal Statistical Society: Series B (Statistical Methodology)*, 76(2), pp.373-397.
<https://doi.org/10.1111/rssb.12033>

[51] David, O. and Friston, K.J., 2003. A neural mass model for MEG/EEG:: coupling and neuronal dynamics. *NeuroImage*, 20(3), pp.1743-1755.
<https://doi.org/10.1016/j.neuroimage.2003.07.015>

[52] Drton, M., Massam, H. and Olkin, I., 2008. Moments of minors of Wishart matrices. *The Annals of Statistics*, 36(5), pp.2261-2283.
<https://doi.org/10.1214/07-AOS522>

[53] Daunizeau, J. and Friston, K.J., 2007. A mesostate-space model for EEG and MEG. *NeuroImage*, 38(1), pp.67-81.
<https://doi.org/10.1016/j.neuroimage.2007.06.034>

[54] Deco, G., Jirsa, V.K., Robinson, P.A., Breakspear, M. and Friston, K., 2008. The dynamic brain: from spiking neurons to neural masses and cortical fields. *PLoS computational biology*, 4(8), p.e1000092.
<https://doi.org/10.1371/journal.pcbi.1000092>

[55] Dempster, A.P., Laird, N.M. and Rubin, D.B., 1977. Maximum likelihood from incomplete data via the EM algorithm. *Journal of the royal statistical society. Series B (methodological)*, pp.1-38.
<https://www.jstor.org/stable/2984875>

[56] Ephremidze, L., Janashia, G. and Lagvilava, E., 2007, September. A new efficient matrix spectral factorization algorithm. In *SICE, 2007 Annual Conference* (pp. 20-23). IEEE.
<https://doi.org/10.1109/SICE.2007.4420943>

[57] Faes, L. and Nollo, G., 2011. Multivariate frequency domain analysis of causal interactions in physiological time series. In *Biomedical Engineering, Trends in Electronics, Communications and Software*. InTech.

[58] Fan J and Li R.: Variable Selection via Nonconcave Penalized Likelihood and Its Oracle Properties. *Journal of the American Statistical Association*. 2001; 96: pp1348-1360.
<https://doi.org/10.1198/016214501753382273>

[59] Freeman WJ (1975) Mass action in the nervous system. New York: Academic Press.

[60] Friston, K., Harrison, L., Daunizeau, J., Kiebel, S., Phillips, C., Trujillo-Barreto, N., Henson, R., Flandin, G. and Mattout, J., 2008. Multiple sparse priors for the M/EEG inverse problem. *NeuroImage*, 39(3), pp.1104-1120.
<https://doi.org/10.1016/j.neuroimage.2007.09.048>

[61] Friston, K., 2009. Causal modelling and brain connectivity in functional magnetic resonance imaging. *PLoS biology*, 7(2), p.e1000033.
<https://doi.org/10.1371/journal.pbio.1000033>

[62] Friston, K.J., 2011. Functional and effective connectivity: a review. *Brain connectivity*, 1(1), pp.13-36.
<https://doi.org/10.1089/brain.2011.0008>

[63] Friedman, J., Hastie, T. and Tibshirani, R., 2008. Sparse inverse covariance estimation with the graphical lasso. *Biostatistics*, 9(3), pp.432-441.

[64] Faes, L., Erla, S. and Nollo, G., 2012. Measuring connectivity in linear multivariate processes: definitions, interpretation, and practical analysis. *Computational and mathematical methods in medicine*, 2012.
<http://dx.doi.org/10.1155/2012/140513>

[65] Faul, A.C. and Tipping, M.E., 2002. Analysis of sparse Bayesian learning. In *Advances in neural information processing systems* (pp. 383-389).

[66] Galka, A., Yamashita, O., Ozaki, T., Biscay, R. and Valdés-Sosa, P., 2004. A solution to the dynamical inverse problem of EEG generation using spatiotemporal Kalman filtering. *NeuroImage*, 23(2), pp.435-453.

[67] <https://doi.org/10.1016/j.neuroimage.2004.02.022>
 Goodman, N.R., 1963. Statistical analysis based on a certain multivariate complex Gaussian distribution (an introduction). *The Annals of mathematical statistics*, 34(1), pp.152-177.
<https://www.jstor.org/stable/2991290>

[68] Honorio, J. and Jaakkola, T.S., 2013. Inverse covariance estimation for high-dimensional data in linear time and space: Spectral methods for riccati and sparse models. *arXiv preprint arXiv:1309.6838*.
<https://arxiv.org/abs/1309.6838>

[69] Jafarian, A. and McWhirter, J.G., 2012, August. A novel method for multichannel spectral factorization. In *Signal Processing Conference (EUSIPCO), 2012 Proceedings of the 20th European* (pp. 1069-1073). IEEE.

[70] Janashia, G., Lagvilava, E. and Ephremidze, L., 2011. A new method of matrix spectral factorization. *IEEE Transactions on information theory*, 57(4), pp.2318-2326.
<https://doi.org/10.1109/TIT.2011.2112233>

[71] Jankova, J. and Van De Geer, S., 2015. Confidence intervals for high-dimensional inverse covariance estimation. *Electronic Journal of Statistics*, 9(1), pp.1205-1229.
<https://doi.org/10.1214/15-EJS1031>

[72] Janková, J. and van de Geer, S., 2017. Honest confidence regions and optimality in high-dimensional precision matrix estimation. *Test*, 26(1), pp.143-162.
<https://doi.org/10.1007/s11749-016-0503-5>

[73] Jankova, J. and van de Geer, S., 2018. Inference in high-dimensional graphical models. *arXiv preprint arXiv:1801.08512*.
<https://arxiv.org/abs/1801.08512>

[74] Jirsa, V.K. and Haken, H., 1996. Field theory of electromagnetic brain activity. *Physical Review Letters*, 77(5), p.960.
<https://doi.org/10.1103/PhysRevLett.77.960>

[75] Jordan, M.I. ed., 1998. *Learning in graphical models* (Vol. 89). Springer Science & Business Media.
<https://doi.org/10.1007/978-94-011-5014-9>

[76] Kaminski, M.J. and Blinowska, K.J., 1991. A new method of the description of the information flow in the brain structures. *Biological cybernetics*, 65(3), pp.203-210.
<https://doi.org/10.1007/BF00198091>

[77] Karahan, E., Rojas-López, P.A., Bringas-Vega, M.L., Valdés-Hernández, P.A. and Valdes-Sosa, P.A., 2015. Tensor Analysis and Fusion of Multimodal Brain Images. *Proceedings of the IEEE*, 103(9), pp.1531-1559.
<https://doi.org/10.1109/JPROC.2015.2455028>

[78] Kyung, M., Gill, J., Ghosh, M. and Casella, G., 2010. Penalized regression, standard errors, and Bayesian lassos. *Bayesian Analysis*, 5(2), pp.369-411.
<https://doi.org/10.1214/10-BA607>

[79] Li, Q. and Lin, N., 2010. The Bayesian elastic net. *Bayesian Analysis*, 5(1), pp.151-170.
<https://doi.org/10.1214/10-BA506>

[80] Lim, Y., 2006. The matrix golden mean and its applications to Riccati matrix equations. *SIAM Journal on Matrix Analysis and Applications*, 29(1), pp.54-66.
<https://doi.org/10.1137/050645026>

[81] Liu, C. and Rubin, D.B., 1994. The ECME algorithm: a simple extension of EM and ECM with faster monotone convergence. *Biometrika*, 81(4), pp.633-648.
<https://doi.org/10.1093/biomet/81.4.633>

[82] Ljung, L. and Glover, K., 1981. Frequency domain versus time domain methods in system identification. *Automatica*, 17(1), pp.71-86.
[https://doi.org/10.1016/0005-1098\(81\)90085-6](https://doi.org/10.1016/0005-1098(81)90085-6)

[83] McLachlan, G. and Krishnan, T., 2007. *The EM algorithm and extensions* (Vol. 382). John Wiley & Sons.

[84] MacKay D J C. *Information Theory, Inference, and Learning Algorithms*. Cambridge University Press 2003.
<https://doi.org/10.2277/0521642981>

[85] Paz-Linares, D., Vega-Hernandez, M., Rojas-Lopez, P.A., Valdes-Hernandez, P.A., Martinez-Montes, E. and Valdes-Sosa, P.A., 2017. Spatio temporal EEG source imaging with the hierarchical bayesian elastic net and elitist lasso models. *Frontiers in neuroscience*, 11, p.635.
<https://doi.org/10.3389/fnins.2017.00635>

[86] Rosenblatt, M., 1956. A central limit theorem and a strong mixing condition. *Proceedings of the National Academy of Sciences*, 42(1), pp.43-47.
<https://doi.org/10.1073/pnas.42.1.43>

[87] Roweis, S. and Ghahramani, Z., 1999. A unifying review of linear Gaussian models. *Neural computation*, 11(2), pp.305-345.

<https://doi.org/10.1162/089976699300016674>

[88] Sayed, A.H. and Kailath, T., 2001. A survey of spectral factorization methods. *Numerical linear algebra with applications*, 8(6-7), pp.467-496.
<https://doi.org/10.1002/bla.250>

[89] Schmolck, A. and Everson, R., 2007. Smooth relevance vector machine: a smoothness prior extension of the RVM. *Machine Learning*, 68(2), pp.107-135.
<https://doi.org/10.1007/s10994-007-5012-z>

[90] Sánchez-Bornot J M, Martínez-Montes E, Lage-Castellanos A, Vega-Hernández M and Valdés-Sosa P A. Uncovering sparse brain effective connectivity: A voxel-based approach using penalized regression. *Statistica Sinica* 2008; 18: 1501-1518.
<https://www.jstor.org/stable/24308566>

[91] Schmidt, M., 2010. Graphical model structure learning with l1-regularization. *University of British Columbia*.

[92] Schoukens, J., Pintelon, R. and Rolain, Y., 2004, June. Time domain identification, frequency domain identification. *Equivalencies? Differences?*. In *American Control Conference*, 2004. *Proceedings of the 2004* (Vol. 1, pp. 661-666). IEEE.
<https://doi.org/10.23919/ACC.2004.1383679>

[93] Srivastava, M.S., 1965. On the complex Wishart distribution. *The Annals of mathematical statistics*, 36(1), pp.313-315.
<https://www.jstor.org/stable/2238098>

[94] Schwartz, B., Gannot, S. and Habets, E.A., 2017. Two Model-Based EM Algorithms for Blind Source Separation in Noisy Environments. *IEEE/ACM Transactions on Audio, Speech, and Language Processing*, 25(11), pp.2209-2222.
<https://doi.org/10.1109/TASLP.2017.2738438>

[95] Tipping, M.E., 2001. Sparse Bayesian learning and the relevance vector machine. *Journal of machine learning research*, 1(Jun), pp.211-244.
<https://doi.org/10.1162/15324430152748236>

[96] Valdés-Sosa, P., Martí, F., García, F. and Casanova, R., 2000. Variable resolution electric-magnetic tomography. In *Biomag 96* (pp. 373-376). Springer, New York, NY.
https://doi.org/10.1007/978-1-4612-1260-7_91

[97] Valdés-Sosa, P.A., Bornot-Sánchez, J.M., Vega-Hernández, M., Melie-García, L., Lage-Castellanos, A. and Canales-Rodríguez, E., 2006. 18 granger causality on spatial manifolds: applications to neuroimaging. *Handbook of time series analysis: recent theoretical developments and applications*, pp.461-491.
<https://doi.org/10.1002/9783527609970.ch18>

[98] Valdés-Sosa, P.A., Sánchez-Bornot, J.M., Lage-Castellanos, A., Vega-Hernández, M., Bosch-Bayard, J., Melie-García, L. and Canales-Rodríguez, E., 2005. Estimating brain functional connectivity with sparse multivariate autoregression. *Philosophical Transactions of the Royal Society of London B: Biological Sciences*, 360(1457), pp.969-981.
<https://doi.org/10.1098/rstb.2005.1654>

[99] Valdés-Sosa, P.A., Roebroek, A., Daunizeau, J. and Friston, K., 2011. Effective connectivity: influence, causality and biophysical modeling. *Neuroimage*, 58(2), pp.339-361.
<https://doi.org/10.1016/j.neuroimage.2011.03.058>

[100] Valdés-Sosa, P.A., Sanchez-Bornot, J.M., Sotero, R.C., Iturria-Medina, Y., Aleman-Gomez, Y., Bosch-Bayard, J., Carbonell, F. and Ozaki, T., 2009. Model driven EEG/fMRI fusion of brain oscillations. *Human brain mapping*, 30(9), pp.2701-2721.
<https://doi.org/10.1002/hbm.20704>

[101] Valdes, P.A., Jiménez, J.C., Riera, J., Biscay, R. and Ozaki, T., 1999. Nonlinear EEG analysis based on a neural mass model. *Biological cybernetics*, 81(5-6), pp.415-424.
<https://doi.org/10.1007/s004220050050>

[102] Valdés-Hernández, P.A., von Ellenrieder, N., Ojeda-Gonzalez, A., Kochen, S., Alemán-Gómez, Y., Muravchik, C. and Valdés-Sosa, P.A., 2009. Approximate average head models for EEG source imaging. *Journal of neuroscience methods*, 185(1), pp.125-132. Valdés-Sosa, P.A., 2004. Spatio-temporal autoregressive models defined over brain manifolds. *Neuroinformatics*, 2(2), pp.239-250.
<https://doi.org/10.1016/j.jneumeth.2009.09.005>

[103] Van Hoey, G., Van de Walle, R., Vanrumste, B., D'Havse, M., Lemahieu, I. and Boon, P., 1999. Beamforming techniques applied in EEG source analysis. *Proc. ProRISC99*, 10, pp.545-549.

[104] Wang, H., 2012. Bayesian graphical lasso models and efficient posterior computation. *Bayesian Analysis*, 7(4), pp.867-886.
<https://doi.org/10.1214/12-BA729>

[105] Wang, H., 2014. Coordinate descent algorithm for covariance graphical lasso. *Statistics and Computing*, 24(4), pp.521-529.
<https://doi.org/10.1007/s11222-013-9385-5>

[106] Wang, X., Quost, B., Chazot, J.D. and Antoni, J., 2016. Estimation of multiple sound sources with data and model uncertainties using the EM and evidential EM algorithms. *Mechanical Systems and Signal Processing*, 66, pp.159-177.

<https://doi.org/10.1016/j.ymssp.2015.06.011>

[107] Wu, W., Nagarajan, S. and Chen, Z., 2016. Bayesian Machine Learning: EEG/MEG signal processing measurements. *IEEE Signal Processing Magazine*, 33(1), pp.14-36.
<https://doi.org/10.1109/MSP.2015.2481559>

[108] Wipf, D.P., Owen, J.P., Attias, H.T., Sekihara, K. and Nagarajan, S.S., 2010. Robust Bayesian estimation of the location, orientation, and time course of multiple correlated neural sources using MEG. *NeuroImage*, 49(1), pp.641-655.
<https://doi.org/10.1016/j.neuroimage.2009.06.083>

[109] Wipf, D. and Nagarajan, S., 2009. A unified Bayesian framework for MEG/EEG source imaging. *NeuroImage*, 44(3), pp.947-966.
<https://doi.org/10.1016/j.neuroimage.2008.02.059>

[110] Wipf, D.P. and Rao, B.D., 2007. An empirical Bayesian strategy for solving the simultaneous sparse approximation problem. *IEEE Transactions on Signal Processing*, 55(7), pp.3704-3716.
<https://doi.org/10.1109/TSP.2007.894265>

[111] Wipf, D.P., Ramirez, R.R., Palmer, J.A., Makeig, S. and Rao, B.D., 2006. Automatic Relevance Determination for Source Localization with MEG and EEG Data. Technical Report, University of California, San Diego.

[112] Wills, A., Ninness, B. and Gibson, S., 2009. Maximum likelihood estimation of state space models from frequency domain data. *IEEE Transactions on Automatic Control*, 54(1), pp.19-33.
<https://doi.org/10.1109/TAC.2008.2009485>

[113] Yuan, G., Tan, H. and Zheng, W.S., 2017. A Coordinate-wise Optimization Algorithm for Sparse Inverse Covariance Selection. arXiv preprint arXiv:1711.07038.
<https://arxiv.org/abs/1711.07038>

[114] Zhang, T. and Zou, H., 2014. Sparse precision matrix estimation via lasso penalized D-trace loss. *Biometrika*, 101(1), pp.103-120.
<https://doi.org/10.1093/biomet/ast059>

[115] Zhang, Y., Wang, Y., Jin, J. and Wang, X., 2017. Sparse Bayesian learning for obtaining sparsity of EEG frequency bands based feature vectors in motor imagery classification. *International journal of neural systems*, 27(02), p.1650032.
<https://doi.org/10.1142/S0129065716500325>

[116] Zhang, Y., Zhou, G., Jin, J., Zhao, Q., Wang, X. and Cichocki, A., 2016. Sparse Bayesian classification of EEG for brain-computer interface. *IEEE transactions on neural networks and learning systems*, 27(11), pp.2256-2267.
<https://doi.org/10.1109/TNNLS.2015.2476656>

[117] Zhang, Z. and Rao, B.D., 2011. Sparse signal recovery with temporally correlated source vectors using sparse Bayesian learning. *IEEE Journal of Selected Topics in Signal Processing*, 5(5), pp.912-926.
<https://doi.org/10.1109/JSTSP.2011.2159773>